Master's thesis

2022

Emil Hansen

NTNU
Norwegian University of
Science and Technology
Faculty of Engineering
Environmental Engineering
Department of Civil and Environmental Engineering

Emil Hansen

A flow path detection algorithm to improve leakage risk assessment through defective jet-grouted cut-off walls

June 2022

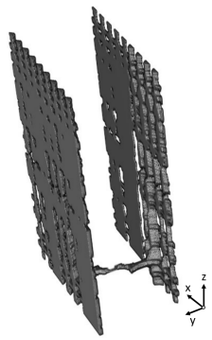

NTNU
Norwegian University of
Science and Technology

NTNU
Norwegian University of
Science and Technology

NTNU
Norwegian University of
Science and Technology

A flow path detection algorithm to improve leakage risk assessment through defective jet-grouted cut-off walls

Emil Hansen

Geotechnical Engineering
Submission date: June 2022
Supervisor: Yutao Pan
Co-supervisor: -

Norwegian University of Science and Technology
Department of Civil and Environmental Engineering

"… in spite of its practical benefits, the construction of a jet-grouting cut-off should be very carefully conceived, because of the dramatic consequences of possible failures."

P. Croce and G. Modoni, 2007

Abstract

Jet-grouted cut-off walls (JGCOWs) is an attractive solution as an artificial water barrier to prevent undesirable ground water seepage in situations where heavy machinery is not applicable. Failure likelihood for uncontrolled seepage has to be restricted as much as possible because of the dramatic consequences that could follow such events. Accurate field measurements of flow rate through defective JGCOWs has been proven difficult to obtain as a sound and recognized empirical framework is lacking. Numerical algorithms has therefore been developed to enable risk assessment and to aid designers. Focus on geometric imperfections, i.e. positioning errors and random variability of column diameter, has been prioritized in the algorithms to properly replicate the likelihood of occasional penetrating seepage passages.

This thesis proposes a flow path detection algorithm (FPDA) as an incremental innovation to describe the risk of undesired seepage flow more accurately. The focus has been dedicated to revising the logic that is used to detect penetrating passages. Instead of using nested *if*-statements, the powerful DBSCAN clustering technique is utilized to search for penetrating flow paths. Statistical robustness has been obtained through Monte Carlo simulations and consistency throughout a parametric study demonstrates high confidence in the results. When the new FPDA method was compared to the former algorithm, it was found that:

1. FPDA suggests **15 % reduced normalized flow rate for JGCOWs consisting of one single row of jet-grouted columns**, allowing a more economic and environmental design.
2. FPDA arrests the former algorithm's lacking ability of properly modelling tortuous flow paths through JGCOWs consisting of more than one row of jet-grouted columns, essentially revealing that the risk of underestimating the seepage flow rate is present in the former algorithm.

Furthermore, the proposed FPDA update serves as an enabler to revise existing knowledge about leakage risk through defective cutoff walls with a subtle, yet substantial, improvement.

Sammendrag

Jetpelevegger er en attraktiv løsning som en kunstig strømningsbarriere for å hindre uønsket strømning av grunnvann i situasjoner hvor tungt utstyr ikke kan anvendes. Sannsynligheten for ukontrollert strømning må begrenses så mye som mulig for å hindre de dramatiske konsekvensene som kan oppstå i visse tilfeller. Pålitelige feltmålinger av strømningsraten gjennom defekte jetpelevegger har vist seg vanskelig å oppnå ettersom det ikke finnes noe annerkjent empirisk rammeverk som beskriver denne risikoen. Numeriske algoritmer har derfor blitt utviklet for å kvantifisere risikoen og for å bistå ingeniører i valg av design. Geometriske avvik har vært et sentralt fokusområde i utviklingen av algoritmene for å kunne beskrive sannsynligheten for sporadiske gjennomstrømningspassasjer.

Denne masteroppgaven foreslår en ny metode kalt FPDA som en inkrementell innovasjon for å beskrive risikoen for gjennomstrømning mer nøyaktig. Arbeidet har vært dedikert til å revidere logikken som brukes for å detektere strømningskanaler gjennom jetpeleveggen. Isteden for å bruke *hvis*-setninger, har den kraftige grupperingsteknikken DBSCAN blitt brukt for å finne strømningskanaler. Monte Carlo simuleringer har blitt gjennomført for å oppnå statistisk signifikante resultater og et sensitivitetsstudie er utført for å underbygge konklusjonen. Når den nye FPDA-metoden sammenlignes med eksisterende algoritmer, viser det seg at:

1. FPDA-metoden foreslår en **15 % reduksjon i normalisert strømningsrate for jetpelevegger bestående av èn rad av jetpeler**. Dette tillater et mindre konservativt design, noe som sparer både penger og miljøet.
2. FPDA-metoden arresterer den eksisterende algoritmens manglende egenskap til å modellere kronglete og svingete strømningskanaler gjennom jetpelevegger bestående av mer enn èn rad av jetpeler. Dette funnet avslører at den eksisterende algoritmen står i fare for å underestimere strømningsraten.

Videre fungerer den nye FPDA-metoden som en muliggjører for å revidere eksisterende kunnskap om lekkasjerisiko gjennom jetpelevegger med en subtil, men betydningsfull, forbedring.

Acknowledgements

Foremost, I would like to thank my supervisor Professor Yutao Pan for his commitment to fundamental understanding and excellent guidance. Our discussions and his ability to express complex technical phenomenons with intuitive layman's words has boosted my motivation throughout the entire semester.

I would also like to thank PhD candidate Rui Tao for valuable feedback at an early stage - the achievements in this thesis would not have been accomplished without his support. He patiently took of his time to understand the problem statement and contributed with new ideas.

Norconsult and Indira Bodø has sequentially accommodated me with a personal high quality office ever since I moved to Bodø 1^{st} of March 2022. It has significantly facilitated the entire thesis production process as well as provided me with a valuable psychosocial working environment. Additionally, I have learned a lot by being present in a professional setting. I do not forget that both companies has treated me with free lunch thoughout the semester.

It is not possible to avoid expressing my gratitude to my girlfriend, Lisa Mari Høgseth. She has had an unconditional positive influence on me over the past half-year and has really constituted a true source of inspiration.

Last, but not least, I would like to thank my little sister Johanne, little brother Arne, mom Hilde and dad Lennart. They have always been a source of motivation and encouragement for me.

Emil Hansen
Bodø, June 2022

Methodology

A summary of the production process for the master thesis is provided in this chapter.

Strategy

Quality and flow efficiency has been prioritized in accordance with the LEAN mindset as summarized elegantly in [1]. To enable quality and flow efficiency, it is important to focus on customer awareness when defining the objective and progress plan. So who is the customer of a master thesis? One could argue that it does not have any customers and that it serves merely as a prerequisite for the candidate to achieve a master's degree. At the same time, many of the process attributes resemble those of a textbook commodity business example with clearly defined customers. More specifically, there is an expectation on what to deliver and when. The artificial customer is expecting some technical work to be presented in a structured manner by 16th June in 2022.

Requirements for the technical work include understanding of fundamental principles, awareness of existing knowledge and an incremental innovation attempt to - in some way or another - add value to the society. The latter can not be understated as the overall purpose of any engineering practice is to 'make it happen' by applying academic knowledge to real-life problems. Clear presentation is of practical importance as it aims to preserve any findings by getting it safely across to the reader. An illustrative model of the quality is presented in Figure 1. Distinct weak links will severely harm the quality and it is therefore important to allocate sufficient consideration to all parts of the bicycle chain to make it sufficiently strong. Required strength is defined by the customer and is concertized with aid from the supervisor.

The first step towards flow efficiency is taken by altering the traditional focus on resource efficiency, where everyone is as occupied as possible, towards progress traction. Flow efficiency aims to prioritize activities that pushes the product, namely the master thesis, towards completion by reducing waste. Loosely speaking, waste can be defined as any activity that does not contribute to progress of the product towards delivery. Two examples are provided to illustrate the concept of waste.

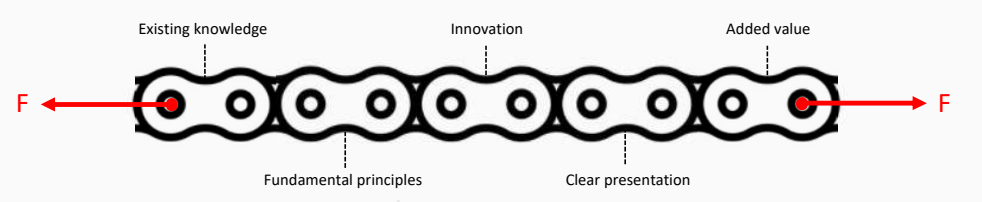

(a) Elements in quality model.

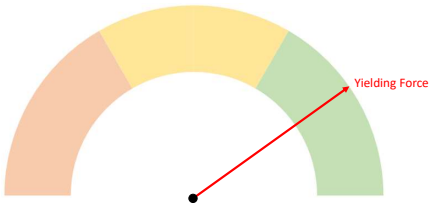

(b) Quality indicator given by yielding force.

Figure 1: Illustrative quality model of the master thesis.

Example 1: Flow Efficiency Analysis

Figure 2 presents a high-level Flow efficiency analysis (FEA) of my previous master thesis in Petroleum Engineering from 2016.

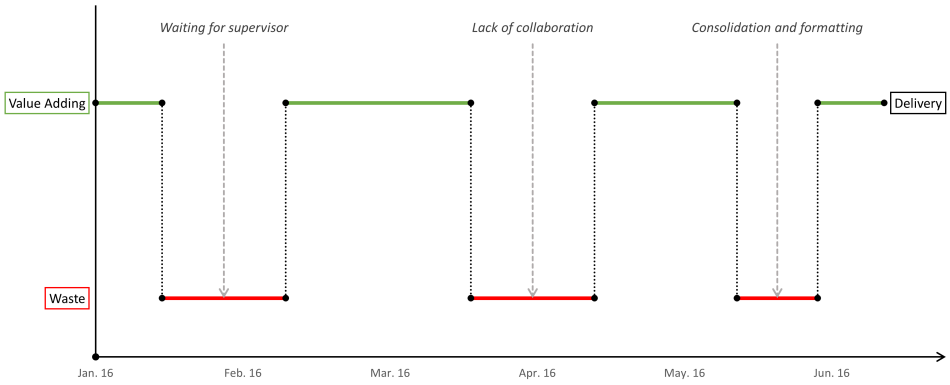

Figure 2: FEA of previous master thesis production process

Supervisor availability is a vital, yet often limited, asset for master thesis candidates and waiting time, as well as irrelevant time usage, can constitute a significant waste element in the activity set. For this thesis, it has been mitigated by scheduling bi-weekly meetings for predictability and establishment of a dedicated Teams channel to allow transparency and demand driven communication throughout the semester. Preparation for the bi-weekly meetings is essential to avoid urgency and to stay on the right track towards delivery.

Another asset for master thesis candidates is collaboration with fellow stu-

dents or other people with interest in the same topic realm. Lack of such collaboration will likely lead to waste by reinventing existing knowledge or insufficient quality control. In 2016, I used a substantial amount of time to develop an appropriate goal seek algorithm before I got in contact with Arnaud Hoffman, which enlightened me with a very intuitive implementation of the bisection method that solved the problem in question efficiently. For this thesis, I early discussed a home made nested if-statement idea to cluster data with PhD candidate Rui Tao and he advised me to test DBSCAN - an existing clustering algorithm that way surpasses both efficiency and accuracy to anything I could have made by myself.

Organizing references, both figures and bibliography, and document formatting serves the purpose of clear presentation and early acknowledgement of these activities can reduce waste. The table of contents can be used as a document skeleton to align thoughts in an early phase with the supervisor to avoid waste generating reorganization later on. Also, continuous input of figures and references will make post administration redundant and therefore reduce waste. An analog example is provided below to clarify.

Imagine you are going on a business trip and that the expenses are refunded afterwards. To get the refund, you have to document your expenses with date, activity (e.g. taxi), amount and a copy of the receipt. Alternative A is to put all the receipts in you pocket and issue the refund claim afterwards. Alternative B is to continuously log the expenses as they occur by documenting the receipt with a photograph and providing metadata (date, activity and amount) while the information is present. The final refund claim is identical for both alternatives, but alternative A requires additional post administration efforts to remember the required metadata for the various receipts afterwards. This additional effort does not add any value and can therefore be considered as waste. Such post administration activities can indeed become substantial for projects in the master thesis order of magnitude.

Example 2: Visualization

In my previous thesis, Figure 3 was presented to describe the data flow in an iterative process. Although the objective of the figure was met, it took 8 hours to generate the figure in Paint with pixel level accuracy. This exemplifies a typical traditional resource efficiency mindset where the resources are occupied, but lacking customer awareness is resulting in lead time to achieve the objective. The same objective could have been met with significant reduction in time usage without loss of quality.

Strategic summary

Based on the given argumentation, the key strategic priorities for this thesis production is quality and flow efficiency.

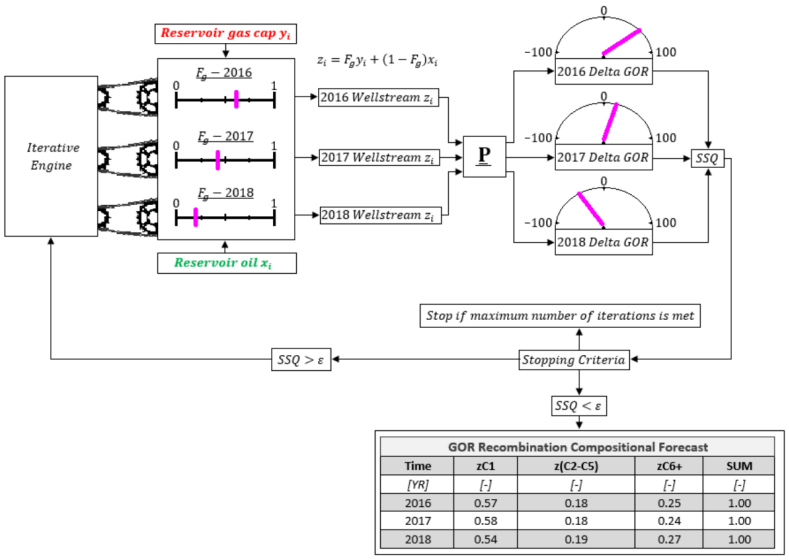

GOR Recombination Compositional Forecast				
Time	zC1	z(C2-C5)	zC6+	SUM
[YR]	[-]	[-]	[-]	[-]
2016	0.57	0.18	0.25	1.00
2017	0.58	0.18	0.24	1.00
2018	0.54	0.19	0.27	1.00

Figure 3: Visualization from previous thesis

Activities

To honour the strategic priorities, a high-level activity set has been generated to allow progress control and transparency throughout the thesis production process. It serves as a guideline on how to utilize the time frame and does not aim to capture all tasks in great detail. A visualization of the planned activity set is given in Figure 4.

One Full time equivalent (FTE) is equivalent to 8 hours per day, 5 days a week with 30 minutes daily lunch break and does not include national Easter holiday. It is used to illustrate the relative amount of time used for the different activities.

Screening

The purpose of the screening activity is to identify a relevant geotechnical topic realm. An initial wide approach increases the probability of finding an appropriate topic that triggers personal motivation as well as being technically feasible and with some value potential to the society. Tasks within this activity include orientation of proposed topics by the geotechnical department, contacting relevant commercial companies, talking to potential supervisors and reading abstracts for technical papers. The screening activity leads to determination of a topic realm and store some back-up topics in case further investigations meets a dead end.

Literature Review

The next phase is dominated by reviewing existing literature. The purpose is to get familiar with the chosen topic realm and to seek for research gaps. Requirements

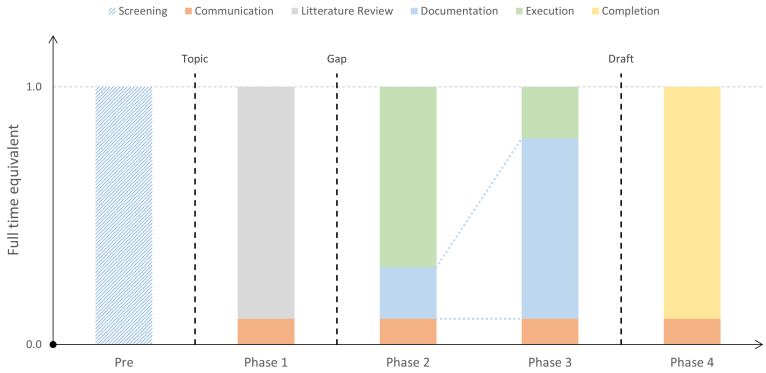

(a) Time allocation management

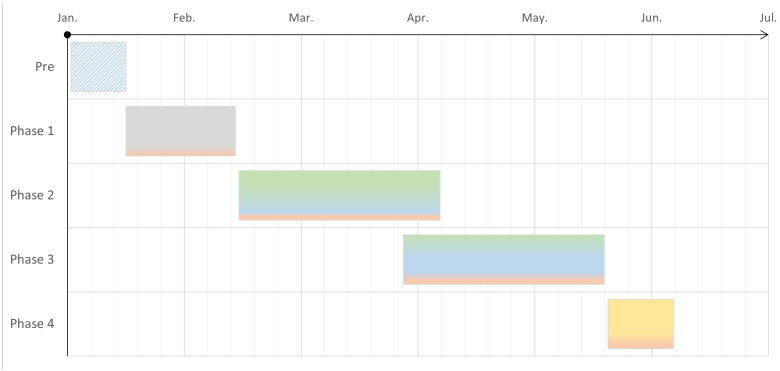

(b) Gantt chart

Figure 4: High-level progress plan for production of master thesis.

for an appropriate research gap includes technical feasibility and that filling the gap indeed adds some value in one way or another. Uniqueness is also important as it gives the thesis an opportunity to contribute with new ideas and findings. Some limitations for the scope going forwards can also be defined to ensure that future effort does not get stretched too thin trying to capture too much.

Communication

Communication is introduced as a separate activity and includes practical administration, e.g. approval of formal thesis contract, collaboration and supervisor communication. The supervisor serves as a counsellor and constitutes a central source of guidance, motivation and technical insight. It is important to underline that the communication goes both ways and that preparation before meetings is essential to extract value. The overall responsibility of the master thesis lays with the candidate and the communication activity serves to help stay on track along the way.

Execution

Execution constitutes the central activity of the master thesis and is where the 'actual work' takes place. The identified research gap is attempted filled by combining existing knowledge with new ideas. For this thesis, Matlab coding has been the main task within the execution activity. Initial proof of concept development, testing, run time optimization, data flow integration, quality control and result interpretation constitute natural elements within the coding task.

Documentation

Documentation goes hand-in-hand with the execution activity and the overlapping transition between phase 2 and 3 is characterized by altering the main focus from execution to documentation. To achieve flow efficiency, these activities are conducted simultaneously to capture knowledge when it is fresh and for transparency for the supervisor. The transition towards more and more focus on documentation follows the execution maturity in a natural manner as the degree of confidence increases in the results. Due to the simultaneity, a flexible documentation approach in LaTeXhas been chosen. Changes in figures, tables and sections can easily be implemented as new findings or ways of visualizing the results occur. It is however important to underline that over documentation in a too early phase can harm the flow efficiency as results are prone to volatility until quality controls and peer reviews are conducted.

Completion

Completion is a collective activity that gathers all tasks related to consolidation and final preparation towards delivery. An important prerequisite for efficient

completion is to establish a common formatting practice when setting up the initial document for consistent layout and phrasing. The main objective of the completion activity is to ensure that the message of the thesis is communicated to the reader is a clear manner.

Note on LEAN Approach

Finally, a couple of comments related to the application of a LEAN approach to master thesis production are provided to emphasize some limitations.

- The LEAN concept constitutes a mindset that is applied worldwide to reduce waste in business processes. It involves a comprehensive list of models and tools, whom only a very few are mentioned and utilized in this thesis work. Also, the FEA is based only on one previous master thesis and application of LEAN is deliberately kept limited to not steal too much time from the actual thesis production. The ambition is not to remove all waste, but to motivate customer awareness to reach a satisfactory degree of quality and flow efficiency. Some residual waste is certainly present within the production process for this thesis.
- Application of LEAN theory in an academic environment can seem somewhat counter intuitive as traditional LEAN examples often concern more practical streamlined processes in commodity businesses. The purpose of this attempt to apply the theory for master thesis production is not to ensure that every effort goes into producing phrases and visualization that goes directly into the final pdf-document, but to ensure that the majority of the effort goes into maturing the thesis project towards delivery. For example, trial and error or run time optimization while coding may not be apparent in the final deliverable, but they are essential in achieving fundamental understanding which in turn enhances the quality of the final product. Flow efficiency is not meant to compete with quality by any means, but the customer awareness is supposed to arrest obvious waste activities.

Contents

Figures

Tables

Code Listings

Acronyms

CDF cumulative distribution function.

COV Coefficient of variation for a given random variable, X. $\mathrm{COV}(X) = \frac{\sigma_X}{\mu_X}$.

DBSCAN Density-based spatial clustering of application with noise.

FEA Flow efficiency analysis.

FEM Finite element method.

FPDA flow path detection algorithm.

FTE Full time equivalent.

IID independent and identically distributed.

JGCOWs Jet-grouted cut-off walls.

MATLAB well known programming language developed by MathWorks.

PDE Partial differential equation.

PDF probability density function.

PhD philosophiae doctor.

SOF scale of fluctuation.

TDA three-dimensional discretized algorithm.

Symbols

A Area, $\left[m^2\right]$.

A_j Cross sectional untreated area for j^{th} slice, $\left[m^2\right]$.

A_w Total cross sectional area of the entire JGCOWs, $\left[m^2\right]$.

H Water head difference, $[m]$.

N_{min} Minimum number of neighbouring points required for a core point in DBSCAN method.

Q Flow rate, $\left[\frac{m^3}{s}\right]$.

Λ_i Jackknife relative impact estimator for the harmonic mean.

Ω Normalized flow rate.

α Azimuth angle as described in Figure 2.6.

β Inclination angle as described in Figure 2.6.

ϵ Threshold distance to neighbouring points in DBSCAN method.

η_i Jackknife impact estimator for the harmonic mean.

μ Mean or expected value for a given random variable.

ω Relative flow rate, $\frac{\Omega_{FPDA}}{\Omega_{TDA}}$.

σ Standard deviation for a given random variable.

$\tilde{x}$ Harmonic mean. $\tilde{x} = \left[\frac{1}{n}\sum_{i=1}^{n} x_i^{-1}\right]^{-1}$.

i Hydraulic gradient $\frac{dh}{dl}$, defines head loss per unit length.

k Permeability coefficient, $\left[\frac{m}{s}\right]$.

n Number of slices as illustrated in Figure 2.2b.

n_{row} Number of rows of jet-grouted columns in cut-off wall construction.

xxx

s_x Along-row spacing.

s_y Across-row spacing.

L Length of JGCOWs as defined in Figure 1.3.

t Thickness of JGCOWs as defined in Figure 1.3.

W Width of JGCOWs as defined in Figure 1.3.

Chapter 1

Introduction

1.1 Jet-Grouted Cutoff Walls

Cutoff walls are widely used to prevent undesirable fluid seepage through water-bearing permeable soils [2–5]. Examples of undesirable seepage include intrusion of water into excavation pits, flow under coffer dams and spreading of buried waste. Such undesirable seepage events can lead to dramatic consequences, as exemplified by the long-term postexcavation settlements on an adjacent building following an uncontrolled outburst of groundwater during construction of a subway station in Shanghai, China [5]. Application of cutoff walls to prevent these unwanted events are illustrated in Figure 1.1. Cutoff walls can be constructed with different techniques, such as jet grouting, secant pile, diaphragm or slurry walls. Jet-grouted cut-off walls (JGCOWs) offers geometrical versatility, rapid installation and relatively light equipment [3, 6]. The latter constitutes a key advantage and decisively outcompetes the alternative techniques for cases where large and heavy equipment cannot be used. Typical examples include densely populated downtown areas or coastal areas with soft ground conditions.

Jet grouting denotes in-situ injection of a fluid slurry to improve ground conditions. The fluid slurry consists of a water-cement mixture and is characterized by solidifying underground some time after casting. The construction procedure [1] is initiated by attaching a grouting monitor to the end of a drill stem and to run it to the desired treatment depth. Fluids are then injected into the ground at high speed through rotating small-diameter nozzles as the drill stem is slowly raised towards ground surface level. After curing, a cemented soil body takes place within the natural soil as shown excavated in Figure 1.2. The material properties of the cemented soil body resembles those of low-quality concrete, and it is therefore denoted soilcrete [2]. Compared to natural soils, soilcrete is characterized by high strength, high stiffness and low permeability [8–10].

The construction procedure yields columnar units of soilcrete within the natural soil. These columnar units are installed in an overlapping fashion to minimize

[1] [7] including descriptive video

[2] [3] page 11

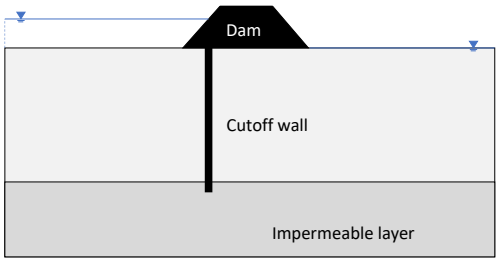

(a) Coffer dam

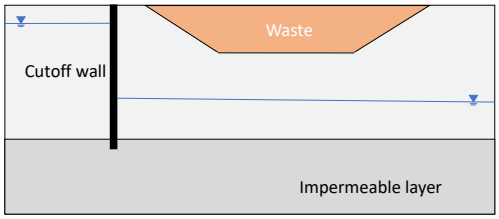

(b) Buried waste

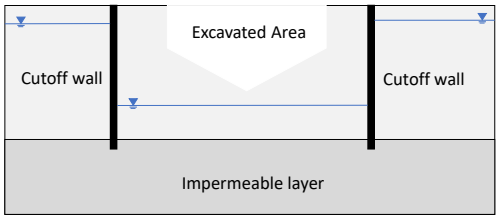

(c) Excavation

Figure 1.1: Typical application of cutoff walls.

the extent of untreated zones within the construction. Untreated zones constitute defects that may significantly harm the water-tightness by shortening seepage passages or indeed provide penetrating flow paths through the entire construction. Although due consideration is taken in the construction phase, untreated zones are likely to occur as real-life jet grouted columns naturally deviate from ideal theoretical columns. More precisely, the consensus is that variation in column diameter and axial direction are the two major root causes for occurrence of untreated zones in JGCOWs [3, 6, 12–16]. An illustration of ideal versus defective calabash shaped jet grouted columns is given by the digital twins in Figure 1.3. Note that the figure also defines axis orientation and JGCOWs geometric properties, W, L and t for width, length and thickness respectively.

Several probabilistic approaches has been implemented to model the leakage risk through JGCOWs with geometric imperfections appropriately [3, 6, 14–16]. In particular, the three-dimensional discretized algorithm (TDA) proposed in [14] and applied in [6, 15, 16] constitutes the current state-of-art solution.

Figure 1.2: Picture of jet grouted columns [11].

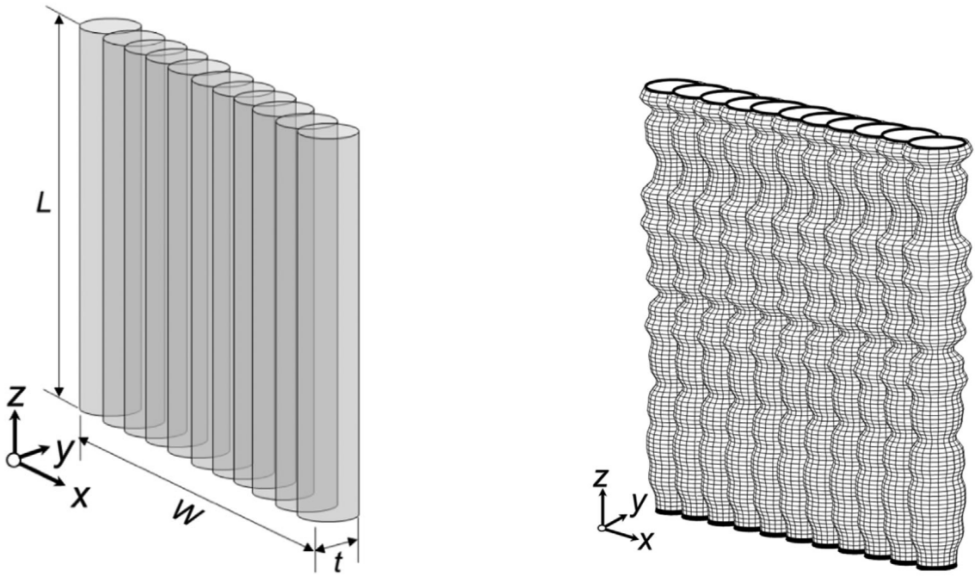

(a) Ideal theoretical **(b)** Defective calabash shaped

Figure 1.3: Ideal versus defective JGCOWs. Taken from [16].

1.2 Objective

The ambition of this thesis is to make an incremental contribution to the existing work related to modelling of leakage risk through JGCOWs with geometric imperfections. The TDA method, as presented by the high level flow chart in Figure 1.4, represents the current research front.

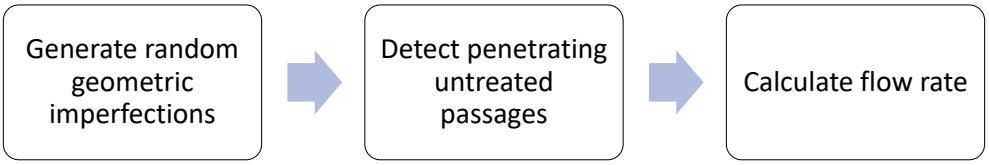

Figure 1.4: High level flow chart for TDA method

Detection of untreated penetrating passages, i.e. flow paths, constitutes an important intermediate step to obtain a reasonable flow rate estimate. The current TDA method holds two limiting assumptions while screening for penetrating untreated seepage passages:

- It applies a 2D bird's-eye view, i.e. a plan view from above, through the cement-treated ground, essentially neglecting the de facto vertical scatter of untreated nodes. Presence of vertical seals are likely and appropriate differentiation does affect the harmonic average based flow rate estimation. This approach also leads to inclusion of untreated nodes that are not necessarily subject to differential hydraulic potential as the communication through the cement-treated ground can be sealed off elsewhere. It is underlined that the vertical scattering of untreated nodes is neglected by the TDA method.
- Looks for penetrating passages in predefined volume segments in-between the soilcrete columns. This implies that the TDA method wrongfully rejects transversal flow as it implicitly assumes no-flow boundaries along the predefined volume segments. Transverse flow paths are indeed likely to occur, especially for JGCOWs configurations with more than one row of jet-grouted columns.

The objective of this thesis is to overcome the two limitations mentioned above to replicate the physical leakage problem more accurately. Improved insight will either lead to more economical and environmental design or increase safety awareness. It is emphatically underlined that this objective could not have been pursued if it was not for the thorough and broad basis provided by the existing work.

1.3 Scope and Limitations

The following list defines the scope boundary of this work by summarizing limitations and assumptions:

- It is known that the minimum thickness, t_{min} as described in Figure 1.5, of treated ground is a significant indicator of water-tightness for cases where no fully penetrating seepage passages exist [3]. For this work, monitoring and evaluation of t_{min} is **not included** as the purpose is to investigate the penetration detection logic. That is, the focus for this work is on cases where the cut-off wall indeed is fully penetrated by seepage passages.

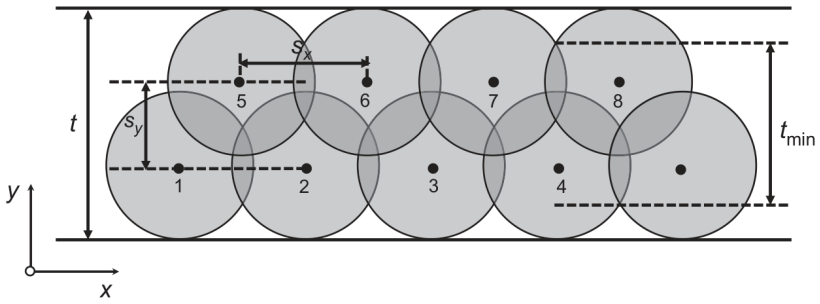

Figure 1.5: Plan view of jet-grouted columns [15]. s_x and s_y describe the along-row and cross-row spacing respectively, whereas t describes the full thickness.

Note that Figure 1.5 illustrates s_x and s_y.

- All flow calculations are conducted in a **steady-state** regime, i.e. $\frac{d}{dt} = 0$, where t denotes time.

- Flow induced erosion effects for granular soils subject to high hydraulic gradient[3] are not considered. Such effects would impose $\frac{d}{dt} \neq 0$ by moving the required calculations out of the steady-state regime. Again, the focus for this work is to investigate the penetration detection logic, naturally leaving this relatively advanced feature out of scope.

- All simulation cases with more than one row of jet-grouted columns assume a triangular design as illustrated in Figure 1.5. Alternative set-ups, such as square layout, are not considered as the triangular design intuitively has a stronger water-tightening effect on horizontal flow through vertical JG-COWs.

- A constant permeability coefficient, k, for the untreated zones is assumed. The benefits of keeping k constant include keeping the flow calculation relative simple as well as protecting the high code efficiency. Appendix B provides an introductory proof of concept to motivate eventual future implementation of stochastic permeability.

- The seepage flow rate evaluations are limited to horizontal seepage through

[3] As exemplified by the Teton dam failure in Idaho, USA in 1976, causing 11 causalities [17].

vertical cutoff walls as illustrated in Figure 1.6 with flow direction perpendicular to the columnar axis. This limitation is introduced to avoid spreading the contribution of this work too wide - making it too thin. The presented methodology in this thesis is directly adaptable to cases with other flow configurations, such as parallel flow through earth-plug constructions.

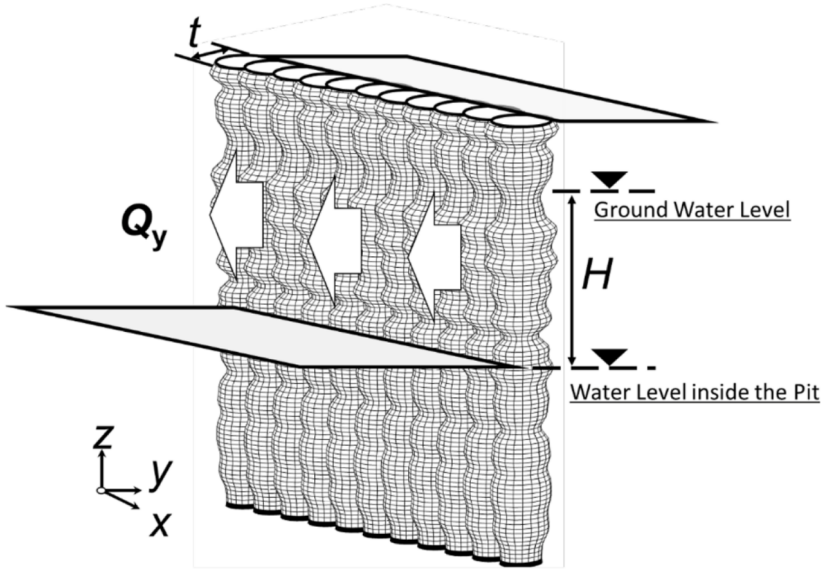

Figure 1.6: Horizontal seepage through vertical JGCOWs [6]

Chapter 2

Theoretical Framework

The purpose of this chapter is to provide a relevant literature review, point at the research gap and to elaborate key fundamental principles used to fill the gap. Motivation for each section in this chapter is given by the below bullet points.

- **Section 2.1 Literature Review**
  Gives an overview of existing work and sets the scene with regards to the work presented in this thesis by describing the research gap.
- **Section 2.2 Geometric Imperfections**
  Geometric imperfection is the main reason for occurrence of untreated zones in cement-treated ground and it describes the three-dimensional appearance of such zones. Hence, proper modelling of geometric imperfection is a key enabler to replicate reality in numerical simulations. One could regard this as the static geometric skeleton in leakage flow rate estimation with TDA.
- **Section 2.3 Leakage Flow Rate**
  Provides the governing equations for physical flow behaviour in porous media. Essential for quantifying flow rate in leakage risk assessment.
- **Section 2.4 Mathematics**[1]
  Elaborates properties of the non-linear **harmonic average** operation as it constitutes a key brick in fluid flow behaviour through matrix with varying capacity. Also, the concept of **data clustering** is introduced as it is extensively used to develop an improved flow path detection algorithm as proposed by this thesis.

Additional theoretical materials are provided in Appendix B Stochastic Permeability and Appendix C Monte Carlo Simulation.

[1] "Examples show how difficult it often is for an experimenter to interpret his results without the aid of mathematics" - **Lord Rayleigh**

2.1 Literature Review

This literature review covers the development of the TDA method as summarized in Table 2.1 and defines the research gap.

Table 2.1: Summary of TDA literature review.

Reference	Takeaways
Croce and Modoni (2007) [3]	Probabilistic framework for leakage risk through JG-COWs established. Includes axis deviation and inter-column diamter variation.
Modoni and Bzówka (2012) [18]	Intracolumn diameter idea noted.
Modoni *et al.* (2016) [12]	Size of geometric defects estimated by evaluating middle layer cross section. Random diameter, but columns assumed to be perfectly cylindrical.
Pan *et al.* (2017) [14]	**TDA launched.** Intracolumn variation incorporated with random field theory. Multi-shaft operation considered and deemed favourable.
Pan *et al.* (2019) [15]	Minimum thickness monitored as additional indicator of water-tightness in TDA. Refined design charts proposed. Anisotropic SOF for orientation parameters.
Pan *et al.* (2019) [6]	Strong correlation with FEM demonstrated. TDA slightly more conservative. High TDA efficiency underlined. Still steady state.
Pan *et al.* (2021) [16]	Diffusivity PDE utilized to capture transient-state behaviour. Strong correlation with FEM comparison.

The TDA method is illustrated by the detailed flowchart given in Figure 2.1[2]. Evaluations related to minimum thickness falls out of scope for this work as the focus is dedicated to proposing an improved algorithm for flow path detection to improve leakage rate calculation. The research gap is annotated in the figure to clearly show where the proposed improvement takes place.

[2] [16] page 113

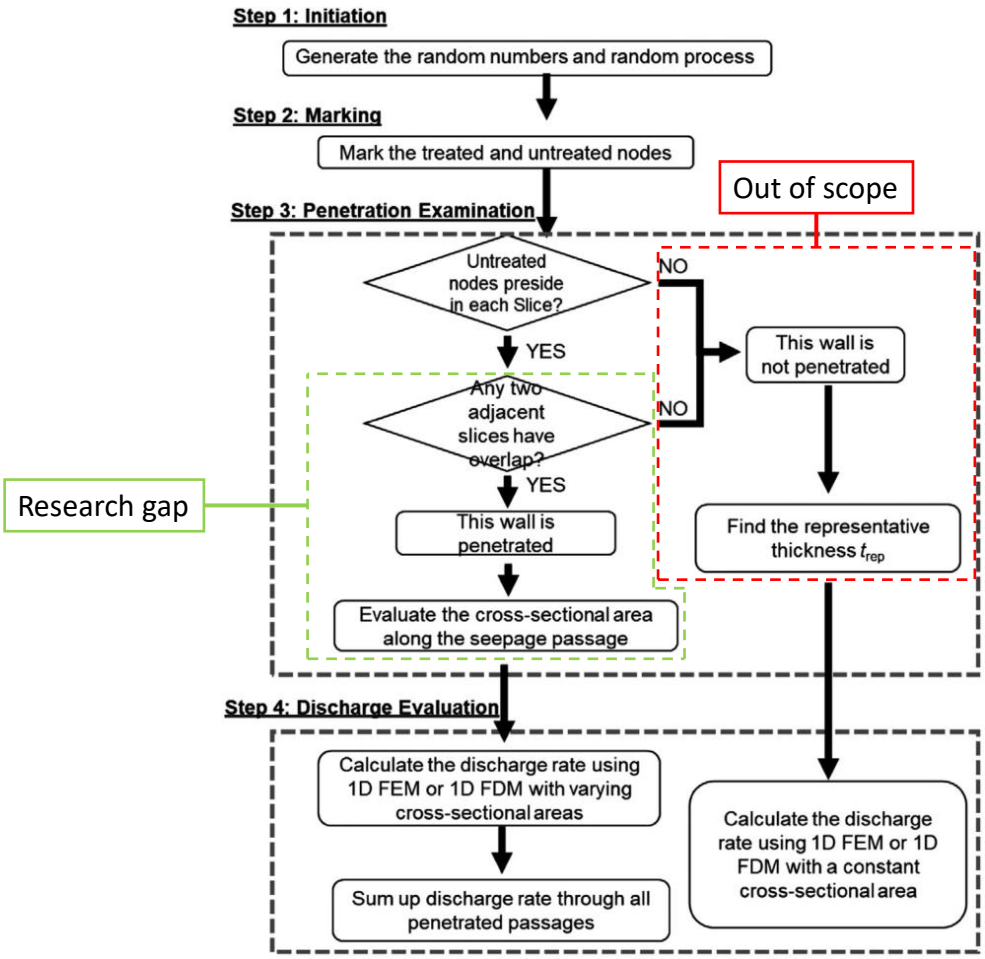

Figure 2.1: Flow chart for TDA method [16] with annotated research gap

More precisely, the research gap is explained by the illustrations provided in Figure 2.2. The **orange** volumetric boxes indicate artificial segments in-between columnar cement-treated units where the current TDA is set to search for penetrating passages. These boundaries are non-physical and implicitly impose no-flow boundaries for potential flow paths as illustrated in Figure 2.3. Transversal flow is wrongfully rejected in the TDA method by the no-flow boundary as indicated by the **red** cross.

Furthermore, the **green** rectangle in Figure 2.2 defines a **slice** perpendicular to the flow direction. The current TDA utilizes a 2D y-x bird's eye view, which is obtained by summing all untreated nodes across the entire depth (z-direction) for each slice, to determine penetrating seepage passages. Neglection of the vertical distribution has two setbacks; *(1)* it includes nodes that are not subject to differential hydraulic potential and *(2)* summation before the harmonic average

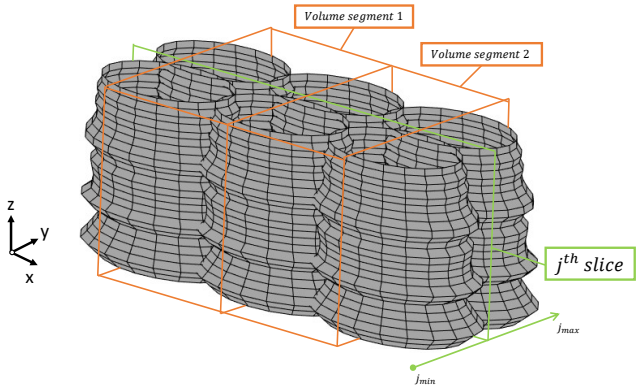

(a) Definition of volume segments and slices

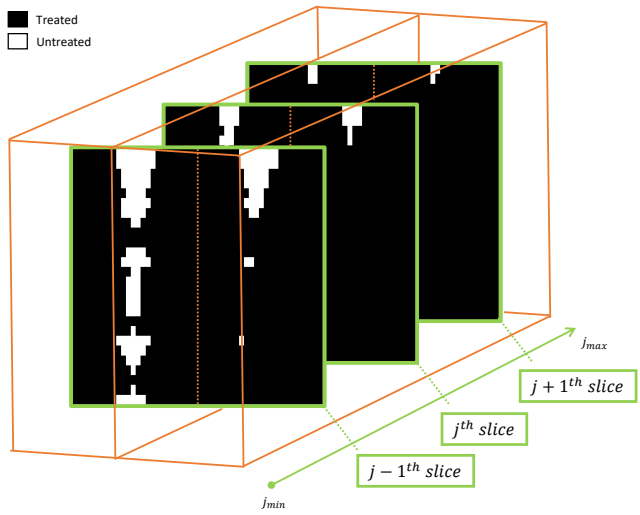

(b) Untreated slice area

Figure 2.2: Definition of slices and volume segments for penetration examination in TDA method.

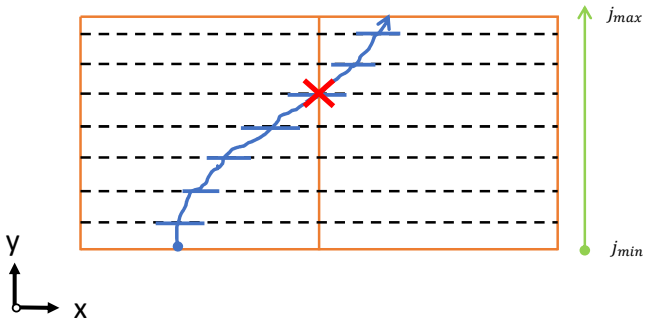

Figure 2.3: Realization 1. Transversal flow rejected by current TDA.

operation affects the calculated leakage rate [3]. An illustrative example is provided in Figure 2.4, where a TDA flow path is defined even though there is no three-dimensional overlap of untreated zones.

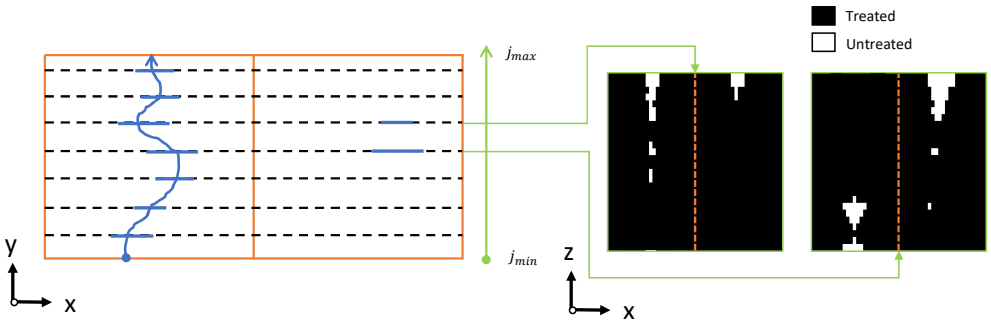

Figure 2.4: Realization 2. Vertical scatter overlooked to allow non-physical flow.

This research gap is of interest because the conservative 2D bird's eye view assumption contains an opportunity for more economical and environmental design if some of the conservatism can be replaced with new insights. The effect of transversal flow is less intuitive as the likelihood for occurrence of transversal flow path depends on the design configuration. In particular, number of rows and relative placement, e.g. triangular set-up, is expected to impact the result.

2.2 Geometric Imperfections

JGCOWs are subject to geometric imperfections given by the nature of the construction process. Variation in column diameter and deviation from perfectly oriented columns are inevitable and its randomness dictates the occurrence of untreated zones [3, 6, 12–16]. These deviations are elaborated in the following subsections.

2.2.1 Diameter Variation

Jet-grouted columns holds intracolumnar variation in diameter as showed in Figure 2.5.

In addition to the controllable jet-grouting operation parameters, the achieved diameter is dependent on the in-situ soil properties strength and permeability [19–22]. Soil properties vary stratigraphically as yielded by the natural depositional history. Such in-situ variation can be replicated theoretically by applying spatial variability and random field theory[4]. The scale of fluctuation (SOF) represents a measure of the largest distance within which significant correlation between two points exists. It is used within a autocorrelation function to apply statistical

[3] Section 2.4.1

[4] These phenomenas are considered well-known and further description falls outside the scope of this thesis.

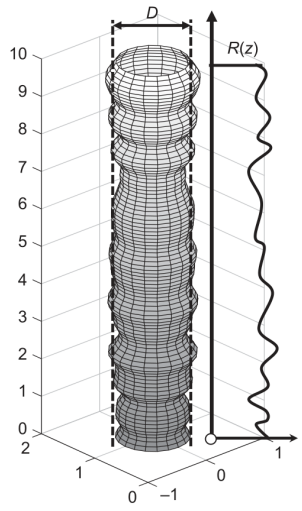

Figure 2.5: Variation in column diameter.

correlation between two points appropriately to replicate natural soil's stratified layout. Note that the SOF in the vertical direction is much smaller than in the horizontal direction [23]. Hence, the TDA assumption of using the same randomly generated column diameter array for all columns seems reasonable.

2.2.2 Random Orientation

Deviation from an ideal axis can be expressed in terms of azimuth (α) and inclination (β) as defined in Figure 2.6.

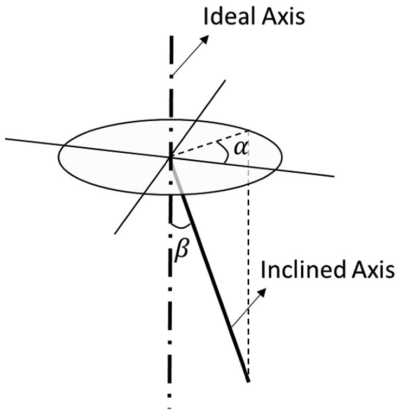

Figure 2.6: Azimuth α and inclination angle β

Azimuth is assumed to be uniformly distributed between $[0, \pi]$, whereas the inclination seem to follow a normal distribution around zero [3, 24] as shown illustratively in Figure 2.7. These parameters can be modelled as independent and identically distributed (IID) variables for each column in single-shaft opera-

tions. The TDA method was enhanced to include random field with autocorrelation structure to improve the de facto correlation between columns for multi-shaft operation in [15]. As a result, the TDA method can efficiently model the random orientation of jet-grouted columns.

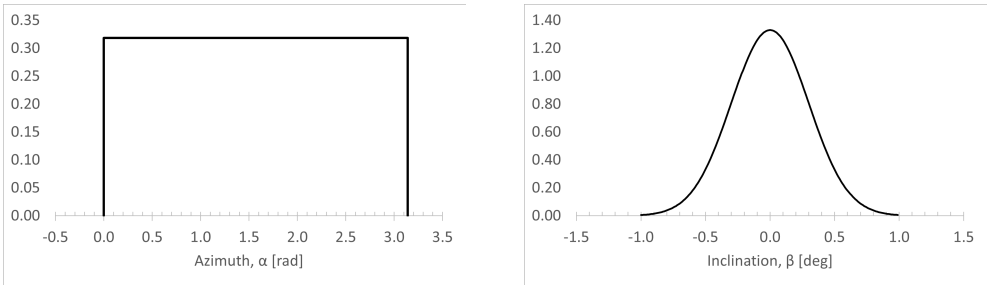

(a) Azimuth, α **(b)** Inclination, β

Figure 2.7: Illustrative PDFs for modelling of random orientation.

2.2.3 Summary

Statistical properties are summarized in Table 2.2. Note that this table is taken directly from [14].

Table 2.2: Statistical characteristics for geometric imperfections. *Obtained from a different site (Isola Serafini). Table taken from [14].

Ref.	Soil type	μ_D [m]	COV(D)	$\sigma(\beta)$ [°]	Remark
[25]	Clay-silt	-	0.02-0.05	-	-
	Sands	-	0.02-0.10	-	-
	Gravels	-	0.05-0.25	-	-
[26]	Sandy clay	1.1	0.06-0.19	-	Derived from field data of diameter at different depths, horizontal column
[3]	Silty sand	0.71-1.11	0.06	0.07*	Vertical columns in Vesuvius site
	Sandy gravel	1.06-1.20	0.19	0.07*	Vertical columns in Polcevera site
[27]	Silty sand	2.5	-	0.16	Vertical columns in Barcelona site
[24]	Sandy clay	0.38	0.13	-	Vertical columns with lower water content
		0.48	0.13	-	Vertical columns with lower water content
		0.75	0.17	0.17	(Sub) Horizontal column

The comingled effect of geometric imperfections in terms of diameter variation and orientational deviation is summarized by the example realization shown in Figure 2.8.

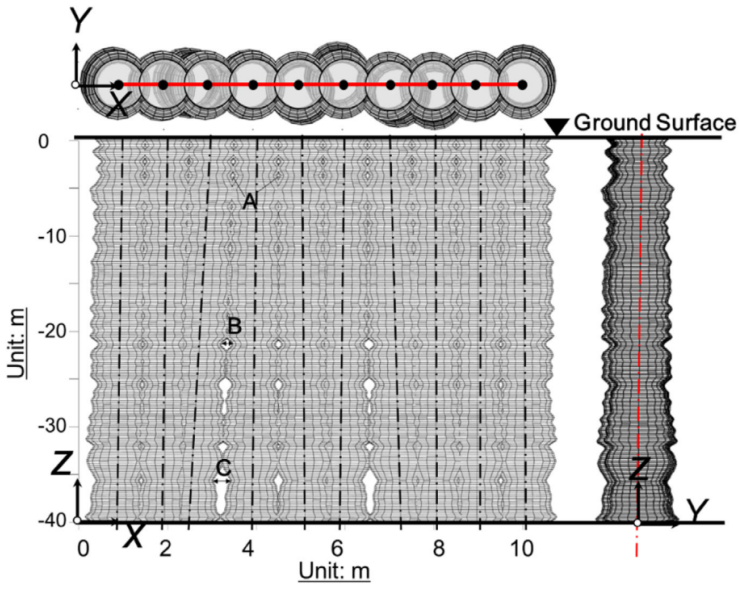

Figure 2.8: A realization with geometric imperfections [16]

Once a random realization is generated, investigation of untreated zones and penetration examination can take place to evaluate the discharge flow rate through the JGCOWs.

2.3 Leakage Flow Rate

Discharge flow rate through the cutoff wall constitutes the key output metric for each realization. For this work, non-zero flow rates are limited to realizations where the cutoff wall suffers from penetrating flow paths. I.e., seepage calculation based on minimum thickness is not regarded. Although the geometric imperfections yield a three-dimensional description of the untreated zones, the leakage flow is assumed to follow a one-dimensional behaviour as it is dominated by flow perpendicular to the wall. An one-dimensional approach also offers increased efficiency, thus enabling a higher volume of Monte Carlo simulations to obtain statistical robustness.

One-dimensional steady state fluid flow though porous media is generally modelled by the well-known Darcy's law:

$$Q = kiA \tag{2.1}$$

where Q is flow rate, k is the coefficient of permeability, i is the hydraulic gradient and A is the cross sectional area of untreated soil along the flow path. k is assumed

to be constant for the natural untreated soil [5] and the hydraulic gradient can be expressed as $i = \frac{dh}{dy}$. Rearranging Equation (2.1) yields

$$\frac{Q}{A(y)}\,dy = k\,dh$$

Assumptions of material balance and water incompressibility yields the following integration

$$\int_0^t \frac{Q}{A(y)}\,dy = \int_0^H k\,dh \;\rightarrow\; Q = \frac{kH}{t}\tilde{A}(t)$$

where H is the water head difference between upstream and downstream, t is the nominal thickness in the flow direction, i.e. y-direction as shown in Figure 1.3, and the harmonic average of untreated area along a flow path is expressed by

$$\tilde{A}(t) = \frac{1}{\frac{1}{t}\int_0^t \frac{1}{A(y)}\,dy} \xrightarrow{Discretization} \tilde{A}(t) = \frac{1}{\frac{1}{n}\sum_{j=1}^{n}\frac{1}{A_j}}$$

where n denotes the number of equally discretized slices and A_j expresses the cross sectional untreated area at the j^{th} slice as illustrated in Figure 2.9.

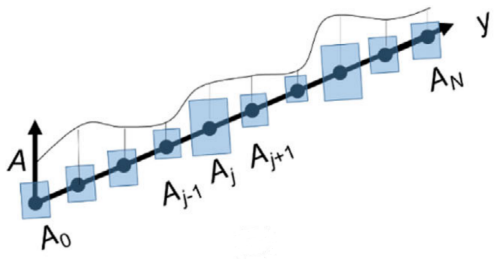

Figure 2.9: Untreated cross sectional area along penetrating flow path. Figure taken from [16] page 114.

Normalization of the flow rate [12] is given by

$$\Omega = \frac{Qt}{kHA} = \frac{\tilde{A}(t)}{A_w} \tag{2.2}$$

where A_w is the total cross sectional area of the entire JGCOWs. Ω constitutes a common performance indicator that can be used for comparison across realizations with different configurations. Furthermore, the total flow rate is calculated by summing up the contribution from each flow path.

[5] See discussion related to random permeability in Appendix B

2.4 Mathematics

2.4.1 Harmonic Average

The harmonic average constitutes one of the classical ancient Pythagorean means. For a dataset $\mathbf{X} = [x_1, x_2, \ldots, x_n]$, it is defined as

$$\tilde{x} = \frac{n}{\frac{1}{x_1} + \frac{1}{x_2} + \cdots + \frac{1}{x_n}} = \left[\frac{1}{n} \sum_{i=1}^{n} x_i^{-1} \right]^{-1}$$

A classical example of application for the harmonic mean is given in Appendix A. Opposed to the well-known arithmetic mean, the harmonic mean is not a linear combination of the given dataset. Hence, its properties are less intuitive and more difficult to evaluate analytically [6]. It has been proven in [29] that for a positive dataset with at least one pair of non-equal values, the harmonic mean is always less than the arithmetic mean. Furthermore, the harmonic mean of a dataset tends to be dominated by the smallest values as its high reciprocals take place in the denominator of the expression for $\tilde{x}$.

Jackknife Analysis

To overcome the analytical complexity of the harmonic mean, a practical approach can be taken to investigate its properties. Jackknife analysis offers a neat way of investigating the relative effect of each element in a dataset by simply removing it to see how much the output varies. It does not necessarily provide a thorough mathematical proof, but it can serve to give guidelines for particular cases and be used to quality control assumptions. An impact estimator can be calculated by

$$\eta_i = \frac{\left(\frac{n}{\frac{1}{x_1} + \cdots + \cancelto{0}{\frac{1}{x_i}} + \cdots + \frac{1}{x_n}} \right)}{\left(\frac{n}{\frac{1}{x_1} + \cdots + \frac{1}{x_i} + \cdots + \frac{1}{x_n}} \right)} = \frac{\frac{1}{x_1} + \cdots + \frac{1}{x_i} + \cdots + \frac{1}{x_n}}{\frac{1}{x_1} + \cdots + \cancelto{0}{\frac{1}{x_i}} + \cdots + \frac{1}{x_n}} \geq 1 \tag{2.3}$$

to estimate the impact of each entity on the harmonic mean of the dataset. η_i describes how much the harmonic mean would change if the i^{th} value of the dataset was effectively removed by setting its reciprocal equal to zero. Note that this estimator deviates somewhat from traditional Jackknife estimators as the sample number, n, is kept unchanged in the numerator. Traditional Jackknife analysis would remove one sample to yield $(n-1)$ in the numerator of the estimator expression. For leakage risk through JGCOWs, the harmonic average arises as an integral along a seepage path through the cement-treated ground. Rationale for keeping all samples, n, in the numerator is based on the fact that the integral has to be taken across the entire wall.

[6] [28] page 267.

Consider a dataset, $\mathbf{Y} = [y_1, y_2, ..., y_{10}]$, where y_i is a uniformly distributed integer within $[1, 100]$. A realization of $\mathbf{Y}$ and calculated impact estimator, η_i, is given in Figure 2.10

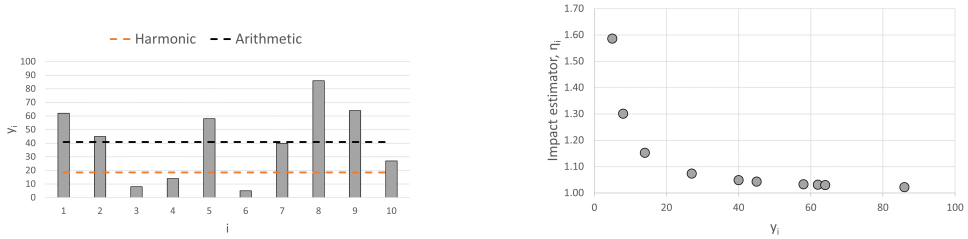

(a) Realization **(b)** Impact estimator, η_i

Figure 2.10: Harmonic mean analysis of example dataset.

The example reveals an asymptotic behaviour for η_i as the i^{th} value approaches zero, which indicates that the harmonic average indeed is dominated by the lowest values of the dataset. Relative impact can further be evaluated by normalizing the impact estimator, η_i, by the lowest value as described by

$$\Lambda_i = \frac{\eta_i - 1}{\eta_{i,min} - 1}$$

and exemplified in Figure 2.11. The example shows that removing the smallest value, 5, would alter the harmonic average **27** times more than removing the biggest value, 86.

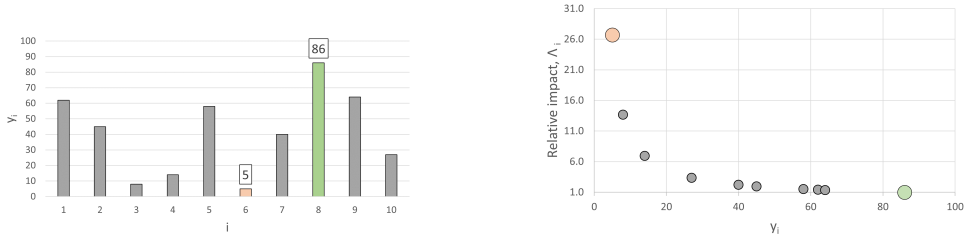

(a) Realization **(b)** Relative impact, Λ_i

Figure 2.11: Harmonic mean analysis of example dataset.

Only one realization of $\mathbf{Y}$ has been investigated so far. To increase the confidence in the indicated behaviour, some statistical analysis has been conducted with $n = 1\ 000$ realizations of $\mathbf{Y}$. Recall that each realization contains 10 integers randomly selected from a uniform distribution between 1 and 100. The statistical analysis is summarized in Figure 2.12.

Figure 2.12a contains all 10 000 integers of all 1 000 realizations and the relative impact is calculated for the given realization. It shows a clear trend of significant increased impact with lower values across all realizations. Figure 2.12b is

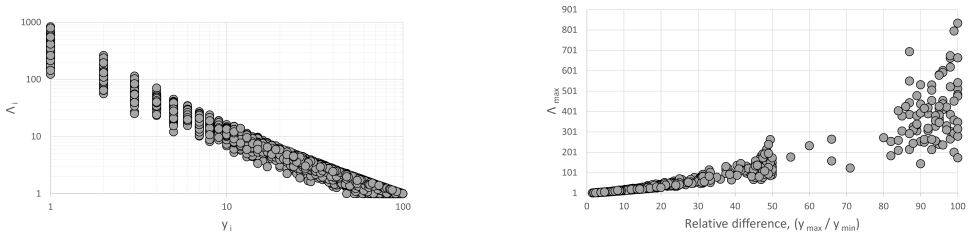

(a) All realizations **(b)** Impact versus relative difference

Figure 2.12: Statistical analysis of harmonic mean behaviour

provided to show the increased impact of removing the smallest value as the relative difference, i.e. contrast, within a realization increases. The relative difference is given by $\frac{y_{max}}{y_{min}}$ for a realization of $\mathbf{Y} = [y_1, y_2, \ldots, y_{10}]$.

Finally, it is emphasized that this Jackknife analysis is inconclusive with regards to providing robust mathematical statements for the generalized behaviour of the harmonic average. It does however provide some indication on the behaviour and demonstrates a usefull toolset that can be used to investigate a particular case and to quality control assumptions.

Summation Properties

Another relevant and somewhat non-intuitive property of the harmonic mean is that the result depends on the summation sequence. That is, the sum of the harmonic mean for each array is not the same as the harmonic mean of the summed array. Table 2.3 is provided to clarify this statement.

Table 2.3: Exemplified summation sequence effect for the harmonic mean

Array						Harmonic	Arithmetic
1	2.651	3.509	0.595	2.780	0.350	0.899	1.977
2	2.229	1.034	0.661	1.128	5.851	1.254	2.180
3	4.262	1.925	0.635	4.830	2.094	1.659	2.749
4	7.328	1.140	0.453	4.506	4.804	1.369	3.646
5	8.862	4.128	0.243	2.106	4.751	0.970	4.018
					SUM	6.151	14.571
SUM	25.332	11.736	2.586	15.350	17.849	7.904	14.571

This inequality has significant practical importance when the harmonic mean is applied to solve physical problems. It also underlines its non-intuitive behavior and that cautious usage is required to avoid mistakes.

2.4.2 Clustering

Clustering analysis denotes the process of dividing a data set into homogeneous subsets. An illustration of the concept is provided in Figure 2.13.

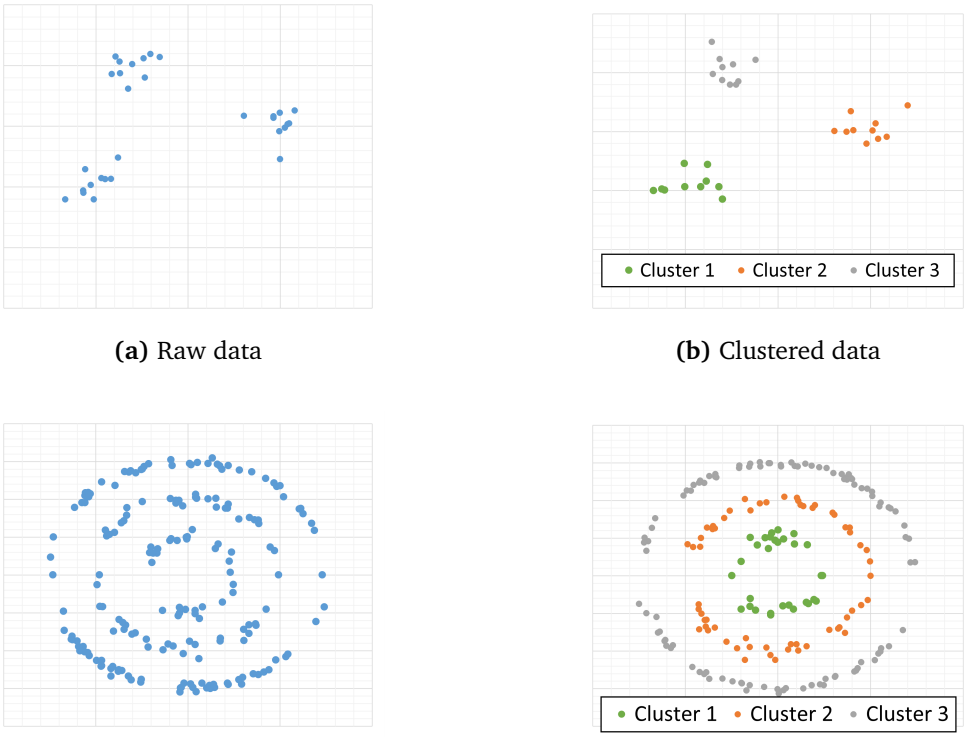

(a) Raw data

(b) Clustered data

(c) Raw data

(d) Clustered data

Figure 2.13: Concept illustration of data clustering.

Application of clustering ranges widely and many different algorithms have been developed to satisfy the broad demand. Common for these algorithms, is that they seek to create subsets in such a way that the objects within one subset are similar yet somehow quite distinct from the objects in the other subsets. Over 50 clustering algorithms are presented in [30] even though the authors underline "... focus on a small number of popular clustering algorithms ..." in the preface. Choosing an appropriate method can therefore be challenging and in many cases several algorithms can produce the same result. In addition to the result, it is important to include efficiency, availability and transparency in the feasibility evaluation when deciding which algorithm to apply. Efficiency serves as an enabler for Monte Carlo simulation and availability is of practical importance for implementation in integrated work flows. The advantage of transparency is achieved through fundamental understanding and aims to avoid hazards related to black box solutions. A density-based clustering algorithm has been found suitable to identify flow paths through JGCOWs and an explanation of the method is given

in Section 2.4.2.

Density-based Spatial Clustering of Applications with Noise

Density-based spatial clustering of application with noise (DBSCAN) was originally proposed in [31] and falls within the density-based category of clustering algorithms. Density-based clustering algorithms are, as the name suggests, characterized by defining clusters as high-density regions separated by regions with low density. Advantages include the ability of detecting arbitrarily shaped clusters, only one scan through the raw data set and few required input parameters [7]. More precisely, DBSCAN requires two input parameters, ϵ and N_{min}. ϵ describes the threshold distance to neighbouring points and N_{min} specifies the minimum number of neighbours required for a core point. These input parameters are intuitively used to detect clusters as demonstrated by the below example.

Figure 2.14a presents a 2D scattered raw data set. Human brain processing immediately clusters the raw data into two clusters and three outliers as shown in Figure 2.14b. DBSCAN attempts to replicate the human brain clustering process by utilizing core points. Core points are defined as points with minimum N_{min} number of neighbours within ϵ distance, as illustrated with $N_{min} = 4$ and $\epsilon = \sqrt{2} \approx 1.414$ in Figure 2.15a and Figure 2.15b.

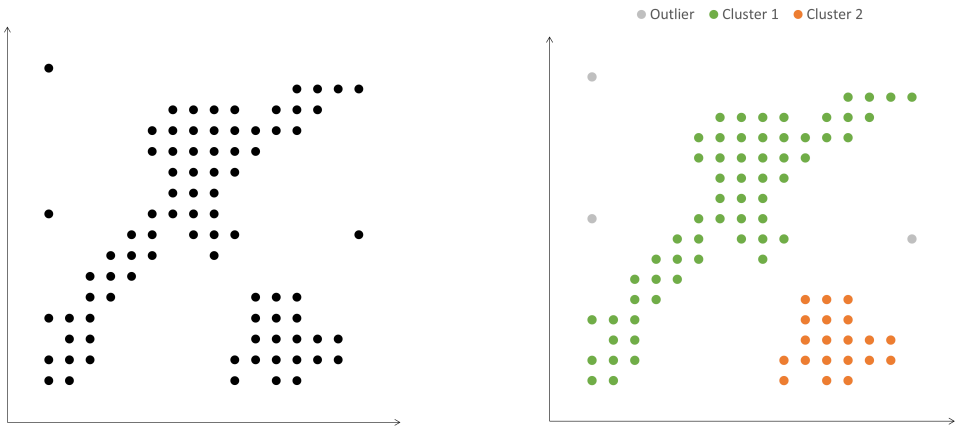

(a) Raw data **(b)** Human brain clustering

Figure 2.14: Raw data and intuitive clustering by the human brain.

Starting with a randomly selected core point and assigning it to the first cluster, all adjacent core points within ϵ distance are assigned to the first cluster. The first cluster is then extended by connecting all proximal core points. An illustration of this process is given in Figure 2.15c and Figure 2.15d. At this stage, the first cluster consists merely of core points. Non-core points adjacent to the first cluster are then

[7] [30] page 219

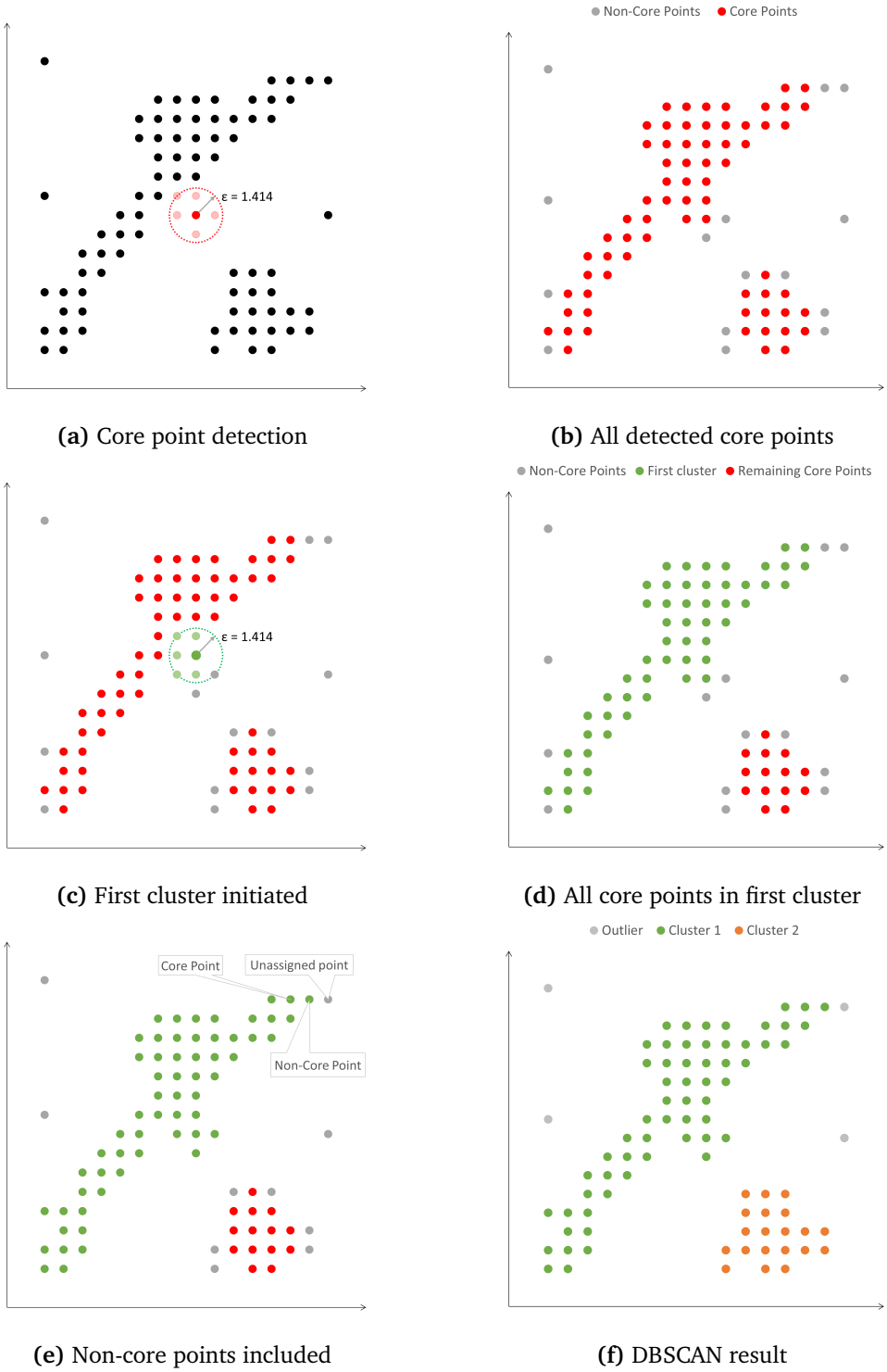

(a) Core point detection

(b) All detected core points

(c) First cluster initiated

(d) All core points in first cluster

(e) Non-core points included

(f) DBSCAN result

Figure 2.15: Visual description of the DBSCAN method with $N_{min} = 4$ and $\epsilon = \sqrt{2}$

added to the first cluster. Note that non-core points are unable to extend the cluster further and can be regarded as boundary points as underlined in Figure 2.15e.

The second cluster is then initiated by regarding an unassigned core point and the same process is repeated to define the second cluster. Remaining points are then categorized as outliers and the 2D raw dataset has been processed by the DBSCAN method to provide the result presented in Figure 2.15f. Note that the result is not identical to the initial human brain processing and some adjustment in the user defined input parameters are necessary to replicate the result exactly. More precisely, reducing the minimum amount of required neighbours required for a core point, N_{min}, from 4 to 3 would exactly replicate the result.

The resulting clusters depends on the user defined input parameters N_{min} and ϵ. A parametric analysis for the example data set given in Figure 2.14a is provided in Figure 2.16 to illustrate the quite intuitive effect of these parameters. Code listing 2.1 was used to conduct the parametric analysis and is provided to demonstrate the straightforward implementation of DBSCAN in MATLAB. Note that N_{min} in MATLAB incorporates the point in question itself as a neighbouring point. I.e., it counts the number of neighbouring points and adds one for comparison with the used defined N_{min} to determine whether a point is a core point or not. This is merely a case of definition and does not interfere with the provided logic of the method.

Code listing 2.1: Matlab implementation for parametric DBSCAN analysis.

```
array = dlmread('dbscan_demo.txt'); % Read dataset

epsilon = [1, sqrt(2), 3];
N_min = [1, 5, 9];
c = 1;
idx=zeros(size(array,1),9);

for nm = [1 2 3]
    for e = [1 2 3]
        idx(:,c) = dbscan(array,epsilon(e),N_min(nm)); % Execute clustering
        c=c+1;
    end
end

run dbscan_demo_viz.m % Visualization script to generate figure
```

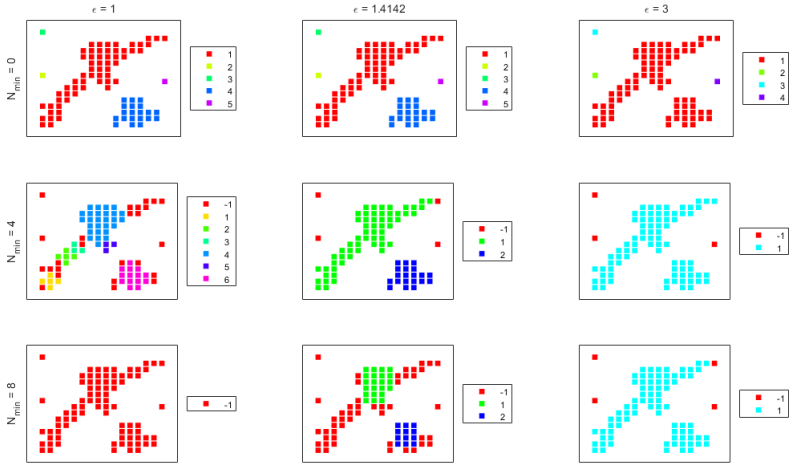

Figure 2.16: DBSCAN results on raw data in Figure 2.14a with varying N_{min} and ϵ

For application in flow path detection through JGCOWs, $N_{min} = 1$ and $\epsilon = \sqrt{2}$ has been found suitable as it clusters all untreated regions surrounded by at least one treated node as shown conceptually in Figure 2.17.

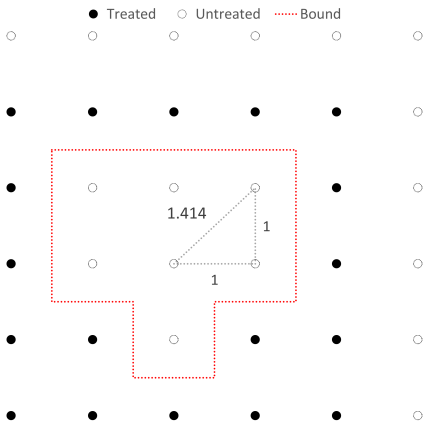

Figure 2.17: Conceptual illustration of DBSCAN configuration for application in flow path detection

Chapter 3

Flow Path Detection Algorithm

This chapter contains a description of the proposed three-dimensional flow path detection algorithm (FPDA). The purpose of the algorithm is to overcome the limiting assumptions in the current TDA [1] to achieve a more accurate representation of the leakage risk. It is developed in MATLAB and is fully incorporated with the existing in-house TDA code as described in Section 2.1. Figure 3.1 shows how the FPDA is connected to the current TDA code. Comparison of the results between the two methods is given in Chapter 4.

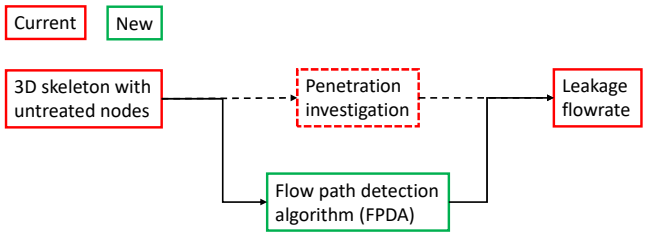

Figure 3.1: Illustration of the connection between FPDA and TDA

3.1 Description

An overall flow chart of the calculation steps in the FPDA is given in Figure 3.2. Each step is elaborated in the following subsections.

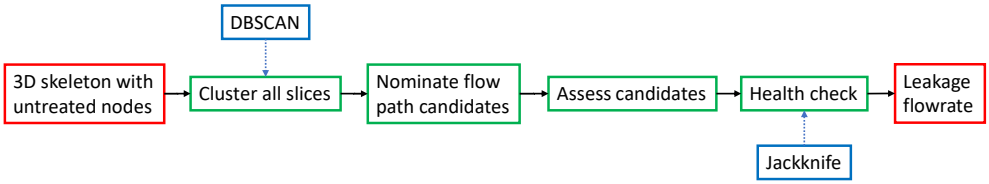

Figure 3.2: Overall flowchart of main calculation steps in FPDA

[1] Elaborated in Section 1.2.

3D skeleton

A three-dimensional digitized model of untreated soil constitutes the starting point for flow path detection. It is taken directly from the current TDA code and represents intact untreated soil volumes where fluid flow is possible. Reorganization to a convenient matrix structure is illustrated in Figure 3.3 and a pseudocode is provided in Code listing 3.1 for transparency. Note that i, j and k constitute a discretization in the x-, y- and z-directions respectively.

Code listing 3.1: Pseudocode for reorganizing geometric data for untreated nodes

```
run TDA.m  % Run existing code to generate 3D untreated skeleton

% Organize untreated nodes variable 'ijk' from nx3 to a 3D matrix

for rows = 1:size(ijk,1)
    ijk_matrix{ijk(rows,2)}(end+1) = [ijk(rows,1) ijk(rows,3)];
end
```

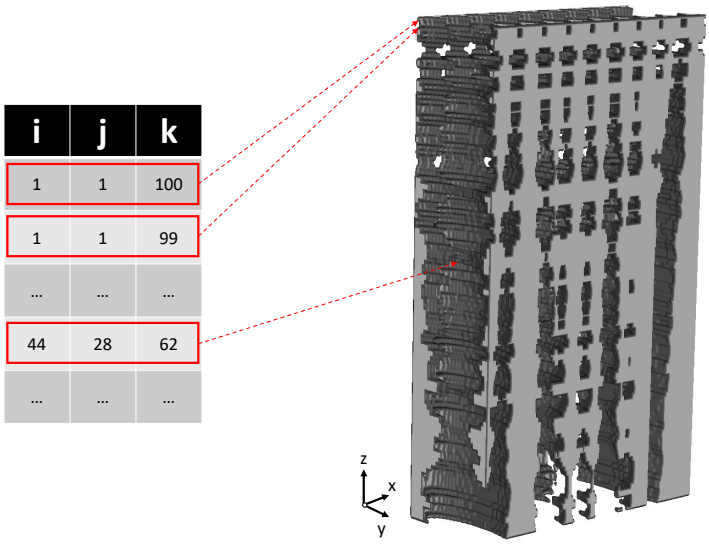

Figure 3.3: Illustration of 3D skeleton of untreated nodes

Cluster all slices

All slices undergo the DBSCAN clustering algorithm[2] with $N_{min} = 1$ and $\epsilon = \sqrt{2}$ to generate 2D clusters for all slices. Each cluster represents a collection of untreated soil nodes that are hydraulically connected and surrounded by sealing treated ground. Note that this is purely a 2D operation and that there is no connection between the defined clusters in each slice. Code listing 3.2 provides a pseudocode and Figure 3.4 illustrates the clustering operation.

Code listing 3.2: Pseudo MATLAB code for clustering per slice

```
ijk_clust = {}; % Empty cell array

for j=1:n
    idx = dbscan(ijk_matrix(j),sqrt(2),1);
    ijk_clust{j} = [ ijk_matrix(j) idx ];
end
```

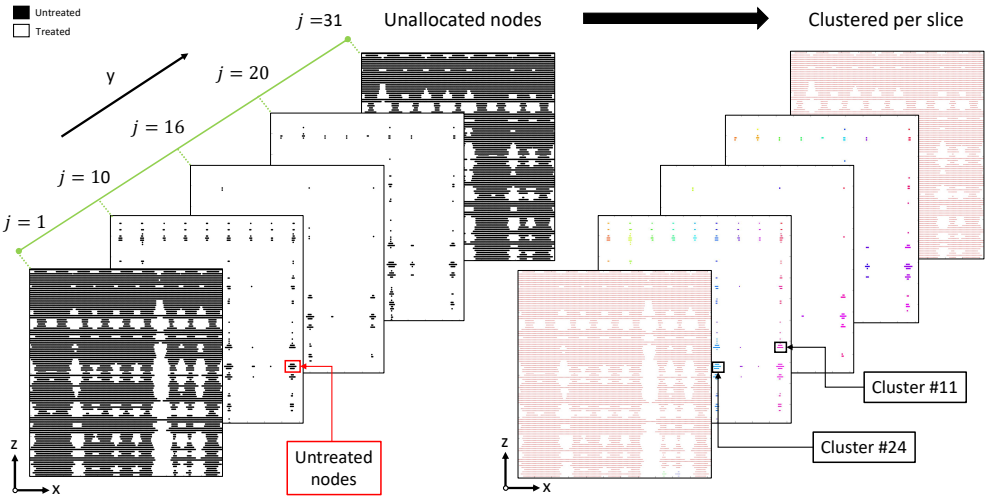

Figure 3.4: Illustration of clustering operation per slice. Left: raw untreated nodes, right: each cluster represents a collection of untreated soil nodes that are hydraulically connected and surrounded by sealing treated ground.

Nominate flow path candidates

Nomination of *potential* flow paths takes place in the slice with the least amount of untreated area. This particular slice has the following characteristics:

- All penetrating flow paths are present.
- Not all clusters constitute penetrating flow paths as they might be sealed off in 'deeper' or 'shallower' slices.

[2]Elaborated in Section 2.4.2

The clusters are enumerated to define the flow path candidates and a boolean array is established for further assessment as explained in the pseudocode in Code listing 3.3. Figure 3.5 provides an example of nomination for flow path candidates for a given slice.

Code listing 3.3: Pseudo MATLAB enumerating flow path candidates

```
[min_val, j_min] = min(cellfun('size', ijk_matrix,1)); % j-slice with minimum area

clust_num = sum(~cellfun(@isempty,ijk_clust)); % Count clusters for each slice

FP_n = clust_num(j_min); % Number of potential flow paths
FP_bool = ones(1,FP_n); % Kept true for penetrating flow paths
```

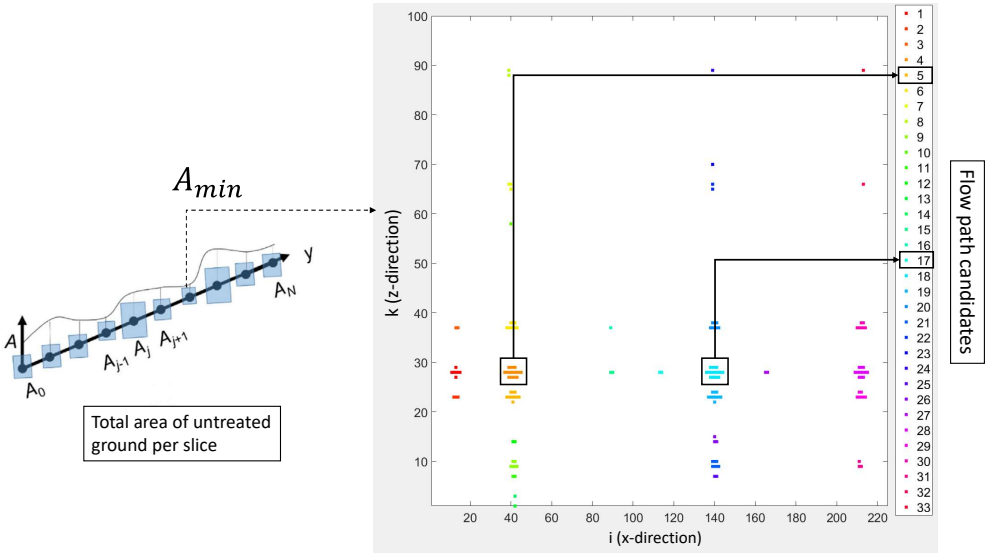

Figure 3.5: Example of identification of flow path candidates.

Assess candidates

The idea is to use the 2D clusters per slice as building bricks to generate 3D flow paths by connecting clusters that are overlaying in the y-direction. Nominated flow path candidates are assessed with two consecutive for-loops as shown in Code listing 3.4. Starting at the slice with the least amount of untreated area, the algorithm searches for overlap in both directions sequentially - towards downstream and upstream the JGCOWs. For each slice, the following evaluation is done:

1. Abandon false flow paths, i.e. break loop if overlap is absent. Exemplified in Figure 3.6.
2. Expand flow path if overlap is detected. As shown in Figure 3.7.

Some of the flow paths will likely share 2D clusters in the same slice. To satisfy material balance, the untreated area within a cluster is evenly distributed to the number of flow paths that share that particular cluster.

Code listing 3.4: Pseudo MATLAB code for flow path candidate assessment

```
for i_FP = 1:FP_n % For-loop through flow path candidates
    for j = j_min-1:-1:1
        % Connect overlapping clusters with @ismember function
        % If no overlap --> FP_bool(i_FP) = 0 --> break.
    end
    for j = j_min+1:1:ylayer(end)
        % Connect overlapping clusters with @ismember function
        % If no overlap --> FP_bool(i_FP) = 0 --> break.
    end
end
```

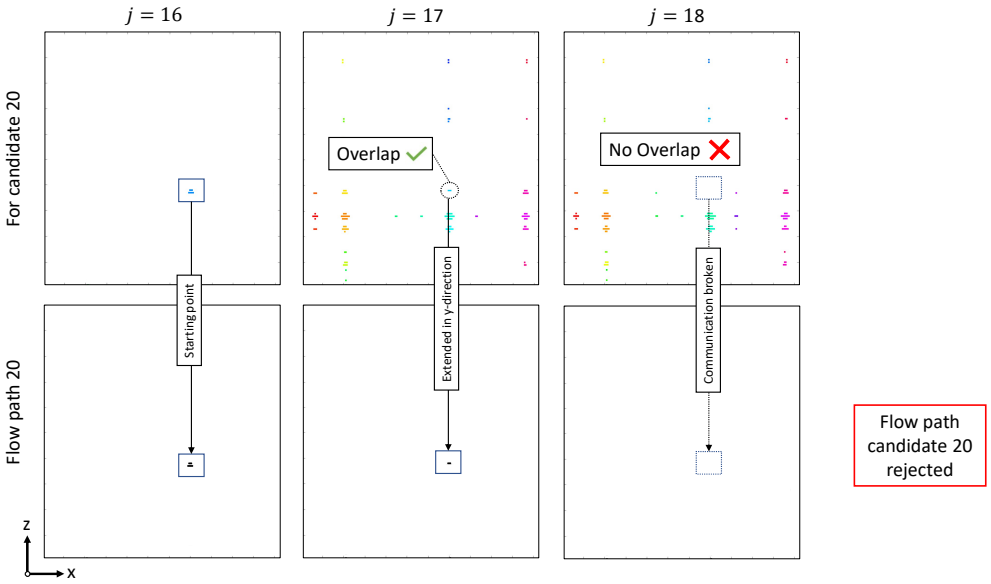

Figure 3.6: Example of rejected flow path candidate

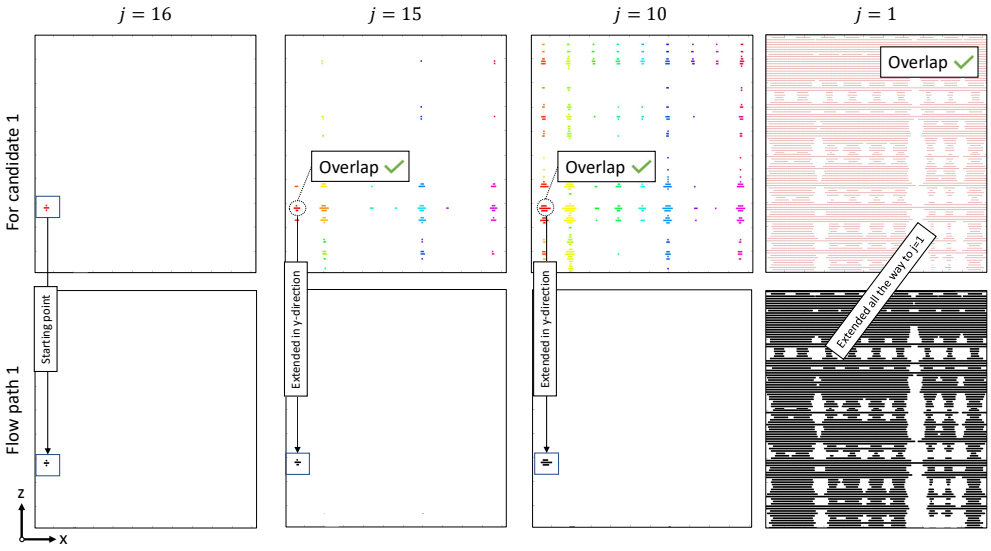

(a) Expansion logic

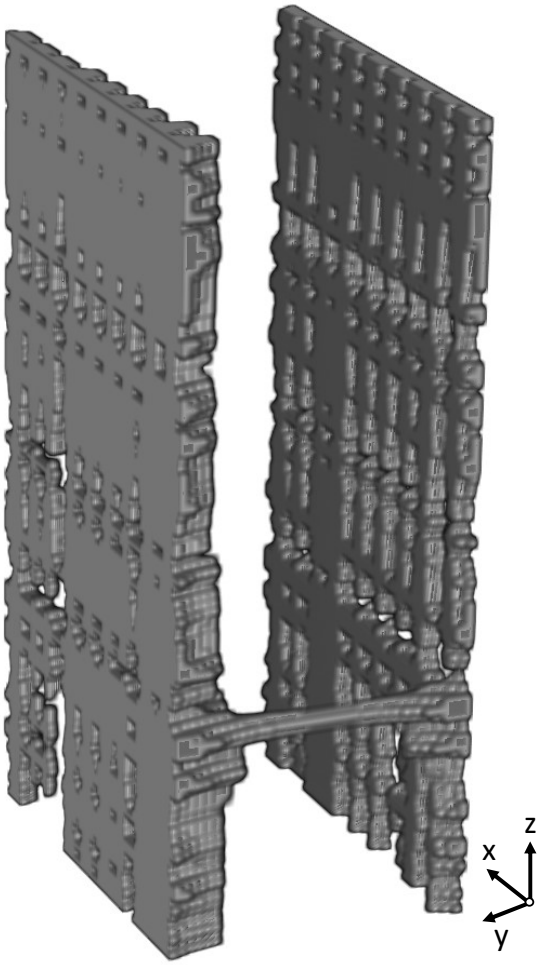

(b) 3D visualization

Figure 3.7: Example of approved flow path candidate

Flow rate calculation

Flow rate calculation follows the same logic as the current TDA method and as described in Section 2.3. Untreated nodes are converted to untreated cross sectional area by multiplying with the unit area. The unit area is given by the mesh size, i.e. how refined the discretization of the continuous soil volume is. Note that the change in flow path identification approach will lead to changes in the results. A comparison of the results is provided in Chapter 4.

Health check

A health check is included to obey best practice for new solutions. It checks whether the calculations makes sense or not and constitutes a slice of cheese in the Swiss Cheese Model[3] to increase the likelihood of preventing severe mistakes in the results. In particular, attributes of the non-intuitive harmonic mean are investigated with Jackknife analysis[4] to verify logical behaviour. Note that the health check does not exclude all possible errors, but it serves to increase the confidence in the result. A realization health check visualization is provided in Figure 3.8.

[3] Assumed to be well-known. Information easily available online.

[4] Elaborated in Section 2.4.1

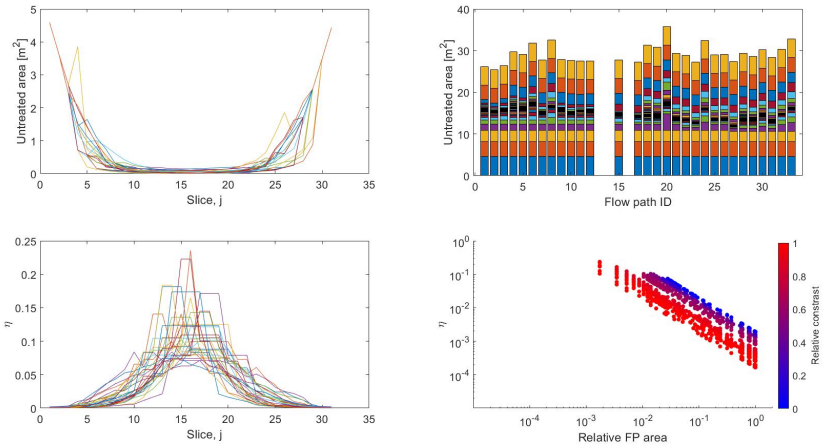

(a) Harmonic average behaviour

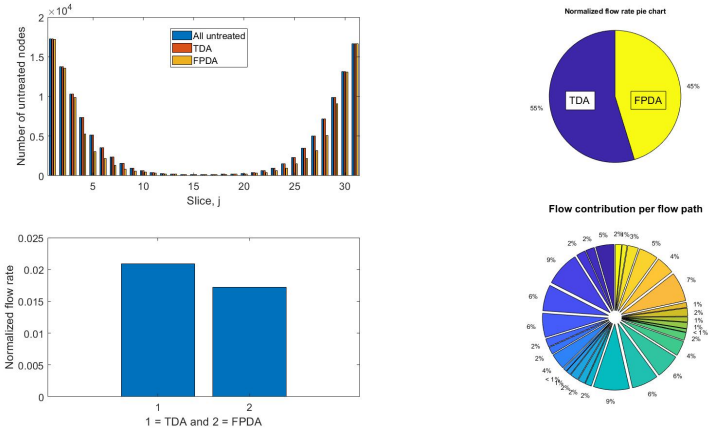

(b) TDA vs FPDA comparison

Figure 3.8: Example visualization of health checks for a realization

Examples

This chapter is rounded off by demonstrating that the objective of the FPDA method is met. The objective of the FPDA is to capture vertical scatter of untreated nodes in the flow calculation and to enable transverse flow paths. Below Figure 3.9 and Figure 3.10 illustrates that the FPDA indeed is able to capture these features.

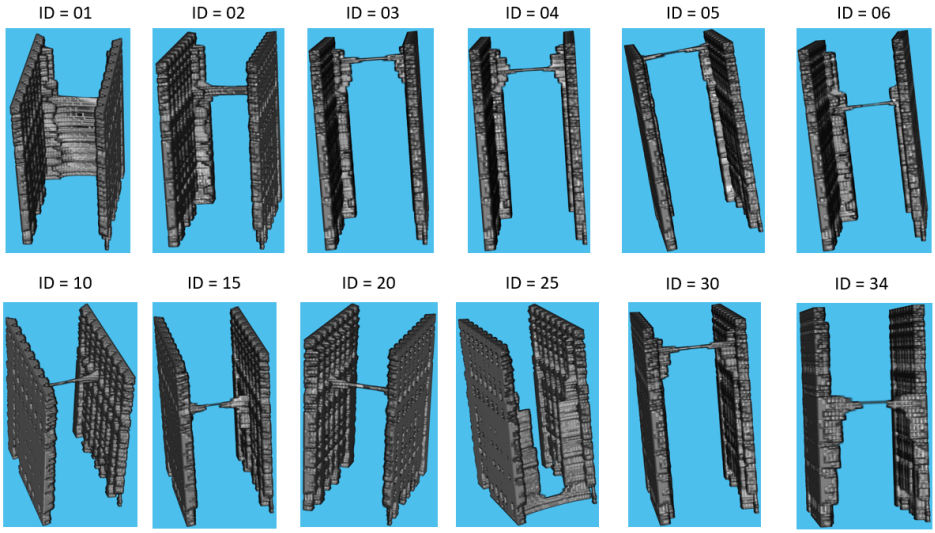

Figure 3.9: Example of identified flow paths for a given FPDA realization

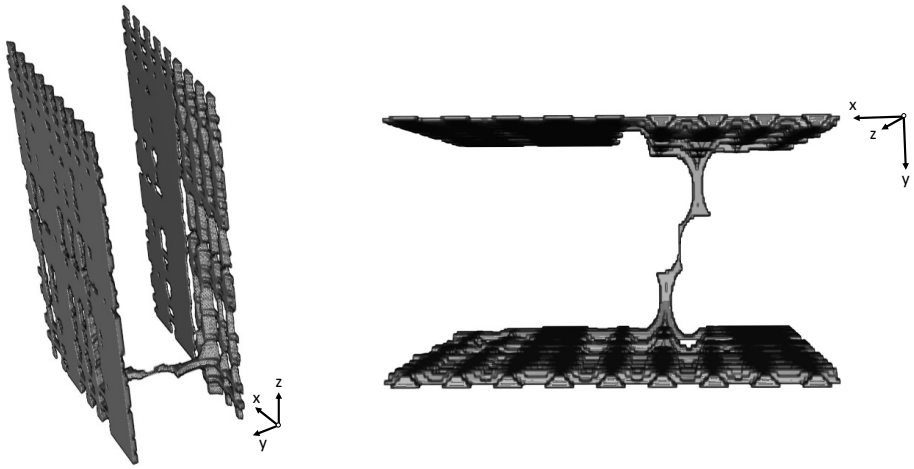

Figure 3.10: Example of transverse flow path for a given FPDA realization

Chapter 4

Results and Discussion

This chapter provides a comparison of the calculated normalized flow rate, Ω[1], for the current TDA versus the proposed FPDA method. Monte Carlo simulations are utilized to obtain a satisfactory degree of statistical robustness. Each realization uses the same random geometric realization to evaluate and compare the flow rate suggested by the two methods as shown in Figure 4.1.

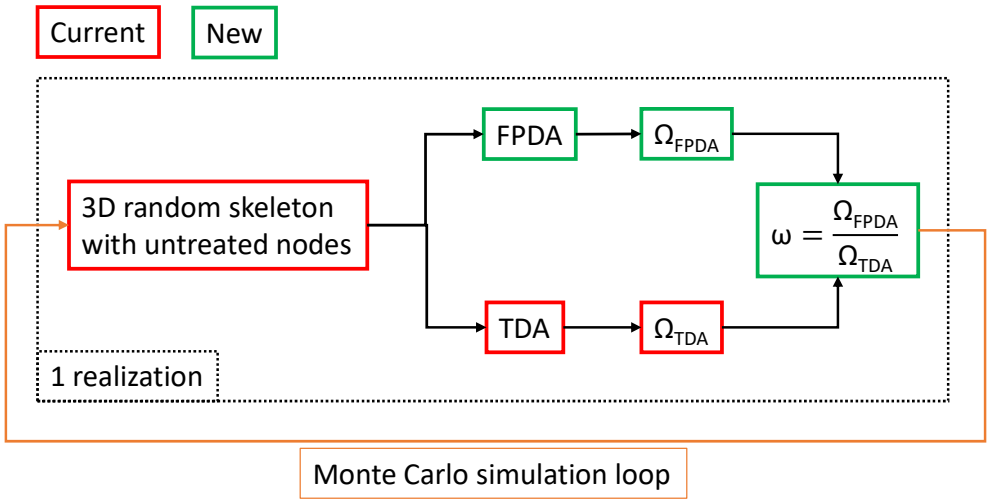

Figure 4.1: Illustration of the Monte Carlo simulation set-up. Ω_{TDA} and Ω_{FPDA} denotes the normalized flow rate for the TDA and FPDA methods respectively.

The comparison is performed both absolute and relative to view the Monte Carlo simulation results from different perspectives. Absolute comparison is a direct comparison of Ω_{TDA} versus Ω_{FPDA} as exemplified in Figure 4.2 by the reference case. 95-percentile values from both methods are determined in addition to the linear regression slope and coefficient of determination, i.e. R^2, to indicate match goodness.

[1]As described by Equation (2.2)

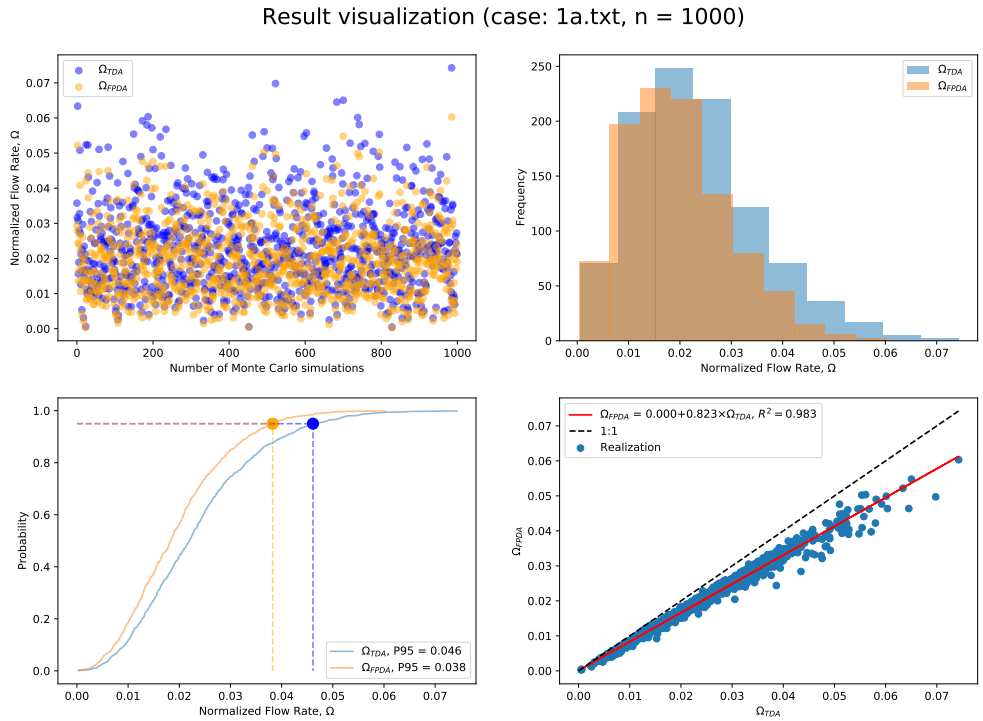

Figure 4.2: Absolute comparison of Ω_{TDA} versus Ω_{FPDA}.

Table 4.1: Categorization of a particular realization

Ω_{FPDA}	Ω_{TDA}	Category	Remark
$=0$	$=0$	A	Wall not penetrated. Excluded in statistical analysis.
$=0$	>0	B	$\omega=0$. Included in statistical analysis.
>0	$=0$	C	Division error. Excluded in statistical analysis
>0	>0	D	$\omega\neq 0$. Included in statistical analysis.

The relative comparison is expressed by

$$\omega = \frac{\Omega_{FPDA}}{\Omega_{TDA}} = \begin{cases} < 1 & \rightarrow \textit{Less conservative design possible} \\ > 1 & \rightarrow \textit{Safety measures required} \end{cases} \tag{4.1}$$

and describes the ratio between the two methods for each realization. ω is prone to acquiring non-physical values if $\Omega_{TDA} = 0$, hence a categorization is used to filter the simulation results as described in Table 4.1. Furthermore, percentile values are extracted from the empirical cumulative distribution function (CDF) as shown in Figure 4.3 to obtain a 90 % confidence interval for ω. Convergency is investigated by tracking the Monte Carlo COV for each simulation.

Former convergency studies [15] are utilized to set the mesh size in x- and y-directions to 0.04 m and 0.2 m in z-direction. Rationale for allowing a coarser discretization in the z-direction is that the wall construction dimension in the z-

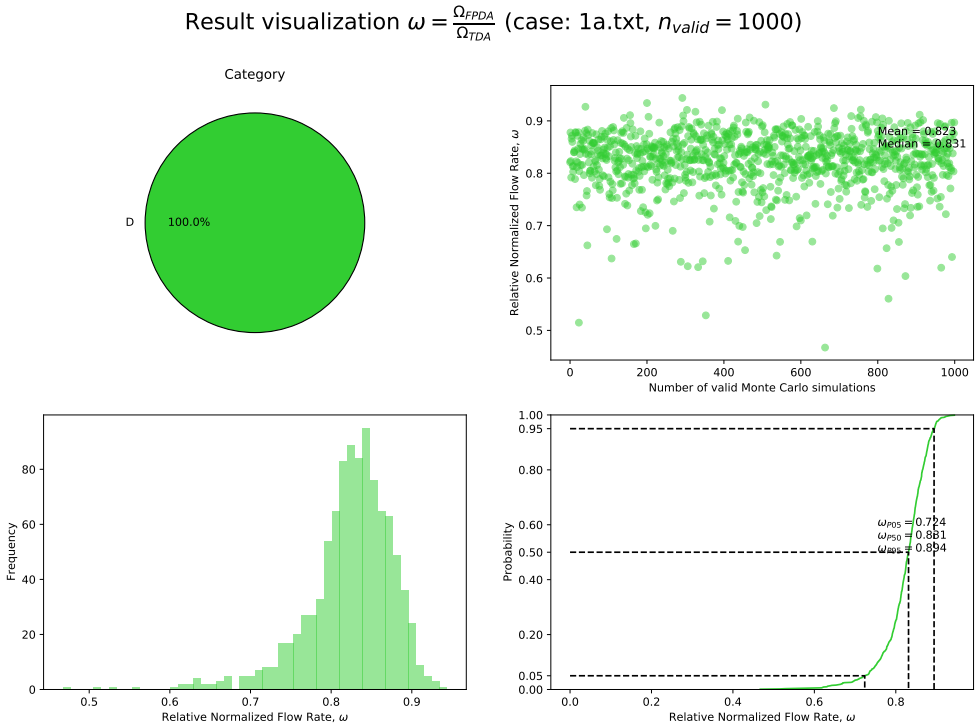

Figure 4.3: Relative comparison of Ω_{TDA} versus Ω_{FPDA}.

direction is much larger than in the other directions. Note that the discretization in the z-direction is adjusted for the cases with varying depth in the parametric study.

4.1 Code Efficiency

Efficient modelling equips the TDA approach with a decisive advantage in competition with its FEM counterpart. Generally, the computational cost of the TDA method is 10^{-3} to 10^{-4} lower than FEM [16]. It is therefore important to underline that the proposed FPDA update does not arrest this advantage, and that code efficiency indeed still constitutes a competitive advantage versus alternative methods. The calculation set-up for each realization as given in Figure 4.1 can be reorganized to systematically track the run time for each task as defined in Figure 4.4a to unravel the impact of the FPDA approach on code efficiency. Figure 4.4b shows the normalized duration for each calculation step. Note that the duration for each step is based on average values for all simulation cases.

Figure 4.4 illustrates that the efficiency advantage is preserved even though some increase in computational time is evident. Computational expenses related

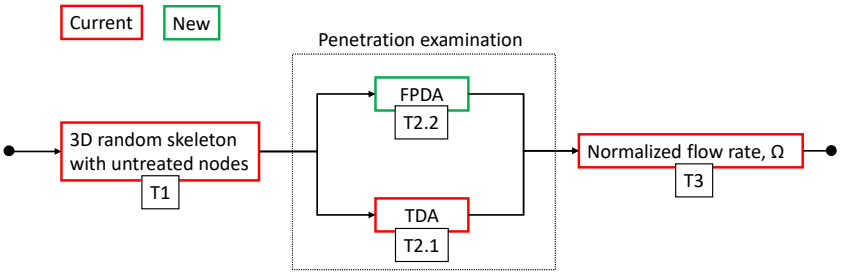

(a) Flow chart with definition of calculation steps

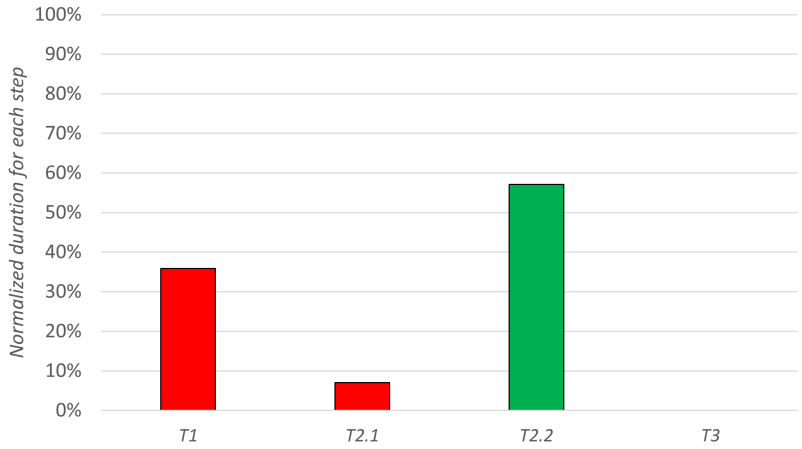

(b) Normalized duration for calculation steps, i.e. the duration of each step divided by the total duration. Based on average values from all simulation cases.

Figure 4.4: Run time analysis

to clustering[2] and flow path assessment[3] explains the increase in computational time, but it is underlined that this increase is neglecatble compared to the FEM counterpart. Also, it is emphasized that, even though some code efficiency measures were taken[4], the focus of this work has been to develop something that works, i.e. produces reliable results *sufficiently* fast rather than eliminating all waste computation in the code. Hence, further code efficiency measures are likely to yield improvements, but the current efficiency is indeed acceptable.

All simulations within this work are run locally on a Lenovo ThinkPad T490 laptop with a i5 Intel Core 8^{th} generation processor. A screenshot of the Windows Task Manager while running the FPDA code is provided in Figure 4.5 for transparency. It reveals 4 cores and a total of 8 logical processors, essentially enabling parallelization of computational tasks into 8 simultaneous processes.

[2]Execution of *DBSCAN* as described on page 27

[3]Execution of the *ismember* function as described on page 28

[4]The first prototype of the FPDA code consumed roughly ×100 more time to complete than the current version. Efficiency measures included application of MATLAB profiler and code restructuring to produce the same result with the same logic roughly ×100 times faster.

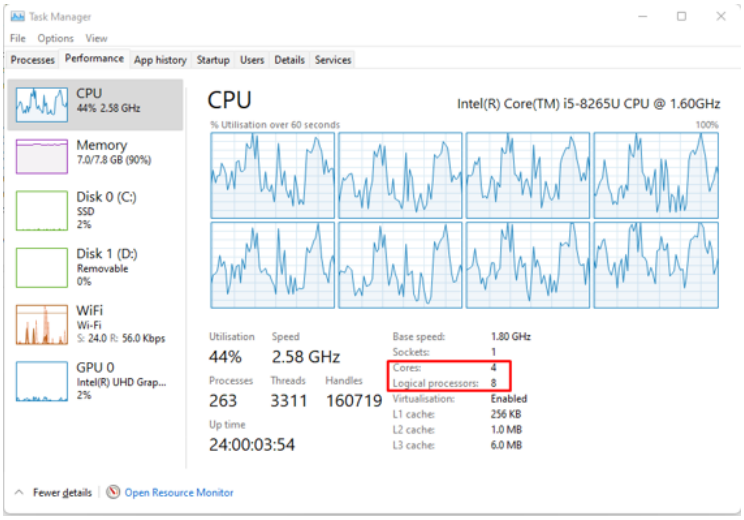

Figure 4.5: Snapshot of Task Manager while running FPDA code

Figure 4.6 provides a run time summary for all 15 simulation cases[5] with $n_{MC} = 100$ and $n_{MC} = 1\,000$ realizations. Note that the comparison origins from separate Monte Carlo executions and that all simulation cases are subject to a total of 1 100 realizations. It demonstrates consistent run time for all cases and the $\times 10$ increase in number of realizations is linearly reflected by a rough $\times 10$ increase in run time suggesting a healthy calculation set-up. Note that the absolute value of run time is dependent on hardware, but the relative difference between the cases is expected to be representative for the run time behaviour of the code.

[5] Ref. Table 4.3

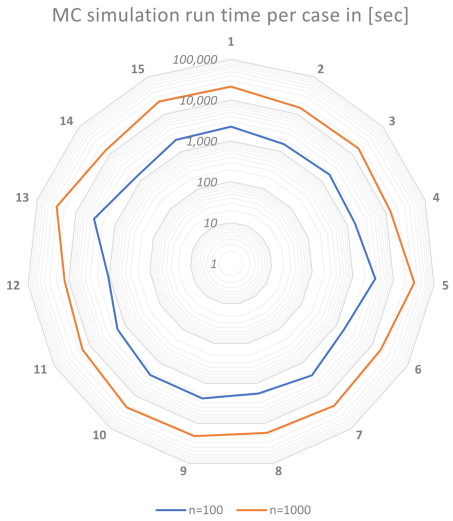

Figure 4.6: Summary of run time for all simulation cases

4.2 Comparison

A concentrated summary of the results is presented in Table 4.3. Appendix E provides visualized summaries of all simulation cases with more details. Robustness is obtained by conducting a parametric study with basis in a reference case. That is, a reference case has been defined based on the statistical characteristics given in Table 2.2 and on typical cutoff wall configuration parameters. Adjustable input parameters are then discretely altered in separate Monte Carlo simulations to investigate variations in the result and to avoid basing the conclusion on a single case. Note the total number of cases - 15 - is somewhat limited by the scope of this work and on reasonable hardware usage. The reference case and the parametric study is given in Table 4.2 and Table 4.3.

Statistical representative results has been obtained by applying $n_{MC} = 1\,000$ realizations to each simulation case as recommended by earlier similar studies [3, 6, 14–16]. Convergency has been quality checked by extracting reasonable histograms, tracking the Monte Carlo coefficient of variation[6] and comparing the results to separate simulation cases with $n_{MC} = 100$ realizations only to observe small changes for all cases. Elaborating details are provided visually in Table E.2 as part of Appendix E.

A graphical representation of Table 4.3 is given in Figure 4.7 for a more intuitive presentation.

[6] As described in Appendix C.

Table 4.2: Configuration for reference case

Case	#1 (Reference case)
d_i [m]	1.2
Columns per row	10
Set-up	Triangular
n_{row}	1
COV(d_i)	0.1
$\sigma(\beta)$ [°]	0.3
Depth, L [m]	20
SOF [m]	0.5
s_x [m]	1
s_y [m]	0.7

Table 4.3: Comparison results of parametric study. **Green** indicates increase and **red** decrease compared to reference case. * Slope refers to the linear regression model in Figure 4.2, ** Category C refers to the categorization given in Table 4.1, *** mesh size in z-direction adjusted to keep same discretization as reference case and **** $n_{row} = 2$ for simulation cases with varying s_y.

			Absolute comparison			Relative comparison			
Case	Vary	To	$\frac{\Omega_{FPDA}^{P95}}{\Omega_{TDA}^{P95}}$	Slope*	R^2	ω_{P05}	ω_{P50}	ω_{P95}	CatC**
# 1			**0.83**	**0.82**	**0.98**	**0.72**	**0.83**	**0.89**	**0**
# 2	n_{row}	**2**	0.72	0.71	0.82	0.00	0.50	1.01	0
# 3		**3**	0.73	0.64	0.68	0.00	0.47	1.91	4 %
# 4	COV(d_i)	**0.05**	0.71	0.69	0.96	0.51	0.78	0.88	0
# 5		**0.20**	0.88	0.88	0.99	0.84	0.89	0.92	0
# 6	$\sigma(\beta)$	**0.1**	0.84	0.85	0.99	0.65	0.80	0.88	0
# 7		**0.5**	0.70	0.66	0.93	0.63	0.80	0.89	0
# 8	Depth***	**15**	0.84	0.87	0.99	0.74	0.84	0.90	0
# 9		**25**	0.74	0.74	0.96	0.69	0.82	0.88	0
# 10	SOF	**0.25**	0.81	0.80	0.98	0.69	0.81	0.86	0
# 11		**1.00**	0.86	0.85	0.98	0.75	0.86	0.92	0
# 12	s_x	**0.9**	0.85	0.84	0.99	0.57	0.82	0.91	0
# 13		**1.1**	0.81	0.77	0.95	0.75	0.84	0.89	0
# 14	s_y****	**0.5**	0.70	0.65	0.81	0.00	0.34	0.90	0.4 %
# 15		**0.9**	1.09	1.02	0.78	0.54	0.93	1.58	0.2 %

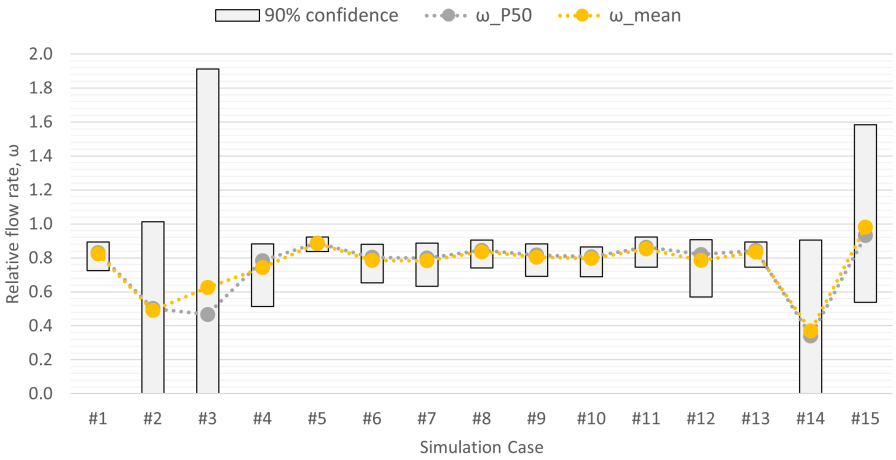

(a) Relative comparison

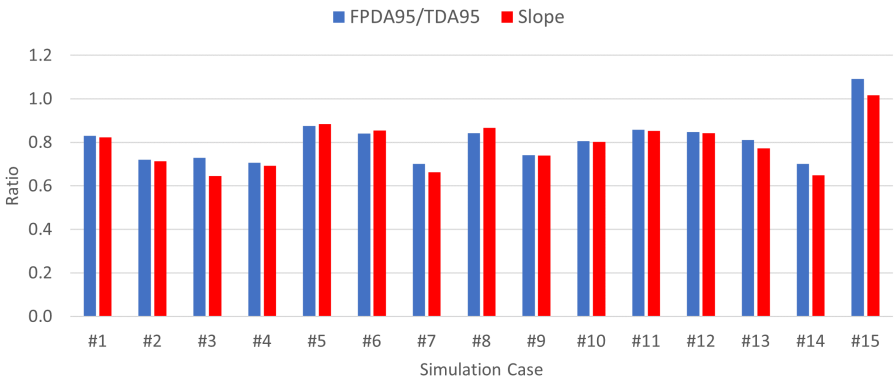

(b) Absolute comparison. FPDA95/TDA95 equivalates to $\frac{\Omega_{FPDA}^{P95}}{\Omega_{TDA}^{P95}}$.

Figure 4.7: Visual representation of the results given in Table 4.3

.

A clear distinction is noticed in the results between simulation cases with one and simulation cases with more than one row of jet-grouted columns. Respective observations are summarized by the below bullet points:

- $n_{row} = 1$ *(Simulation cases 1 and 4-13)*

  Even though some variation in the results are present, there is an overall strong indication of reduced flow rate with the FPDA approach. The **amount of reduction** varies somewhat for the different simulation cases, but the size **is roughly 15 %**. Note that 15 % constitutes a conservative estimate based on the simulation results. Rationale for a conservative approach is: (1) limited volume of simulation cases and (2) that the results are case specific, e.g. changing COV(d_i) seem to have a larger impact than altering the SOF, hence it is reasonable to keep the take-away value on the conservative side of the tested cases.

- $n_{row} > 1$ *(Simulation cases 2,3,14 and 15)*

  Shows a wide span in the confidence interval for relative flow rate, ω, as well as signs of higher volatility in terms of a bigger scatter in the result parameters. Both minimum (simulation case 14) and maximum (simulation case 15) values for the entire study can be found within the simulation cases with more than one row of jet-grouted columns. Note that the absolute comparison for simulation case 15 suggests that the TDA method is underestimating seepage flow rate.

These observations are discussed in the next section.

4.3 Discussion

The results reveal a distinct behavior for simulation cases with only one and for cases with more than one row of jet-grouted columns, n_{row}. This discussion section has therefore been sectionized accordingly.

4.3.1 JGCOWs With More Than One Row of Jet-Grouted Columns

In particular, Figure 4.7a reveals a large span in the confidence interval for simulation cases 2, 3, 14 and 15 - all cases with more than one row. This observations can be attributed to:

- On a general basis, the flow rate through JGCOWs with $n_{row} > 1$ is expected to be low due to the overlapping fashion of the triangular design. This is indeed verified in the results as the normalized flow rate, Ω, for both FPDA and TDA is in the 10^{-3} order of magnitude as opposed to 10^{-2} for all cases

with one row [7]. Small numbers are prone to increased sensitivity as a small change constitutes a larger fraction of the original number.

- Estimated normalized flow rate, Ω, is directly linked to the harmonic average of the untreated area per slice [8] going through the wall. Furthermore, Jackknife analysis [9] reveal that the bottleneck values in a dataset dominates its harmonic average in a non-linear fashion. Hence, even small changes to already small numbers is expected to yield increased volatility in the results.
- Increased number of rows naturally yield a requirement for a longer sequence of connected untreated nodes to generate a flow path. Furthermore, the penetrating passages are more intricate, i.e. tortuous, as they can not 'just find a way' through the volume in-between two columns due to the overlapping design as opposed to realizations with $n_{row} = 1$. The increased degree of complexity in the flow path geometry makes the fundamental difference between the FPDA and TDA methods more apparent in the results, both in terms of high relative volatility and low coefficient of determination, R^2.
- More tortuous flow paths increases the likelihood of transverse flow. Transverse flow is rejected by the TDA method[10], but incorporated in the FPDA method. Note that this subtle difference equips the FPDA approach with an opportunity to capture cases where physical flow will take place in a realization yet to be wrongfully rejected by the TDA method. This phenomena becomes apparent when comparing simulation cases 14 and 15 - two cases with n_{row}= 2 differentiated by the cross-row spacing, s_y. When compared to the TDA method, transverse flow is captured for both cases, but the amount of transverse flow that is rejected by the TDA is larger for simulation case 15 due to the increased cross-row spacing - essentially increasing the amount of untreated nodes present in the transverse flow paths. This features gives the FPDA method an important advantage over the TDA approach.

4.3.2 JGCOWs With One Row of Jet-Grouted Columns

For simulation cases with only one row, the flow paths are intuitively less tortuous as they 'just have to find a way' in-between two columns to penetrate the entire wall. The intuition is confirmed by consistent results, with low scatter and narrow 90 % confidence interval, across all simulation cases with $n_{row} = 1$. A clear indication of reduced flow rate with the FPDA approach is observed in terms of result parameters $\frac{\Omega^{P95}_{FPDA}}{\Omega^{P95}_{TDA}}$, slope, ω_{P50} and even ω_{P95} being less than 1 as summarized in Table 4.3. The observed reduction can be decoded by investigating the fundamental difference between the TDA and FPDA methods. Figure 4.8 illustrates the essential distinction between the methods.

[7] See Appendix E.
[8] As described in Section 2.3.
[9] As described in Section 2.4.1
[10] See Figure 2.3

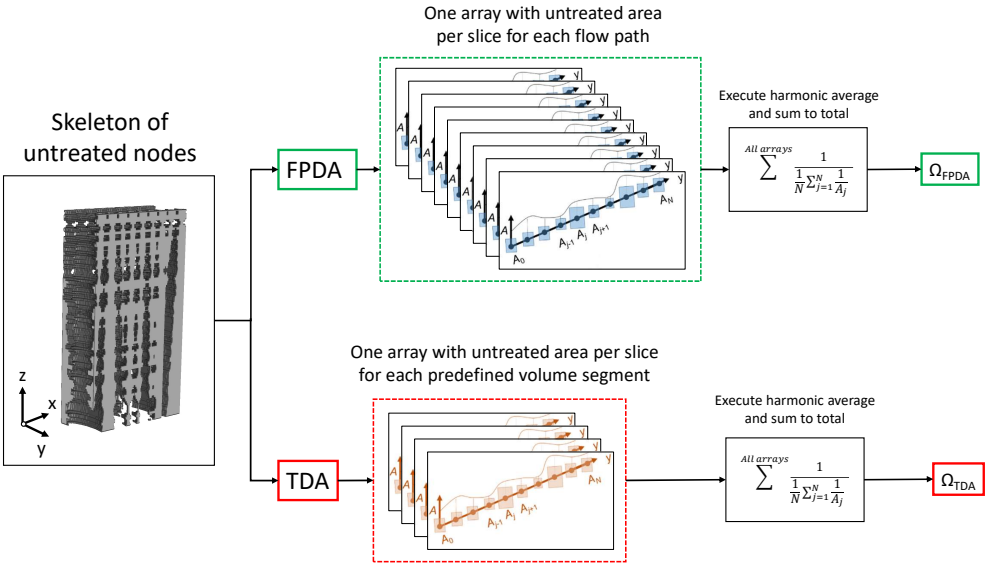

Figure 4.8: Illustration of the fundamental difference between the TDA and the FPDA method

In layman's terms, the only difference between the two methods in how the skeleton of untreated nodes is converted to arrays of untreated area. The TDA method 'searches' within predefined volume segments[11], whereas the FPDA method connects adjacent clusters of untreated nodes. Resulting differences between the sets of untreated area arrays and its implications are elaborated by the below bullet points.

- **Inactive nodes** (*minor effect* ↓)
  Inactive nodes are defined as untreated nodes that are included in the TDA flow rate evaluation even though they are not subject to physical differential hydraulic potential. That is, the hydraulic gradient is zero[12], hence the flow rate contribution should also be zero, but the inactive nodes are included as untreated area in the harmonic average operation to estimate flow rate. Figure 4.9 is taken from a realization to clarify the definition of inactive nodes.
  With reference to Figure 4.9, inactive nodes are exemplified by the annotated untreated nodes in slice $j = 10$ that are included in the TDA flow rate estimation even though the potential flow channel is sealed off in slice $j = 15$.
  Further realization investigation, as presented in Figure 4.10 , show a typical distribution of untreated nodes for all slices through a JGCOWs with one row. Note that the untreated nodes in Figure 4.10 are those who survive the conversion to arrays of untreated area, hence are included in the harmonic

[11] Described in Section 2.1 and illustrated in Figure 2.3
[12] $i = \frac{\Delta h}{\Delta l} = \frac{0}{\Delta l} = 0$

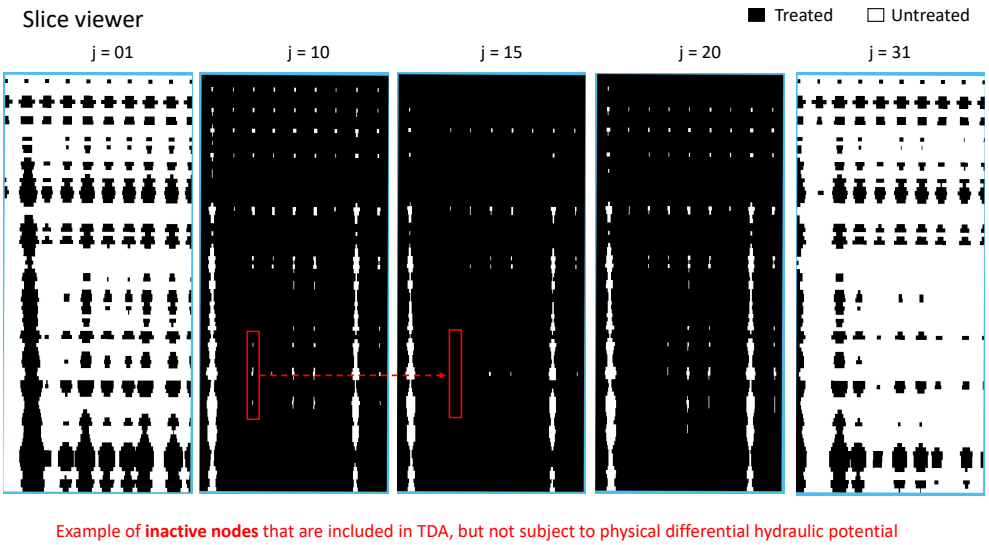

Figure 4.9: Exemplification of inactive nodes.

average operation to yield flow rate estimates

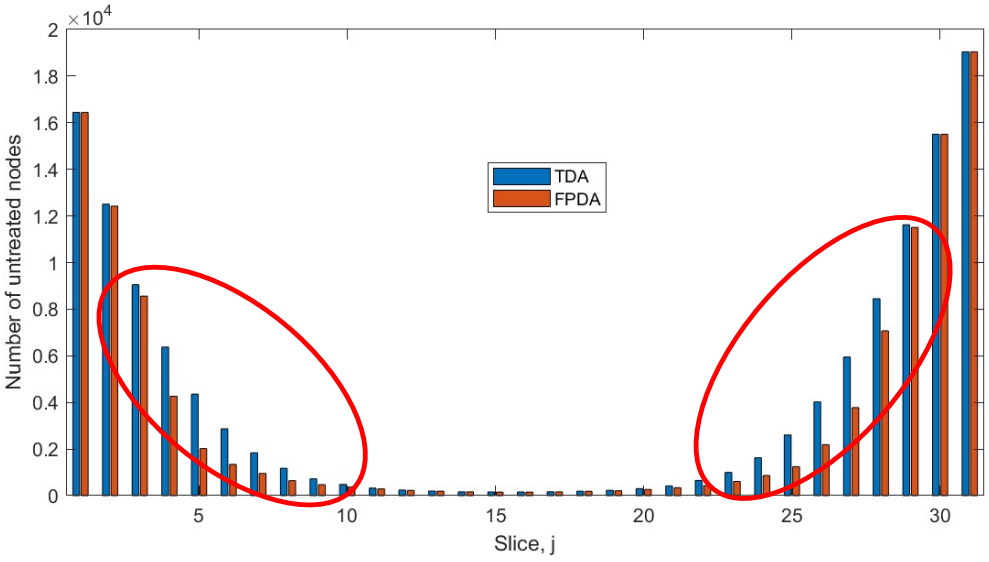

Figure 4.10: Typical distribution of untreated nodes for a realization. Red ellipses annotate 'intermediate' slices.

It becomes clear that the FPDA method omits inactive nodes to reduce the total amount of untreated nodes and furthermore also reduce the estimated flow rate. Note that the difference is most apparent for the 'intermediate' annotated slices in Figure 4.10, whereas the total number of untreated nodes is more similar towards the edges, i.e. downstream and upstream, and for the middle slices. This observation is logical as the occurrence of inactive

nodes in the bottleneck middle slices are unlikely as there is a high chance of continuous hydraulic communication through the wall once there are untreated nodes present in the middle of the wall. Furthermore, since the bottleneck values dominate the harmonic average[13], the effect of omitting inactive nodes is expected to have a minor, but always decreasing, effect.

- **Subdivision of untreated nodes** (*major effect* ↓↓)

  The TDA method is limited by a predefined number[14] of volume segments, whereas the FPDA approach *theoretically* allows an infinite number of flow paths. In practice, this leads to allocation of the untreated nodes to a higher number of arrays for the FPDA approach in the method differentiator 'conversion' process as illustrated in Figure 4.8. That is, the untreated nodes are generally divided on a higher number of flow paths in the FPDA method than there are predefined volume segments in the TDA method. The implication is a consistent lower rate estimation for the FPDA method because of the summation sequence property of the harmonic average operation[15]. Additionally, the vertical scatter in the skeleton of untreated nodes is neglected by the TDA method, but captured by the FPDA method. Even though this is a subtle difference, the subdivision of untreated nodes explains the **major** reason for **why** the estimated normalized flow rate, Ω, is **lower** for the FPDA approach in simulation cases with $n_{row} = 1$.

- **Transverse flow** (*no effect*)

  Intuitively, transverse flow for JGCOWs with one row is unlikely. Aided by the realization categorization defined in Table 4.1, category C, i.e. $\Omega_{FPDA} > 0$ and $\Omega_{TDA} = 0$, can be used as an indication for probability of occurrence of transverse flow. None of the realizations from the simulation cases with one row [16] falls into category C, strongly indicating that transverse flow indeed does not occur for such cases. It is therefore regarded that the transverse flow phenomena is irrelevant for cases with $n_{row} = 1$.

Figure 4.11 is provided as a summary to visualize the reason for why the FPDA method predicts lower flow rate than the TDA method for simulation cases with $n_{row} = 1$.

[13] As demonstrated in Section 2.4.1

[14] $(n_{column} - 1)$, where n_{column} is the number of jet-grouted columns in one row

[15] Section 2.4.1

[16] Summing to a total of 11 000 + 1 100 = 12 100 realizations

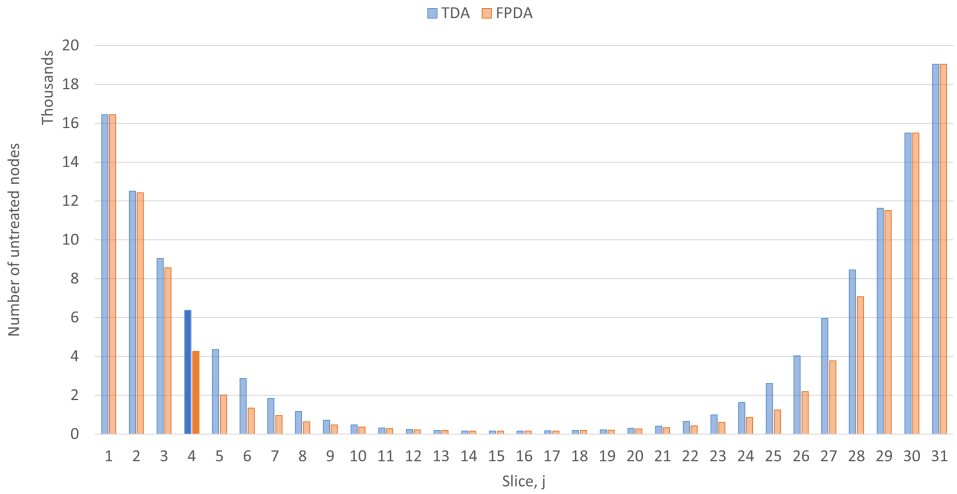

(a) Example distribution of untreated nodes per slices through a cutoff wall

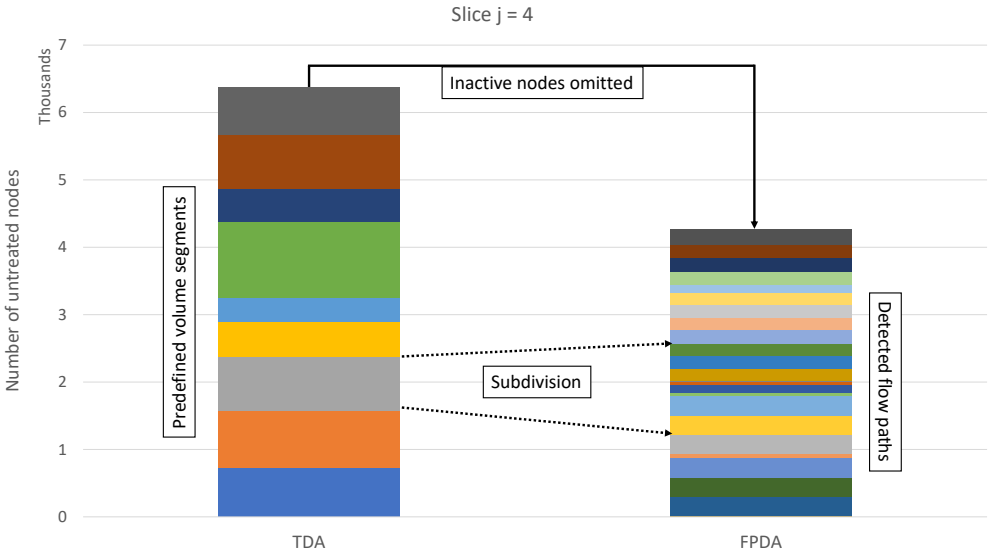

(b) Investigation of slice $j = 4$

Figure 4.11: Visual explanation for why the FPDA method predicts lower flow rate than the TDA method

4.3.3 FEM Comment

Former comparison studies [6] has revealed that equivalent FEM simulations yield roughly 20 % lower normalized flow rate estimates than the TDA method. The reduction was rationally attributed to the flow path lengthening effect as illustrated by the train of thought provided in Figure 4.12.

The reduction effect due to the lengthened seepage distance is obvious, but it is notable that the order of magnitude for the reduction is the same as the FPDA

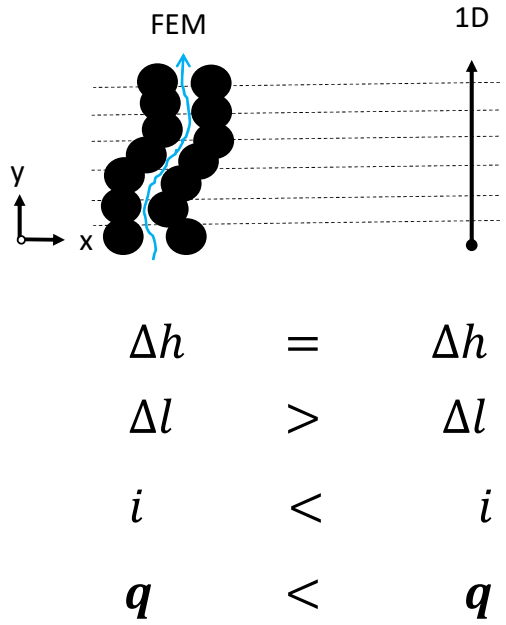

Figure 4.12: Train of thought for FEM induced lengthening effect on estimated flow rate. q equivalates to flow rate, Q.

effect presented in this study and perhaps it can collaborate with the lengthening phenomena to fully explain the observed reduction. Note that the purpose of this statement is purely to comment on a relevant connection to existing knowledge.

Chapter 5

Conclusion

5.1 Concluding Remarks

A flow path detection algorithm (FPDA) has been proposed to improve the seepage flow rate estimation through defective jet-grouted cut-off walls. Geometric imperfections in terms of positioning errors and random variability of column diameter are included to allow occasional penetrating seepage passages to occur. Monte Carlo simulations are then utilized to gain sufficient statistical significance to properly describe the risk of seepage flow through the wall. The FPDA approach differs from previous work in terms of how the seepage flow paths are detected. Where the former three-dimensional discretized algorithm uses nested *if*-statements to execute a simplified penetration investigation, the FPDA method utilizes the powerfull DBSCAN technique to capture the physical flow behaviour in a better way. When the new FPDA method was compared to the former algorithm, it was found that:

1. FPDA suggests **15 % reduced normalized flow rate for JGCOWs with one single row of jet-grouted columns**, allowing a more economic and environmental design.
   Main reason: Subdivision of untreated zones activates the summation sequence property of the harmonic average.

2. FPDA arrests the former algorithm's lacking ability of properly modelling tortuous flow paths through JGCOWs with more than one row, essentially revealing that the risk of underestimating the seepage flow rate is present in the former algorithm.
   Main reason: JGCOWs with more than one row induce more tortuous flow paths which increases the likelihood of transverse flow. Transverse flow is wrongly rejected by the TDA method, but captured in the FPDA update.

5.2 Future Work

The proposed FPDA update serves as an enabler to revise existing knowledge about leakage risk through defective cutoff walls. The following suggestions for future work are meant to pick-up from where this thesis ends:

- **Volume of simulation cases**
  The parametric study in this work is based on a somewhat limited number of simulation cases. Instead of deterministically setting up a stepwise discretized set of simulation cases, all input variables could be described by a probability density function (PDF) and one could monitor the normalized flow rate, Ω, through a large number of random simulation cases. An interesting output could be a tornado plot, as illustrated in Figure 5.1, to visualize the sensitivities for the various input parameters, e.g. SOF or inclination angle, β, to reveal the intra-importance.

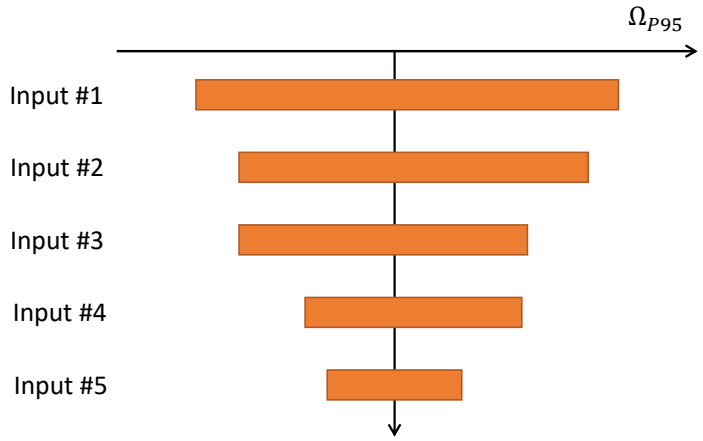

Figure 5.1: Illustration of a tornado plot

  The tornado plot can be used to determine which input parameters deserve extra attention. E.g., what has the largest impact on normalized flow rate of SOF and inclination angle? If it is SOF, one could argue that additional ground investigations are valuable to improve knowledge about the soil layering or if it is the inclination angle, attention should be allocated to the jet-grouting operation. Additionally, extra volume of simulation cases would test new input parameter combinations that could reveal new insights.

- **Stochastic permeability**
  The TDA method (including the FPDA update) assumes constant permeability coefficient for the untreated zones even though existing knowledge considers the permeability to be one of the most variable soil properties with COV as high as three [32, 33]. Former investigations show "... reduction in the expected flow rate with increased permeability variance ... (because) ... the greater the permeability variance, the greater the volume of low per-

meability material that must be negotiated along any flow path." [34]. This statement indicates a potential upside in design to save both money and the environment, but the full implication of stochastic permeability on leakage risk through defective JGCOWs is difficult to foresee without proper implementation. A proof of concept is provided in Appendix B.

- **Improve code**
  The focus for the work in this thesis has been to develop a solution that works. That strategy has materialized in a MATLAB code that runs correctly and sufficiently fast, but some upside in efficiency is probably still possible to realize. More importantly, code availability and adaptability with other solutions can be improved to increase transparency and make it available for more people to contribute. Potential conflicts may be invoked if the code later proves to be of significant monetary value.

- **Laboratory or field data**
  Former similar studies points at "... a lack of experimental or field measurement of groundwater flow through buried JGCOWs." [15]. It is not possible to get around that the fact that lack of representative field or laboratory data to calibrate the numerical algorithms constitutes a weakness in leakage risk modelling through defective JGCOWs. Acquisition of such data - in one way or another - would immensely improve the knowledge.

- **Contribution per flow path**
  The FPDA method adds new information about flow path behaviour that potentially can be used to execute mitigate measures if seepage flow occurs through defective JGCOWs. Figure 5.2 exemplifies a distribution of total flow among all penetrating flow paths for a given realization.
  Further investigations could yield knowledge about the flow path behaviour in terms of where the majority of flow occurs. E.g., if it turns out that > 95 % of the total flow on average goes through one single flow path, a mitigating measure could be to install one additional jet-grouted column in the suspected location to prevent almost all flow from occurring.

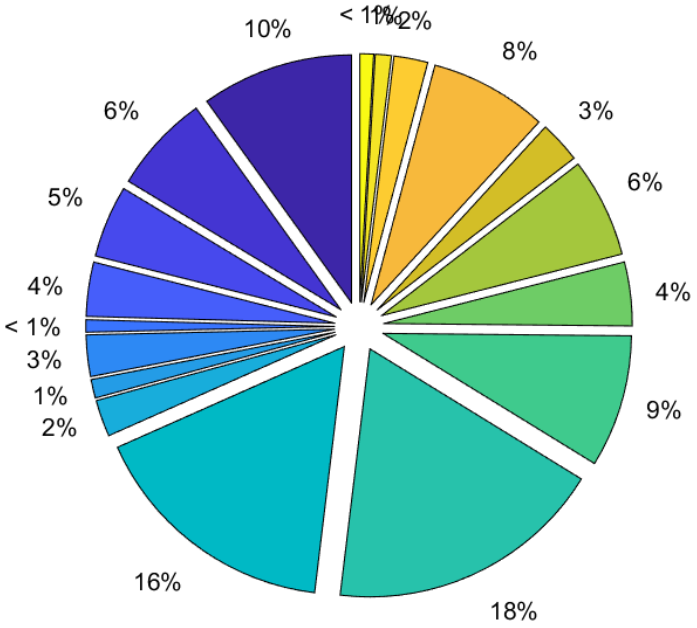

Figure 5.2: Flow contribution per flow path for an example realization. Each slice represents a separate flow path.

- **Formulate design charts**
  As of now, the proposed FPDA method has been developed, tested and compared to an existing algorithm to demonstrate its potential and limitations. To extract value, the method has to be made available to practicing engineers for them to strike a balance among the various JGCOWs design parameters. One way of doing that is to generate intuitive design charts for use by designers. An important enabler to generate proper design charts is to quite significantly increase the number of simulations cases far above what is conducted in this thesis. [15] provides neat design charts and procedures that could be revised with the new insights provided by the FPDA method.

- **Quantify potential savings**
  The purpose of this idea is to further tie the FPDA innovation to an added value contribution. The treatment volume for the reference simulation case in this study can **very simplified** be estimated by the below calculation.

$$V_{treatment} = \frac{d_i^2 \pi L n_{columns}}{4} = \frac{(1.2\ m)^2 \pi (20\ m) 10}{4} = \mathbf{226\ m^3}$$

  Further simplifications of assuming pure concrete as treatment slurry and setting the density of concrete to $\rho_{concrete} = 2\,400\ \frac{kg}{m^3}$ yields

$$m_{concrete} = \rho_{concrete} \times V_{treatment}$$
$$= 2\,400\ \frac{kg}{m^3} \times 226\ m^3 = 542\,400\ kg = \mathbf{542.4\ tons}$$

Further conversion to monetary value is conducted by the below evaluation[1]:

$$\mathbf{Cost} = m_{concrete} \times \text{Concrete price}$$
$$= 542.4\ tons \times 1\,500\ \frac{NOK}{ton} = \mathbf{813\ 600\ NOK}$$

It is emphatically underlined that the above evaluations are *extremely* rough estimates as the purpose is to provide a back-of-the-envelope estimate of the order of magnitude for the potential economic project savings. For JGCOWs with n_{row}= 1, the findings in this thesis suggest roughly 15 % reduced flow rate which can be 'pseduo-forwarded' to the above estimate to get an idea of the potential value. Recommended future work involves arresting all simplifications in the above evaluation by presenting the value potential in a proper manner. It should also include operational and environmental aspects.

[1]Price assumption for concrete collected from professor Klaartje de Weerdt. E-mail correspondence documented in Appendix D. Note that pricing indeed is subject to market variations.

Bibliography

[1] N. Modig and P. Åhlström, 'This is lean: Resolving the efficiency paradox,' *Rheologica Publishing*, 2012.

[2] P. G. Sembenelli and G. Sembenelli, 'Deep jet-grouted cut-offs in riverine alluvia for ertan cofferdams,' *Journal of Geotechnical and Geoenvironmental Engineering*, vol. 125, no. 2, pp. 142–153, 1999.

[3] P. Croce and G. Modoni, 'Design of jet-grouting cut-offs,' *Ground Improvement*, vol. 11, no. 1, pp. 11–19, 2007.

[4] E. Koda and P. Osinski, 'Bentonite cut-off walls: Solution for landfill remedial works,' *Environmental Geotechnics*, vol. 4, no. 4, pp. 223–232, 2016.

[5] Y. Tan and Y. Lu, 'Forensic diagnosis of a leaking accident during excavation,' *Performance of Constructed Facilities*, vol. 31, no. 5, 2017.

[6] Y. Pan, J. Yi, S.-H. Goh, J. Hu, W. Wang and Y. Liu, 'A three-dimensional algorithm for estimating water-tightness of cement-treated ground with geometric imperfections,' *Computers and Geotechnics*, vol. 115, 2019.

[7] Keller, *Jet grouting*, Read: 19.04.2022. [Online]. Available: `https://www.keller.co.uk/expertise/techniques/jet-grouting`.

[8] S. Chew, H. M. Kamruzzaman and F. H. Lee, 'Physicochemical and engineering behaviour of cement treated clays,' *Geotechnical and Geoenvironmental Engineering*, vol. 130, no. 7, pp. 696–706, 2004.

[9] S. Horpibulsuk, N. Miura and T. S. Nagaraj, 'Assessment of strength development in cement-admixed high water content clays with abrams' law as a basis,' *Géotechnique*, vol. 53, no. 4, pp. 439–444, 2003.

[10] H. W. Xiao, F. H. Lee and K. G. Chin, 'Yielding of cement-treated marine clay,' *Soils and Foundations*, vol. 54, no. 3, pp. 488–501, 2014.

[11] *Underground consulting*, Read: 20.04.2022. [Online]. Available: `https://www.undergroundconsulting.it/images/competenza/tn_01c_Jet_grouting_Tuttle_Creek.jpg`.

[12] G. Modoni, A. Flora, S. Lirer, M. Ochmański and P. Croce, 'Design of jet grouted excavation bottom plugs,' *Geotechnical and Geoenvironmental Engineering*, vol. 142, no. 7, 2016.

[13] K. Wang, Z. Li, H. Zheng, X. Xu and H. He, 'A theoretical model for estimating the water-tightness of jet-grouted cut-off walls with geometric imperfections,' *Computers and Geotechnics*, vol. 138, 2021.

[14] Y. Pan, Y. Liu, J. Hu, M. Sun and W. Wang, 'Probabilistic investigations on the watertightness of jet-grouted ground considering geometric imperfections in diameter and position,' *Canadian Geotechnical Journal*, vol. 54, no. 10, pp. 1447–1459, 2017.

[15] Y. Pan, Y. Liu and E. J. Chen, 'Probabilistic investigation on defective jet-grouted cut-off wall with random geometric imperfections,' *Géotechnique*, vol. 69, no. 5, pp. 420–433, 2019.

[16] Y. Pan, M. A. Hicks and W. Broere, 'An efficient transient-state algorithm for evaluation of leakage through defective cutoff walls,' *International Journal for Numerical and Analytical Methods in Geomechanics*, vol. 45, pp. 108–131, 2021.

[17] B. of Reclamation, *Teton dam history*, Read: 15.05.2022, 2020. [Online]. Available: `https://www.usbr.gov/pn/snakeriver/dams/uppersnake/teton/index.html`.

[18] G. Modoni and J. Bzówka, 'Analysis of foundations reinforced with jet grouting,' *Geotechnical and Geoenvironmental Engineering*, vol. 138, no. 12, pp. 1442–1454, 2012.

[19] S.-L. Shen, Z.-F. Wang, J. Yang and C.-E. Ho, 'Generalized approach for prediction of jet grout column diameter,' *Geotechnical and Geoenvironmental Engineering*, vol. 139, no. 12, pp. 2060–2069, 2013.

[20] A. Flora, G. Modoni, S. Lirer and P. Croce, 'The diameter of single, double and triple fluid jet grouting columns: Prediction method and field trial results,' *Géotechnique*, vol. 63, no. 11, pp. 934–945, 2013.

[21] C. E. Ho, 'Fluid-soil interaction model for jet grouting,' *GSP 168 Grouting for Ground Improvement*, pp. 1–10, 2007.

[22] G. Modoni, P. Croce and L. Mongiovì, 'Theoretical modelling of jet grouting,' *Géotechnique*, vol. 56, no. 5, pp. 335–347, 2006.

[23] K.-K. Phoon and F. H. Kulhawy, 'Characterization of geotechnical variability,' *Canadian Geotechnical Journal*, vol. 36, no. 4, pp. 612–624, 1999.

[24] M. Arroyo, A. Gens, P. Croce and G. Modoni, 'Design of jet-grouting for tunnel waterproofing,' *7th International Symposium on Geotechnical Aspects of Underground Construction in Soft Ground*, 2011.

[25] P. Croce, A. Flora and G. Modoni, 'Jet grouting: Tecninca, progetto e controllo,' *Hevelius*, 2004.

[26] O. S. Langhorst, B. J. Schat, J. C. W. M. de Wit, P. J. Bogaards, R. D. Essler, J. Maertens, B. K. J. Obladen, C. F. Bosma, J. J. Sleuwaegen and H. Dekker, 'Design and validation of jet grouting for the amsterdam central station,' *Geotechniek ECSMGE*, pp. 18–21, 2007.

[27] N. Eramo, G. Modoni and M. Arroyo Alvarez de Toledo, 'Design control and monitoring of a jet grouted excavation bottom plug,' *7th International Symposium on Geotechnical Aspects of Underground Construction in Soft Ground*, 2011.

[28] J. L. Jensen, S. D. Thomas and P. W. M. Corbett, 'On the bias and sampling variation of the harmonic average,' *Mathematical Geology*, vol. 29, no. 2, pp. 267–276, 1997.

[29] D.-F. Xia, S.-L. Xu and F. Qi, 'A proof of the arithmetic mean - geometic mean - harmonic mean inequalitites,' *RGMIA Research Report Collection*, vol. 2, no. 1, pp. 85–87, 1999.

[30] G. Gan, C. Ma and J. Wu, 'Data clustering: Theory, algorithms and applications,' *ASA-SIAM Series on Statistics and Applied Probability*, 2007.

[31] M. Ester, H. Kriegel, J. Sander and X. Xu, 'A density-based algorithm for discovering clusters in large spatial databases with noise,' *Second international conference on knowledge discovery and data mining*, pp. 226–231, 1996.

[32] I. K. Lee, W. White and O. G. Ingles, 'Geotechnical engineering,' *Pitman Publishing, Ltd.*, 1983.

[33] F. H. Kulhawy, M. J. S. Roth and M. D. Grigoriu, 'Some statistical evaluations of geotechnical properties,' *Proc.,ICASP6, 6th Int. Conf. Appl. Statistical Problems in Civ. Engrg.*, 1991.

[34] D. V. Griffiths and G. A. Fenton, 'Three-dimensional seepage through spatially random soil,' *Journal of geotechnical and geoenvironmental engineering*, vol. 123, no. 2, pp. 153–160, 1997.

[35] W. Li, 'Risk assessment of power systems: Models, methods and applications,' *The Institute of Electrical and Electronics Engineers, Inc.*, pp. 489–495, 2014.

Appendix A

Harmonic Average Example

This appendix provides a classical example where it is appropriate to apply the harmonic average. The purpose is to demonstrate its usability.

Imagine that a car is driving with varying speed as described in Table A.1 and the objective is to find the average speed.

Table A.1: Distance and speed data for harmonic mean example

n	Distance [km]	Speed [km/h]
1	10	60
2	10	80
3	10	40

The average speed, $\bar{v}$ is given by

$$\overline{v} = \frac{\text{Distance}}{\text{Time}} = \frac{10\text{ km} + 10\text{ km} + 10\text{ km}}{\frac{10\text{ km}}{60\text{ km/h}} + \frac{10\text{ km}}{80\text{ km/h}} + \frac{10\text{ km}}{40\text{ km/h}}} = \frac{3}{\frac{1}{60\text{ km/h}} + \frac{1}{80\text{ km/h}} + \frac{1}{40\text{ km/h}}} = 55.4\,\text{km/h}$$

The average speed is given by the harmonic average, which is lower than the arithmetic average, $\frac{60+80+40}{3} = 60$ km/h. The difference comes from the fact that there is variation in required duration to reach 10 km for the different speeds. The exact same feature occurs in fluid flow through porous media with varying flow capacity.

Appendix B

Stochastic Permeability

The purpose of this appendix is to share an initial proof of concept for the effect of stochastic permeability with regards to seepage flow rate through defective cutoff walls. It has been developed in Excel and limited to evaluating the flow rate through 'artificial' flow paths. Evaluation of flow rate requires adjustments to the flow equations presented in Section 2.3 from:

$$\textbf{Constant k}: \quad Q = kA(y)\frac{dh}{dy} \rightarrow Q = \frac{kH}{t}\tilde{A}(t)$$

where

$$\tilde{A}(t) = \frac{1}{\frac{1}{t}\int_0^t \frac{1}{A(y)}\,dy} \xrightarrow{Discretization} \tilde{A}(t) = \frac{1}{\frac{1}{n}\sum_{j=1}^{n}\frac{1}{A_j}}$$

to:

$$\textbf{Varying k}: \quad Q = k(y)A(y)\frac{dh}{dy} \rightarrow Q = \frac{H}{t}\tilde{Ak}(t)$$

where

$$\tilde{Ak}(t) = \frac{1}{\frac{1}{t}\int_0^t \frac{1}{A(y)k(y)}\,dy} \xrightarrow{Discretization} \tilde{Ak}(t) = \frac{1}{\frac{1}{n}\sum_{j=1}^{n}\frac{1}{A_j k_j}}$$

When the permeability coefficient, k, varies, it can no longer be taken out of the integral operation as a constant. Modelling of varying permeability has been done with a log-normal distribution without any autocorrelation function, i.e. spatial variability is not considered. Resulting flow rate is compared to a homogeneous case with constant k as benchmark. Note that the mean value of the log-normally distributed varying permeability coefficient equals the constant k in the homogeneous case and the COV is varying for different cases. A visualization of the model is given by Figure B.1.

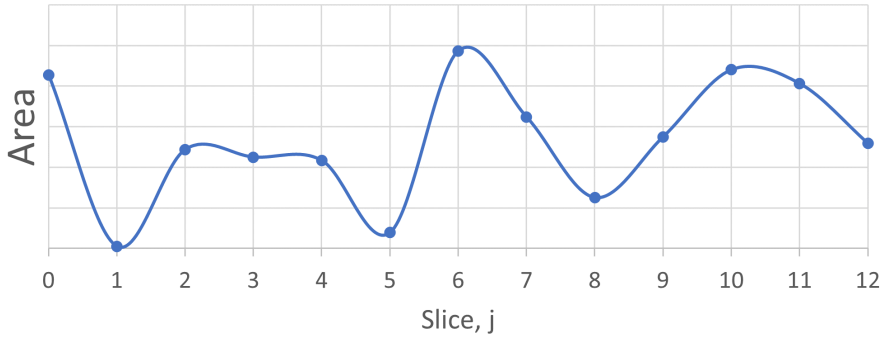

(a) Array of untreated area along 'artificial' flow path

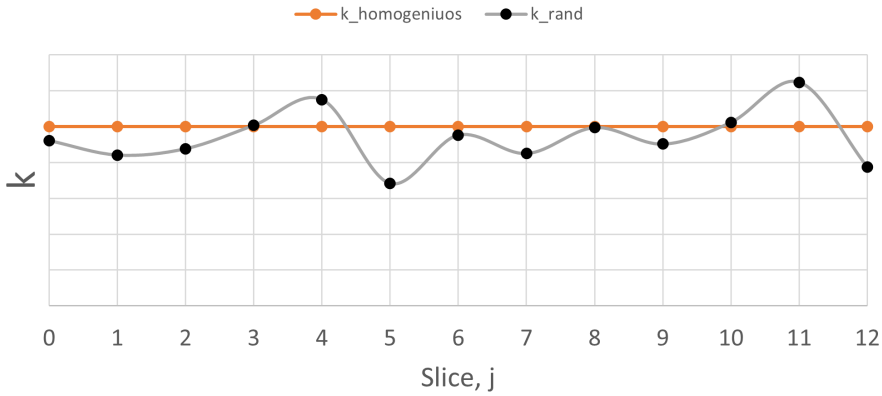

(b) Permeability coefficient, k

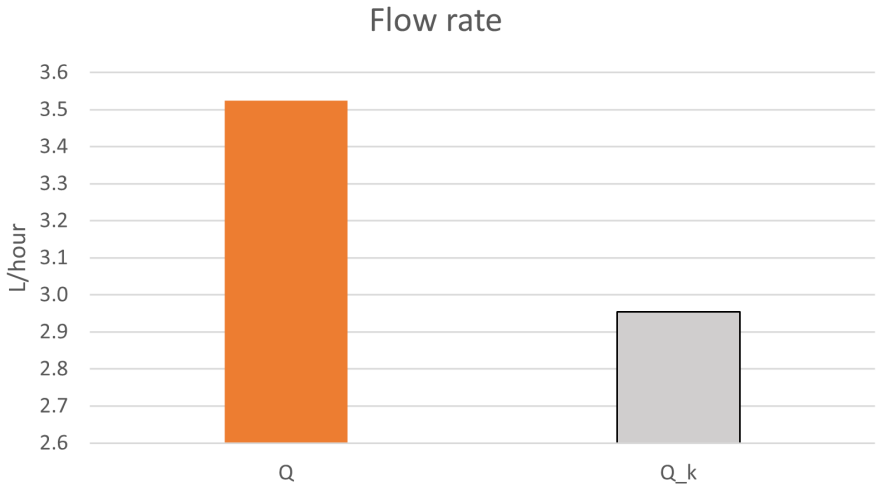

(c) Flow rate. Q for homogeneous k and Q_k for random k

Figure B.1: Visual representation of the flow calculation model

A total of 7 simulation cases with changing COV has been executed. All simulation cases consist of flow paths with 10 slices and undergo 100 realizations in a Monte Carlo simulation set-up to reach a satisfactory degree of statistical significance. Raw data for one Monte Carlo simulation case is given in Figure B.2.

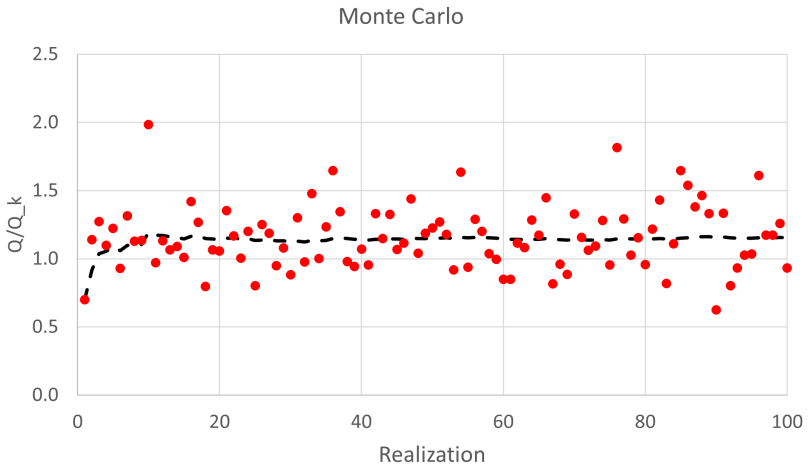

(a) Raw data with running average

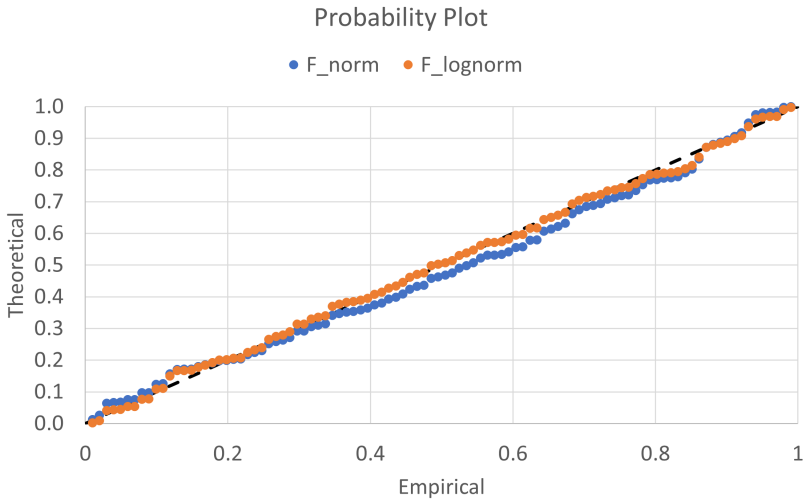

(b) Probability paper

Figure B.2: Monte Carlo simulation summary for a given simulation case

Note that the output variable Q/Q_k describes the ratio between flow rate with homogeneous and varying k. That is, values above one indicates that varying k leads to a reduction in flow rate and vice versa. A summary of all simulation cases is provided in Figure B.3.

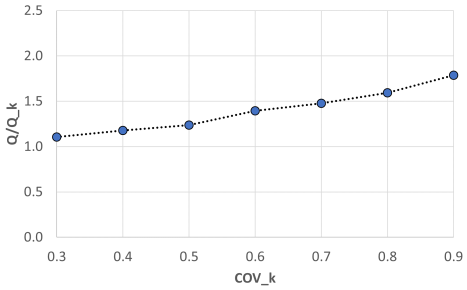

(a) Sample average for Q/Q_k ratio

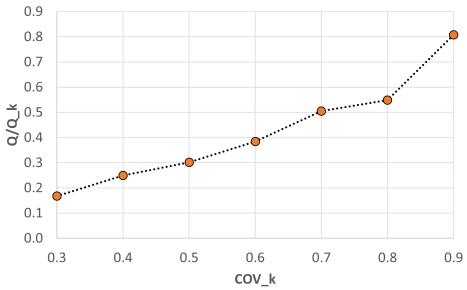

(b) Sample standard deviation for Q/Q_k ratio

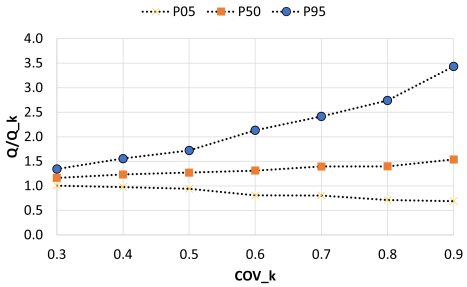

(c) Percentile fraction values

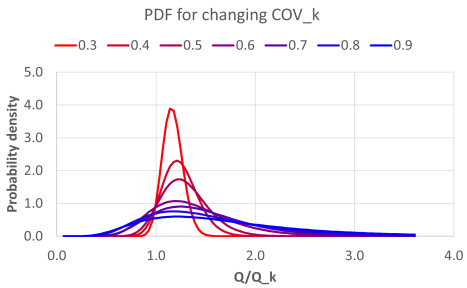

(d) PDF with varying COV_k

Figure B.3: Summary of all simulation cases with stochastic permeability

The summary in Figure B.3 concludes this proof of concept as it demonstrates an expected reduction in flow rate for increased permeability variance, as witnessed by the increasing Q/Q_k trend in Figure B.3a. This observation aligns with the findings of Griffiths and Fenton from 1997 [34], but increased variance in the output flow rate is also observed. In fact, the P05-percentile demonstrates a negative trend with increased variance, evident in Figure B.3c, and perhaps that is exactly what is crucial with regards to design. The full implication of these findings are not easily upscaled to three-dimensional defective JGCOWs, but the proof of concept does indeed demonstrate some potentially decisive new insights.

Appendix C

Monte Carlo Simulation

Monte Carlo simulation constitutes a convenient technique to cope with situations where it is impractical to develop accurate analytical solutions. It bombards the problem with a high number of random realizations to gain knowledge about the stochastic output behaviour and furthermore aids to draw conclusions. Fundamental elements of the Monte Carlo technique is considered well-known and this appendix focuses on presenting a widely used convergency approach [35]. This explanation is based on analysing the relative flow rate, ω_i, as output from one realization, i, in a Monte Carlo simulation with a total of n_{MC} realizations.

Expected value for ω is given by

$$\mu_\omega = \frac{1}{n_{MC}} \sum_{i=1}^{n_{MC}} \omega_i$$

and the sample variance is defined by

$$\sigma_\omega^2 = \frac{1}{n_{MC}-1} \sum_{i=1}^{n_{MC}} (\omega_i - \mu_\omega)^2$$

Note that μ_ω itself is a random variable whos uncertainty can be estimated by

$$\sigma_{\mu_\omega}^2 = \frac{\sigma_\omega^2}{n_{MC}} = \frac{1}{n_{MC}(n_{MC}-1)} \sum_{i=1}^{n_{MC}} (\omega_i - \mu_\omega)^2$$

Furthermore, the standard deviation given by

$$\sigma_{\mu_\omega} = \frac{\sigma_\omega}{\sqrt{n_{MC}}}$$

can be normalized by the expected value to yield the Monte Carlo COV;

$$COV_{MC} = \frac{\sigma_{\mu_\omega}}{\mu_\omega} = \frac{\sigma_\omega}{\sqrt{n_{MC}}\mu_\omega}$$

Note that this expresses the COV for the expected mean value and that confidence in μ_ω increases as the COV decreases. The expression reveals that two strategies

can be taken to reduce the uncertainty, i.e. increase the confidence of the Monte Carlo estimate: reduce sample variance, σ_{ω}^2, or increase the number of realizations, n_{MC}, in the evaluation. Since the former can not be controlled, the number of realizations has to be sufficiently high to achieve a satisfactory degree of confidence. COV_{MC} can either be used as a stopping criteria in Monte Carlo simulations or it can simply be tracked to quality assure the results.

Appendix D

Concrete Price Estimate

Sv: Overslagstall pris / utslipp 1 m^3 betong

Emil Hansen <emilhan@stud.ntnu.no>

to. 12.05.2022 13:25

Til: Klaartje De Weerdt <klaartje.d.weerdt@ntnu.no>

Mange takk Klaartje - både for god hjelp og lykkeønskning.

Mvh,
Emil

Fra: Klaartje De Weerdt <klaartje.d.weerdt@ntnu.no>
Sendt: torsdag 12. mai 2022 12:17
Til: Emil Hansen <emilhan@stud.ntnu.no>
Emne: RE: Overslagstall pris / utslipp 1 m^3 betong

Hei Emil

Når det gjelder prisen for sement så spurte jeg Tone Østnor (marketsjef hos Norcem) for noen uker siden i forbindelse med en emneoppgave til en student (Julie).
Jeg fikk svaret nedenfor:

Hei begge to

Beklager dere må vente på svar fra meg.

Snittpris pr i dag levert er kr.1500 NOK/tonn.

Som dere vet er verden i raske forandringer for tiden.

Lykke til med emneoppgave, Julie.

Mvh Tone

Når det gjelder prisen for betong så finner du prislister på nettet, f.eks.:
https://betongost.no/wp-content/uploads/2020/01/2020-Prisliste-Betong-Tr%C3%B8ndelag.pdf
https://static1.squarespace.com/static/57a07ee36b8f5bcfaa10e364/t/5ff2facd18d44937a927e9a8/1609759438330/Velde+Betong+priser+2021.pdf
Om du ønsker oppdaterte lister kan du ta kontakt med leverandørene (f.eks. Unicon, Norbetong eller BetongØst) direkte.

Jeg håper det hjalp 😊

Lykke til med masteroppgaven!

Hilsen, Klaartje

From: Emil Hansen <emilhan@stud.ntnu.no>
Sent: Thursday, May 12, 2022 9:47 AM
To: Klaartje De Weerdt <klaartje.d.weerdt@ntnu.no>
Subject: Overslagstall pris / utslipp 1 m^3 betong

Klaartje,

> Ble introdusert for deg gjennom BM1 høsten 2020 og Betongkonstruksjoner 1 vår 2021. Skriver nå masteroppgave i geoteknikk om jetpeler.
>
> Søker kilde med overslagstall for pris og utslipp for 1 m^3 med betong eller sement.
>
> Vet du om noe slikt?
>
> Takk,
> Emil

Appendix E

Result Details

Loosely speaking, the purpose of this appendix is to provide a solid foundation to the results presented in Chapter 4 as illustrated in Figure E.1. Table E.1 provides an overview of the cases in the parametric study with figure reference to detailed visualizations of the results. Furthermore, all simulation cases where run separately with both $n_{MC} = 100$ and $n_{MC} = 1\ 000$ for convergency investigations as presented in Table E.2.

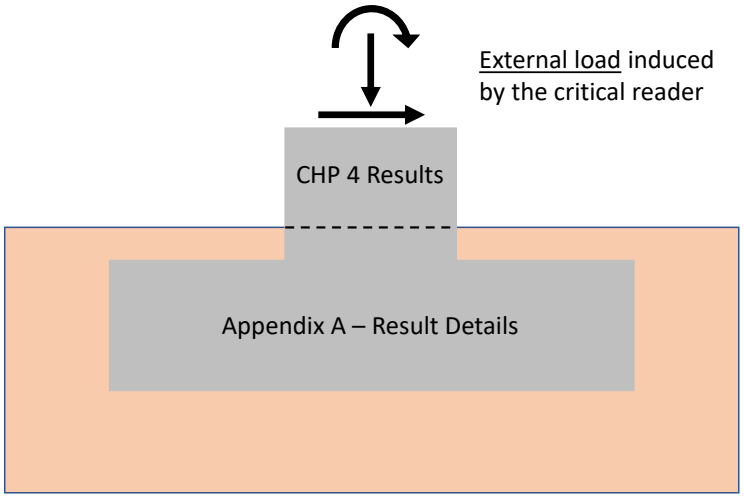

Figure E.1: Illustration of the purpose of Appendix E.

Table E.1: Overview of cases in parametric study. **Green** indicates increase and **red** decrease compared to reference case.

Case	n_{row}	COV(d_i)	$\sigma(\beta)$ [°]	Depth [m]	SOF [m]	s_x [m]	s_y [m]	Figure Reference
# 1	**1**	**0.1**	**0.3**	**20**	**0.5**	**1**	**0.7**	Figure E.2
# 2	**2**	0.1	0.3	20	0.5	1	0.7	Figure E.3
# 3	**3**	0.1	0.3	20	0.5	1	0.7	Figure E.4
# 4	1	**0.05**	0.3	20	0.5	1	0.7	Figure E.5
# 5	1	**0.2**	0.3	20	0.5	1	0.7	Figure E.6
# 6	1	0.1	**0.1**	20	0.5	1	0.7	Figure E.7
# 7	1	0.1	**0.5**	20	0.5	1	0.7	Figure E.8
# 8	1	0.1	0.3	**15**	0.5	1	0.7	Figure E.9
# 9	1	0.1	0.3	**25**	0.5	1	0.7	Figure E.10
# 10	1	0.1	0.3	20	**0.25**	1	0.7	Figure E.11
# 11	1	0.1	0.3	20	**1.00**	1	0.7	Figure E.12
# 12	1	0.1	0.3	20	0.5	**0.9**	0.7	Figure E.13
# 13	1	0.1	0.3	20	0.5	**1.1**	0.7	Figure E.14
# 14	**2**	0.1	0.3	20	0.5	1	**0.5**	Figure E.15
# 15	**2**	0.1	0.3	20	0.5	1	**0.9**	Figure E.16

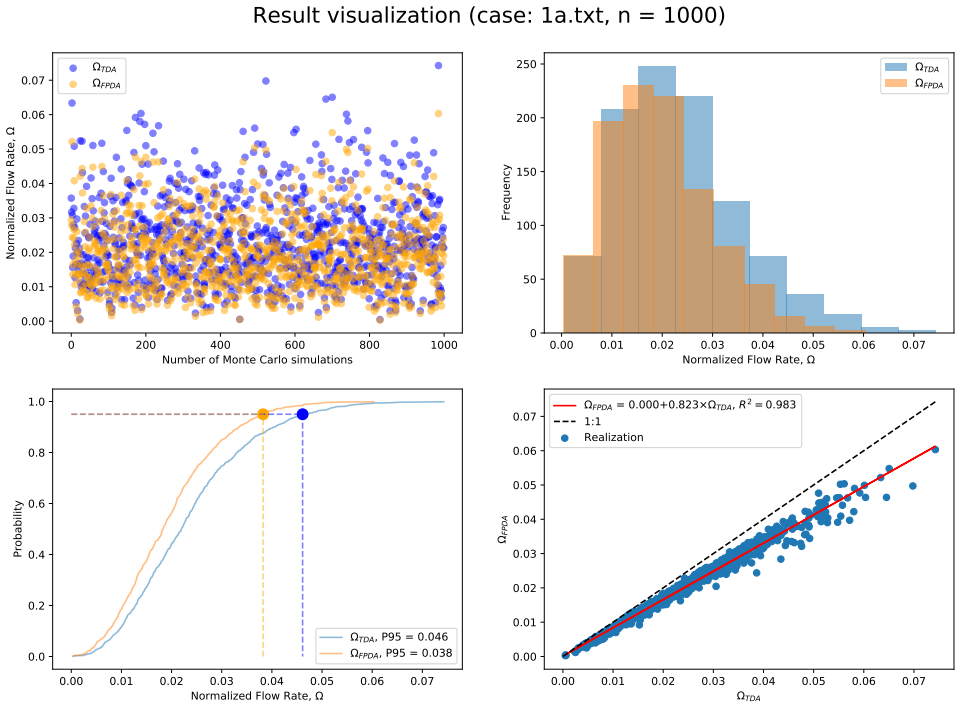

(a) Direct comparison, Ω_{TDA} vs. Ω_{FPDA}

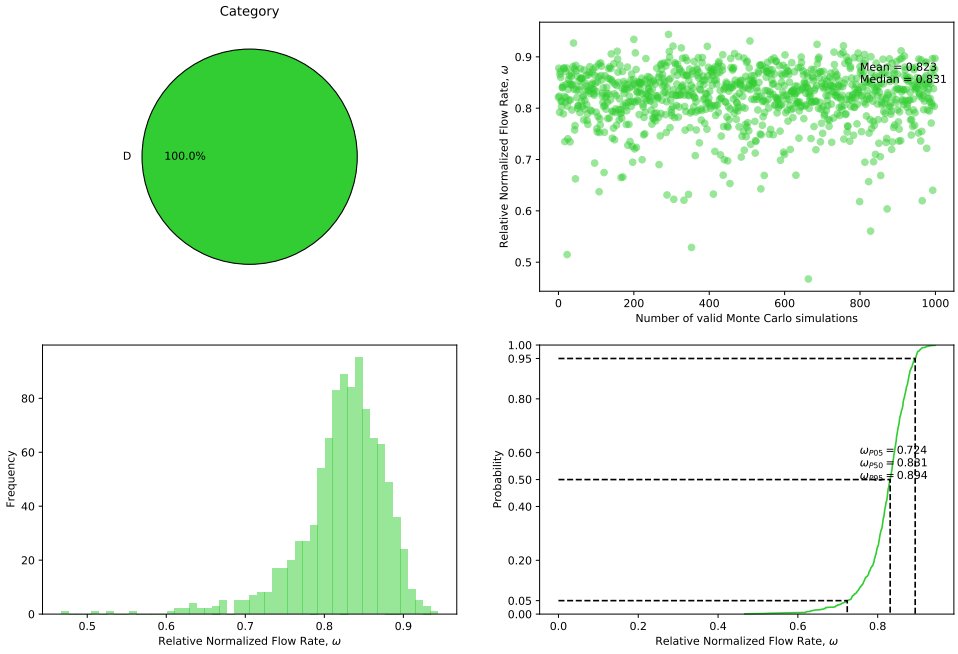

(b) Relative comparison, ω.

Figure E.2: Detailed results for case # 1

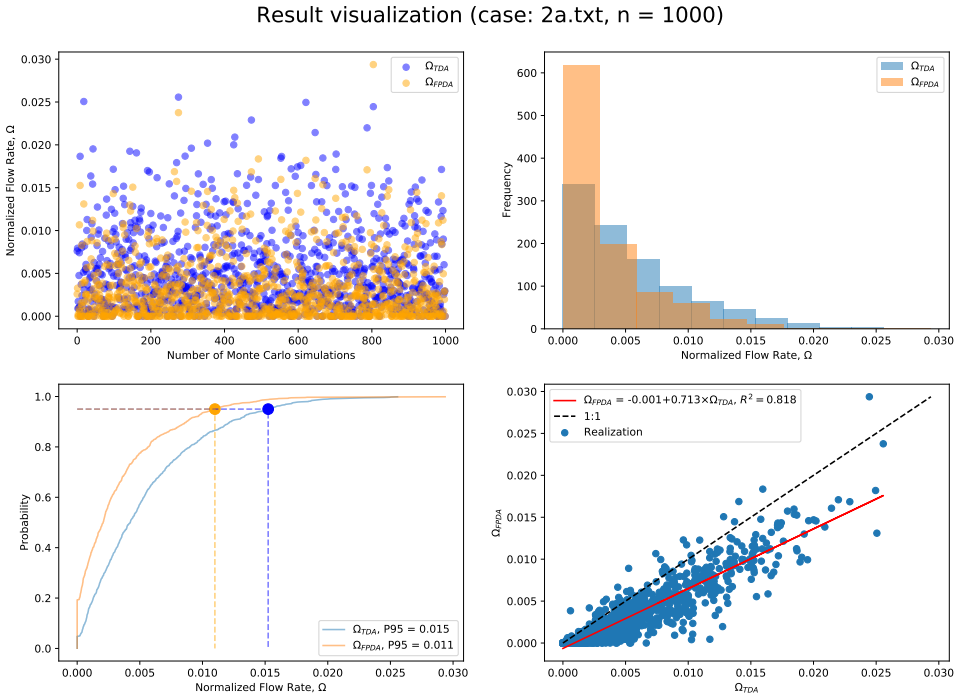

(a) Direct comparison, Ω_{TDA} vs. Ω_{FPDA}

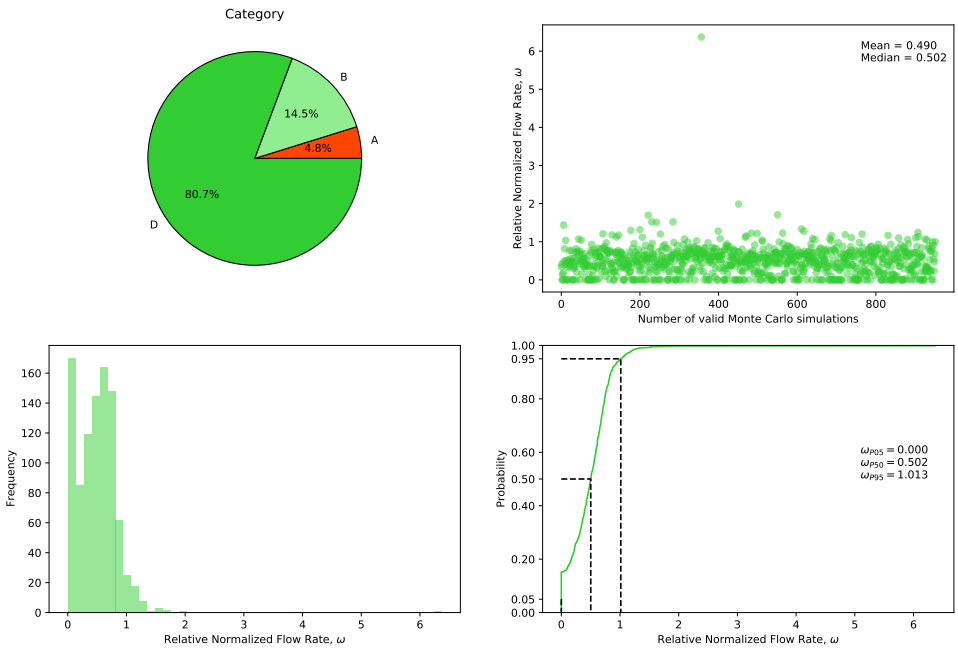

(b) Relative comparison, ω.

Figure E.3: Detailed results for case # 2

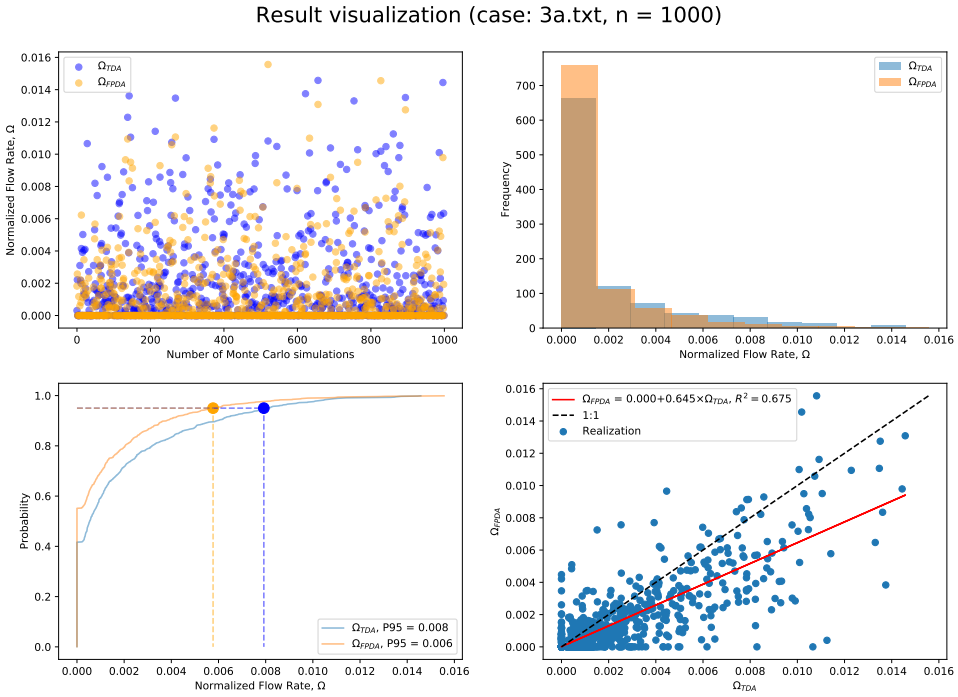

(a) Direct comparison, Ω_{TDA} vs. Ω_{FPDA}

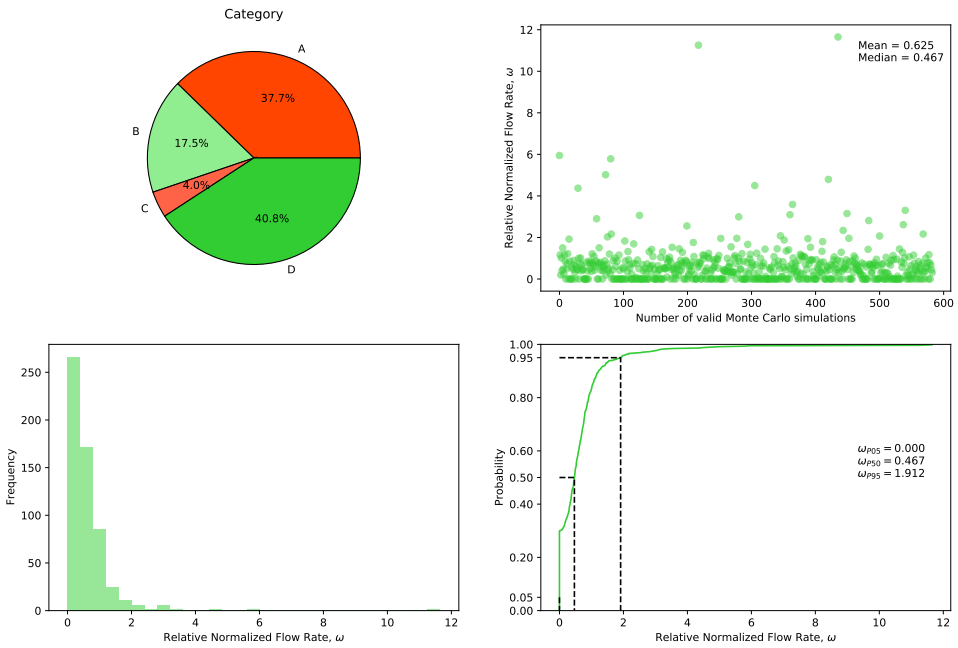

(b) Relative comparison, ω.

Figure E.4: Detailed results for case # 3

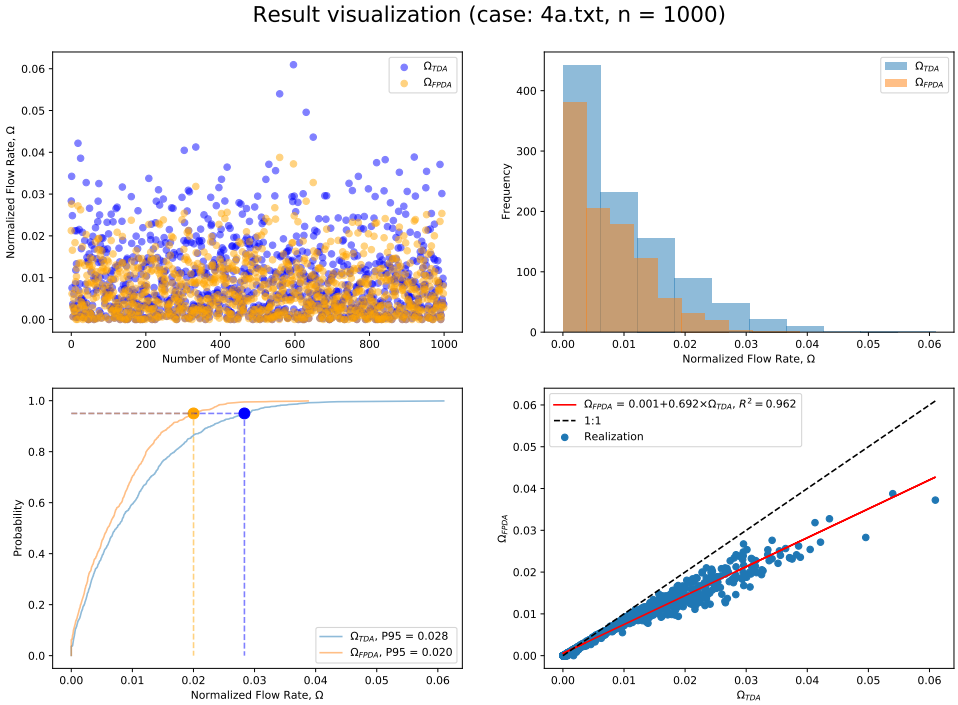

(a) Direct comparison, Ω_{TDA} vs. Ω_{FPDA}

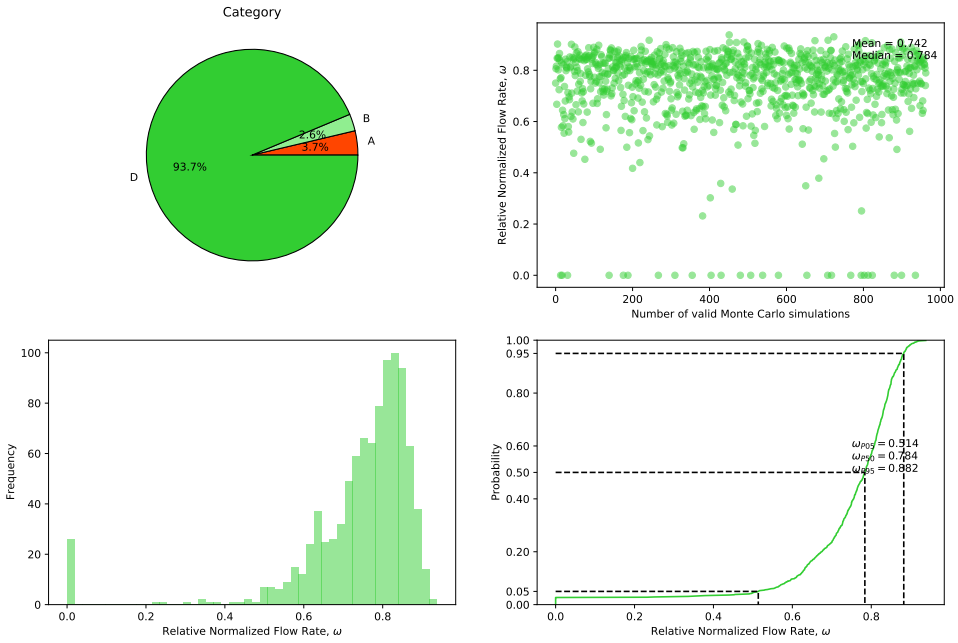

(b) Relative comparison, ω.

Figure E.5: Detailed results for case # 4

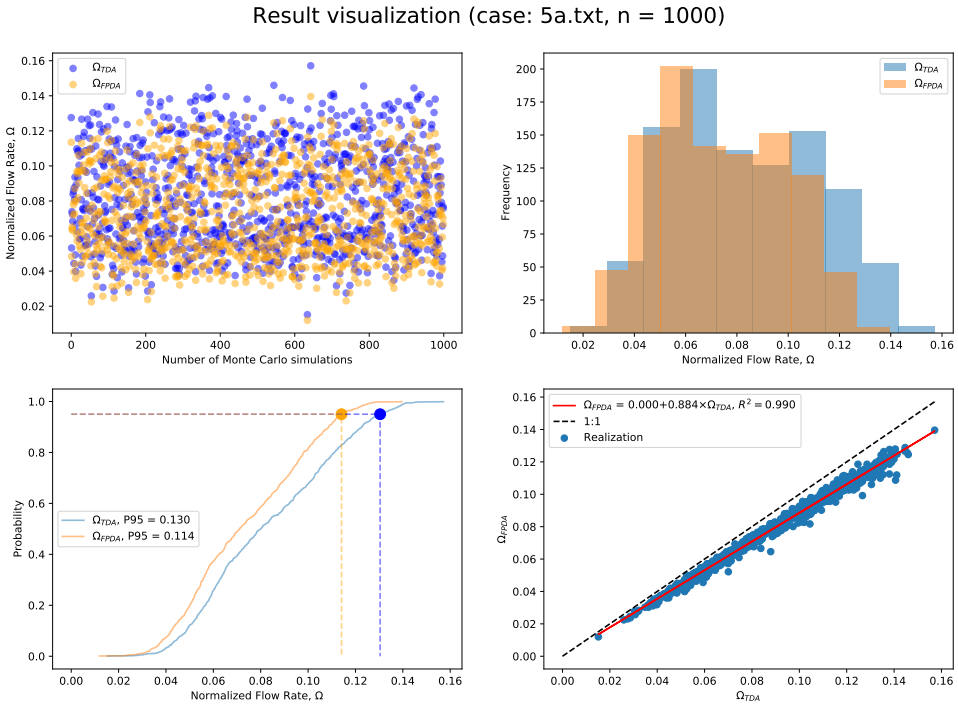

(a) Direct comparison, Ω_{TDA} vs. Ω_{FPDA}

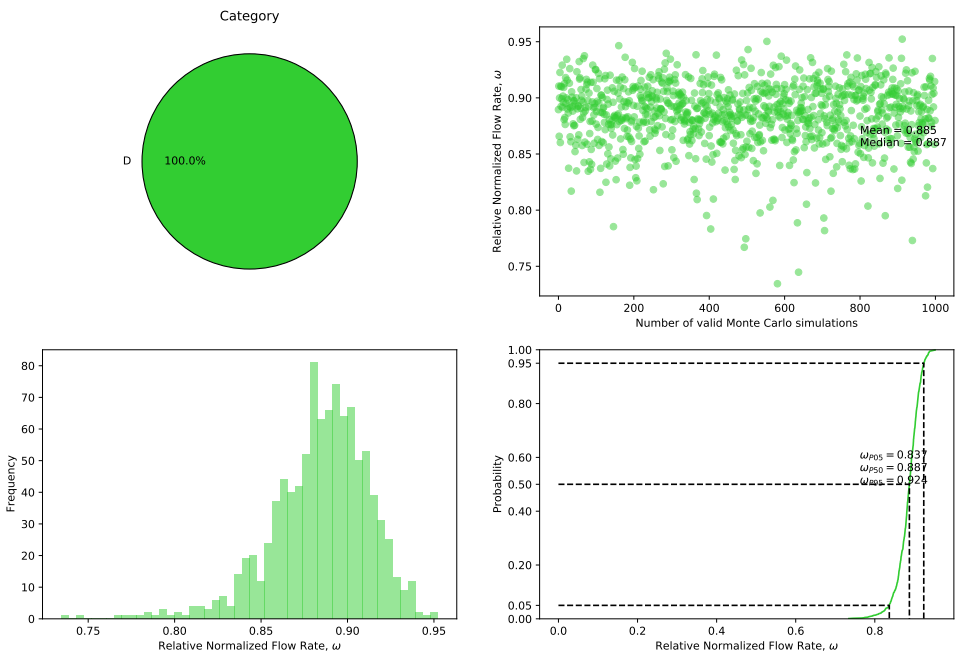

(b) Relative comparison, ω.

Figure E.6: Detailed results for case # 5

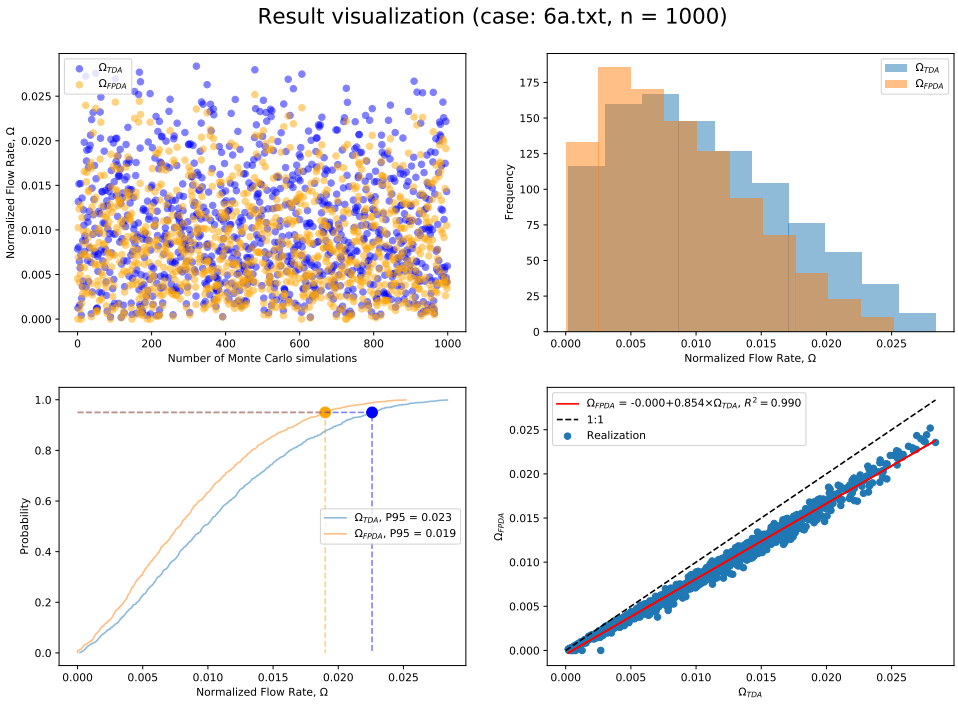

(a) Direct comparison, Ω_{TDA} vs. Ω_{FPDA}

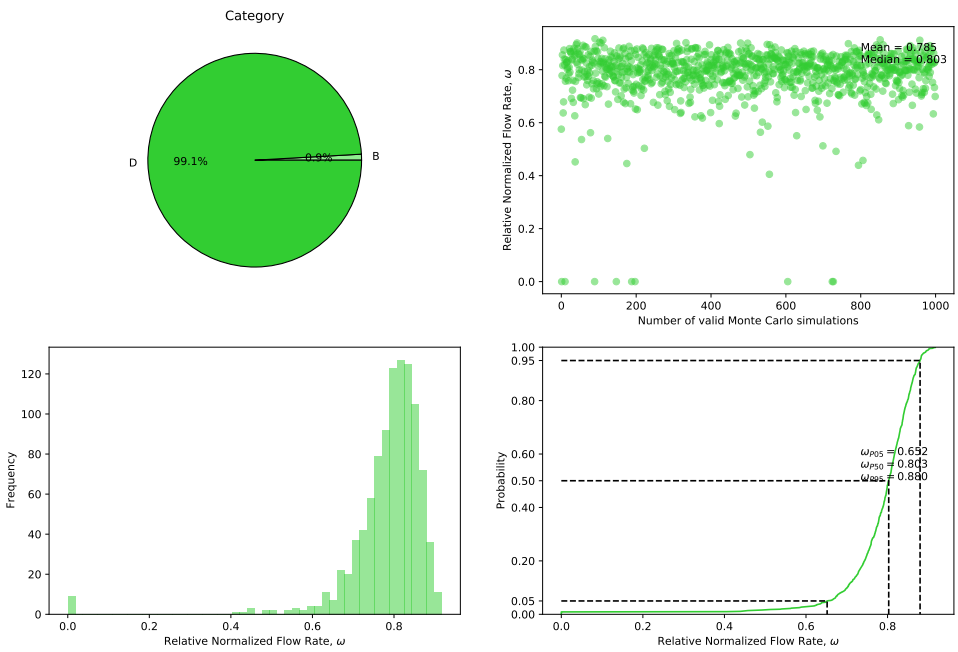

(b) Relative comparison, ω.

Figure E.7: Detailed results for case # 6

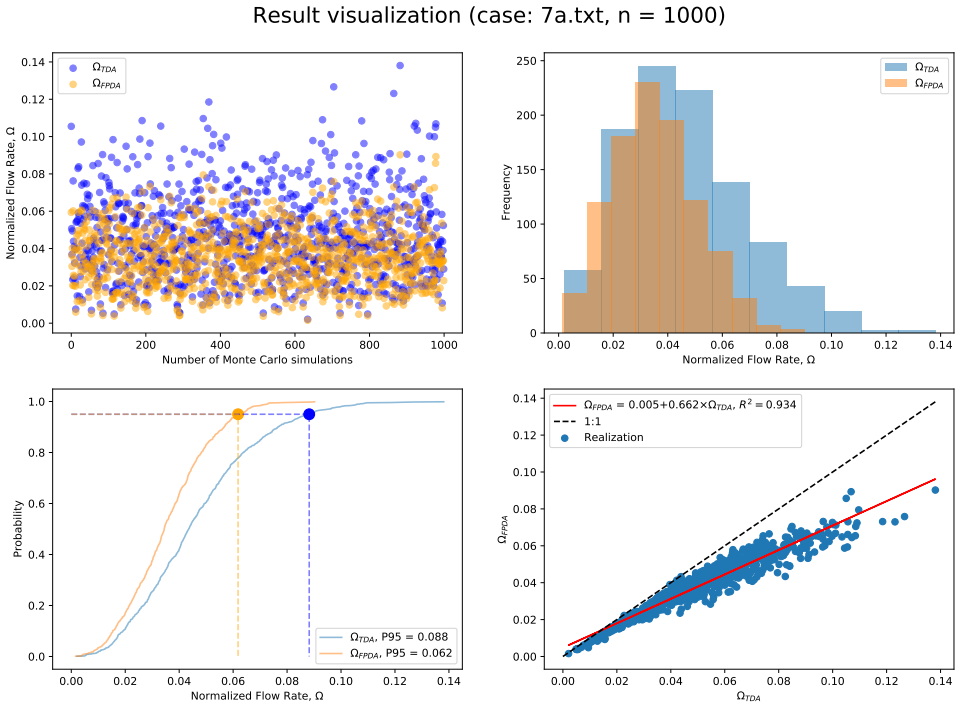

(a) Direct comparison, Ω_{TDA} vs. Ω_{FPDA}

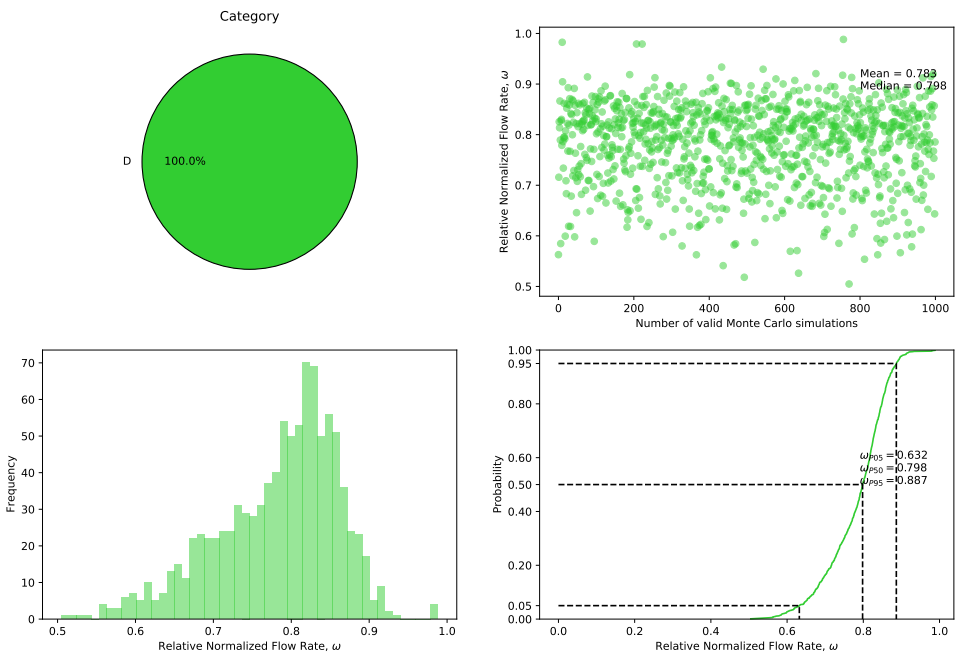

(b) Relative comparison, ω.

Figure E.8: Detailed results for case # 7

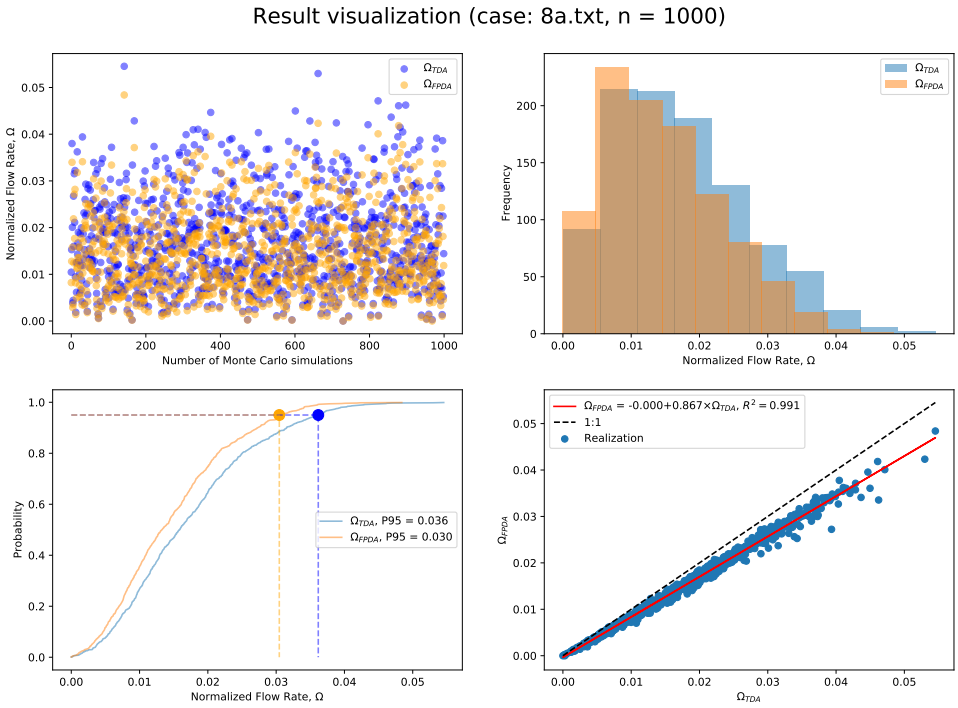

(a) Direct comparison, Ω_{TDA} vs. Ω_{FPDA}

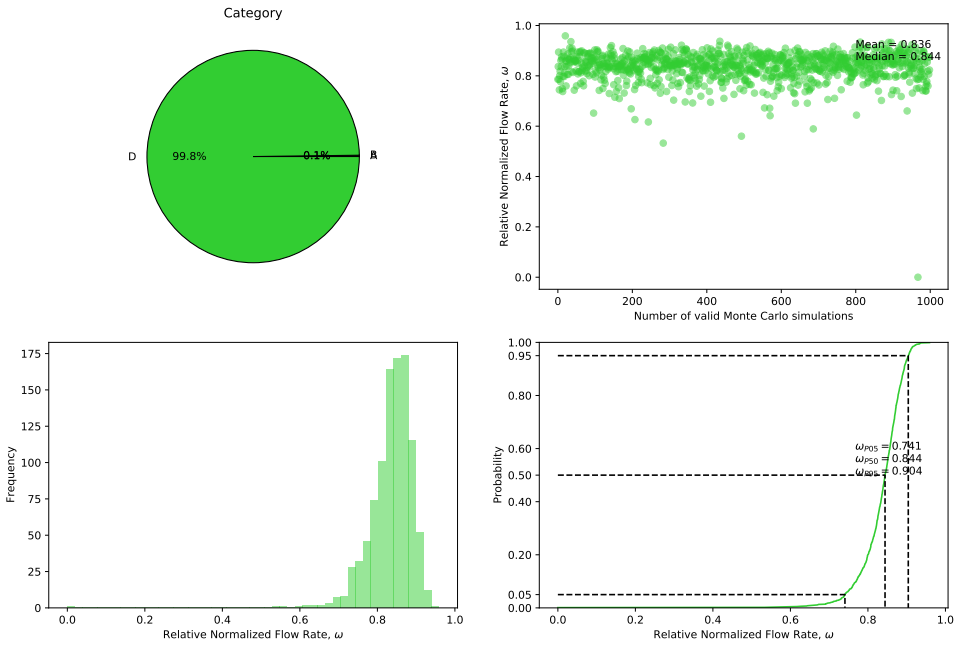

(b) Relative comparison, ω.

Figure E.9: Detailed results for case # 8

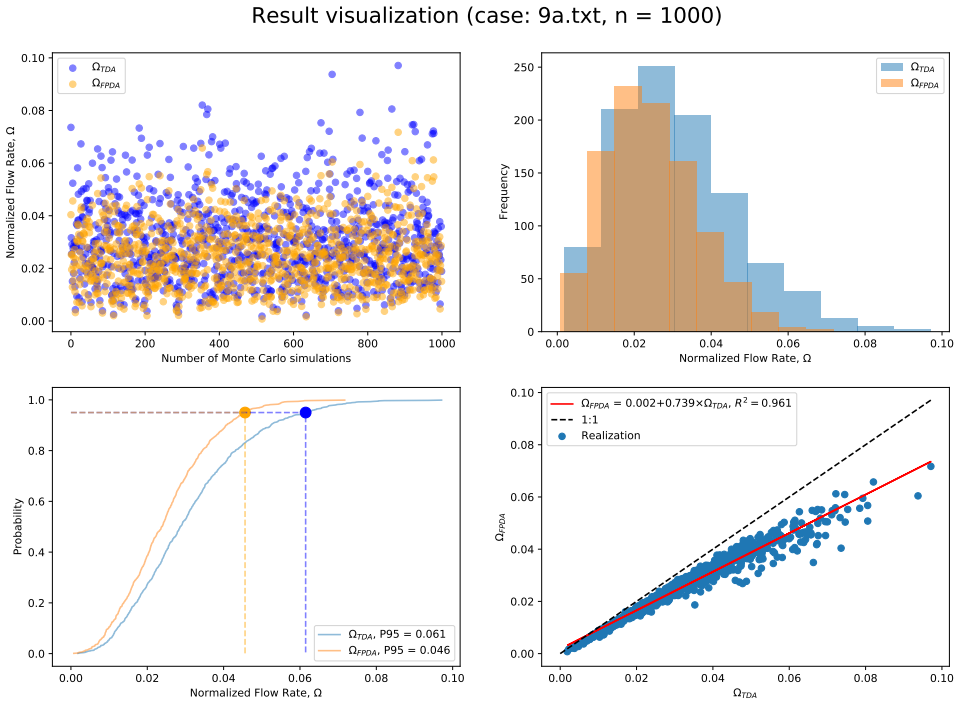

(a) Direct comparison, Ω_{TDA} vs. Ω_{FPDA}

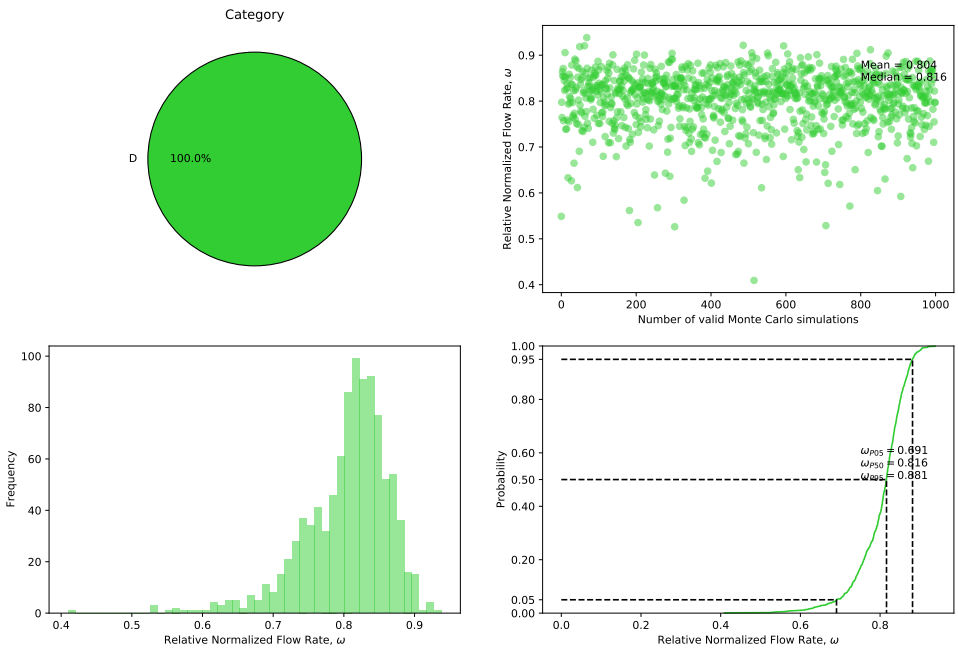

(b) Relative comparison, ω.

Figure E.10: Detailed results for case # 9

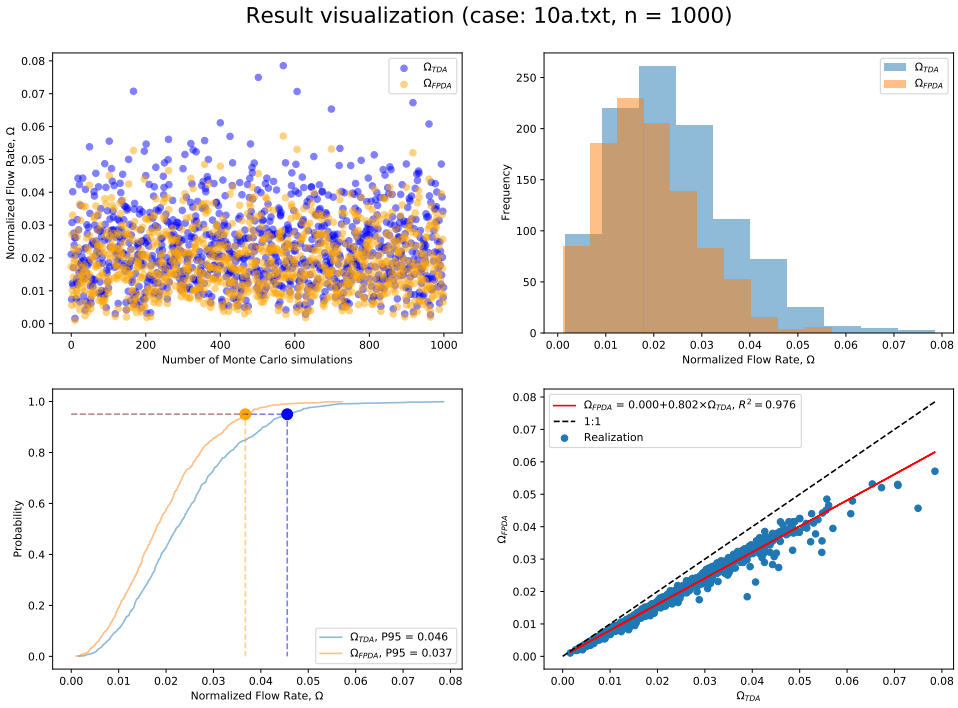

(a) Direct comparison, Ω_{TDA} vs. Ω_{FPDA}

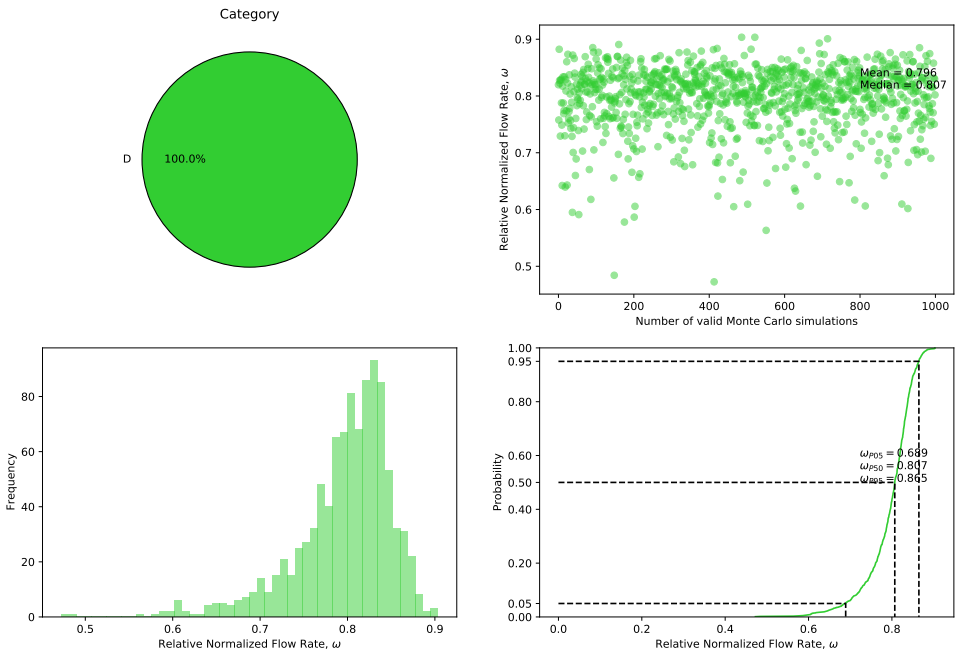

(b) Relative comparison, ω.

Figure E.11: Detailed results for case # 10

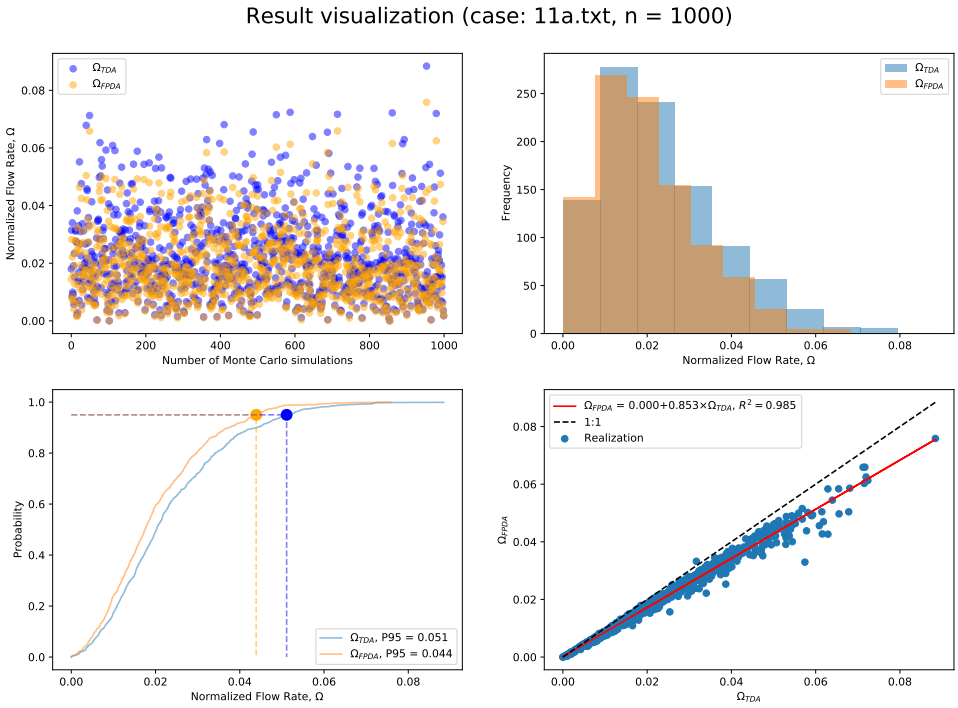

(a) Direct comparison, Ω_{TDA} vs. Ω_{FPDA}

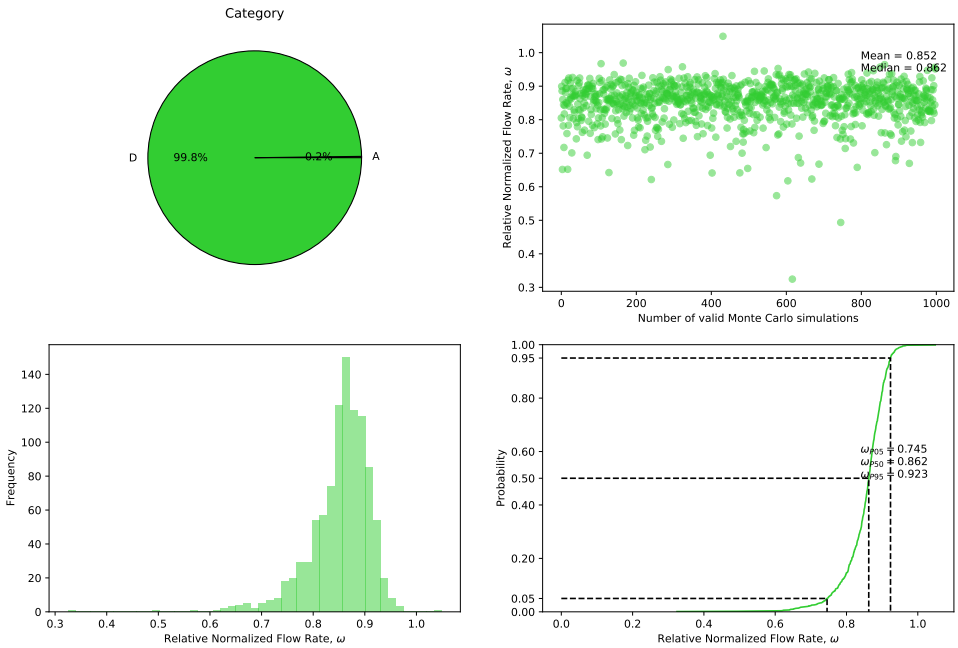

(b) Relative comparison, ω.

Figure E.12: Detailed results for case # 11

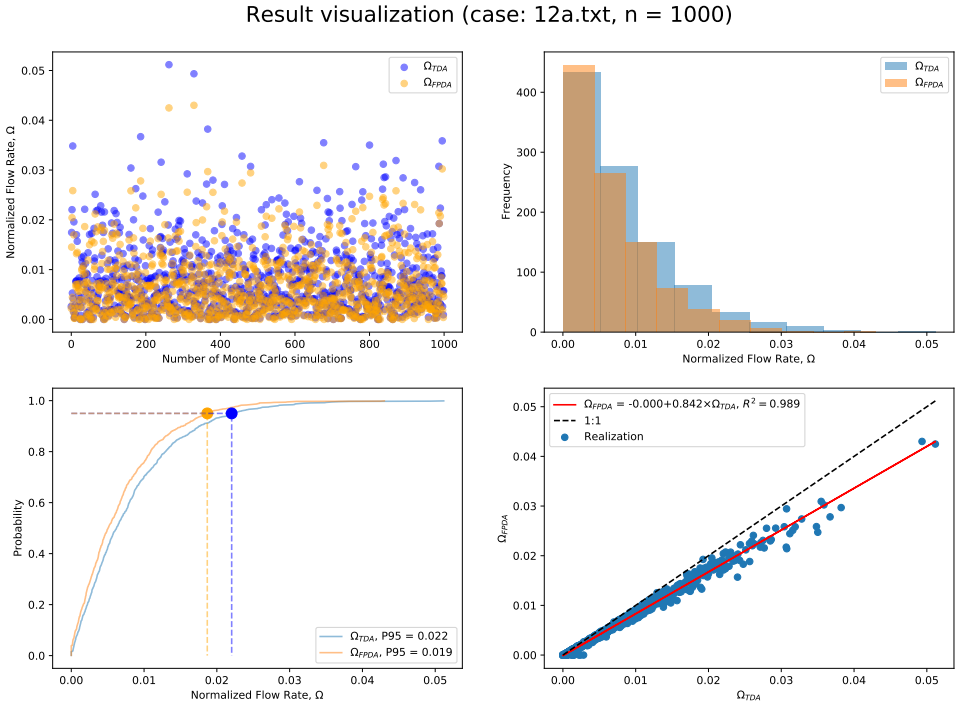

(a) Direct comparison, Ω_{TDA} vs. Ω_{FPDA}

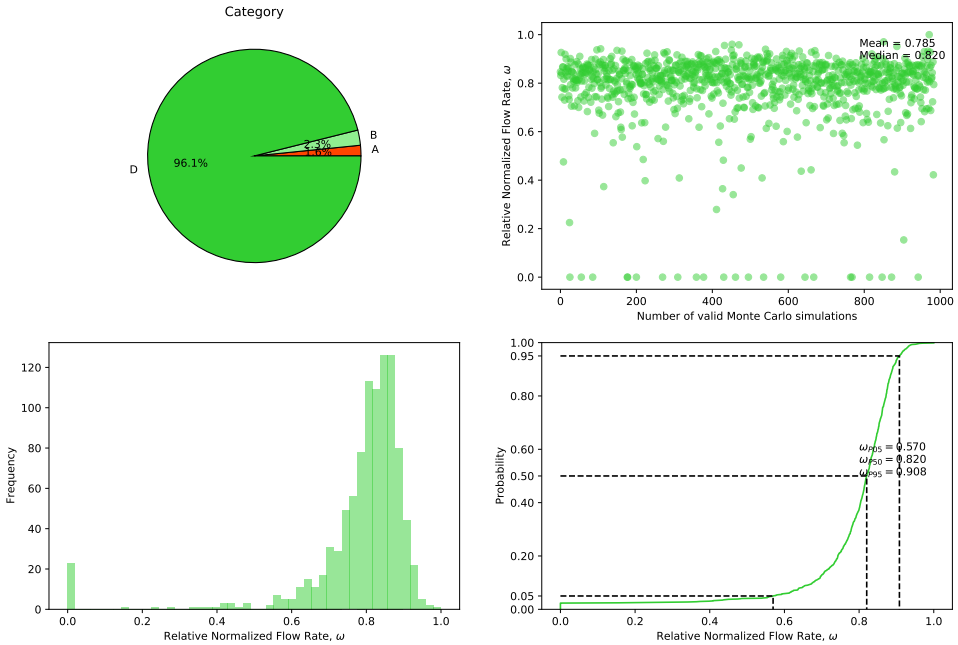

(b) Relative comparison, ω.

Figure E.13: Detailed results for case # 12

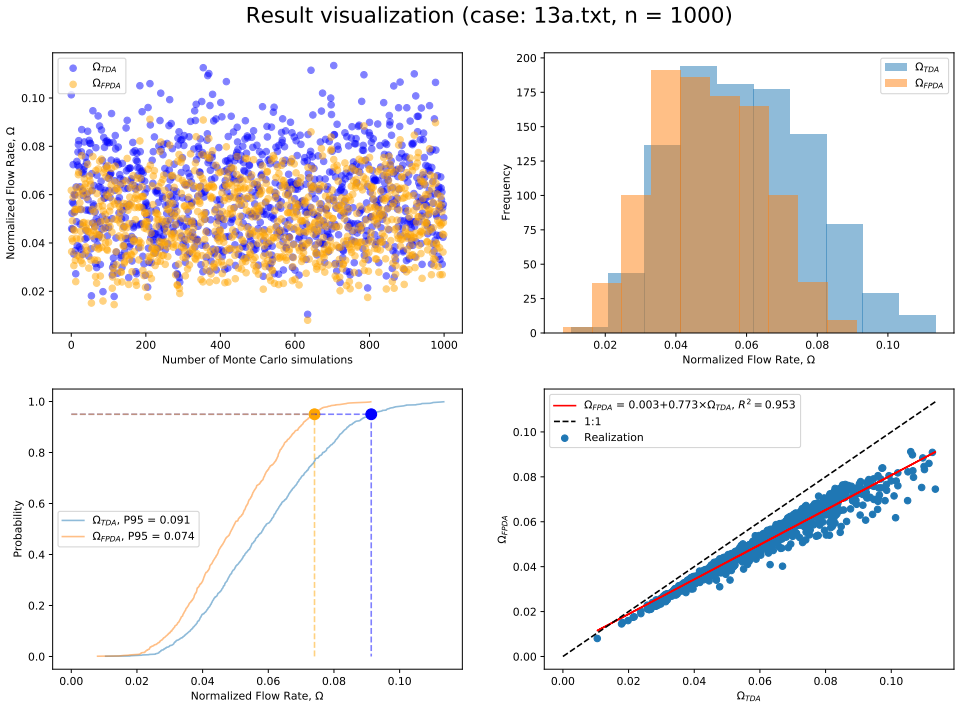

(a) Direct comparison, Ω_{TDA} vs. Ω_{FPDA}

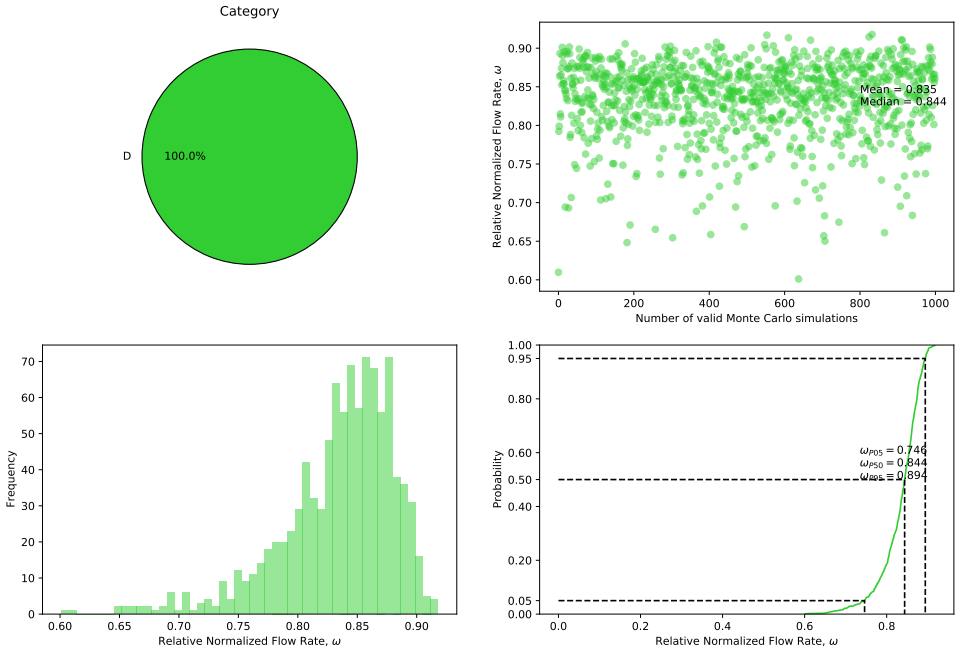

(b) Relative comparison, ω.

Figure E.14: Detailed results for case # 13

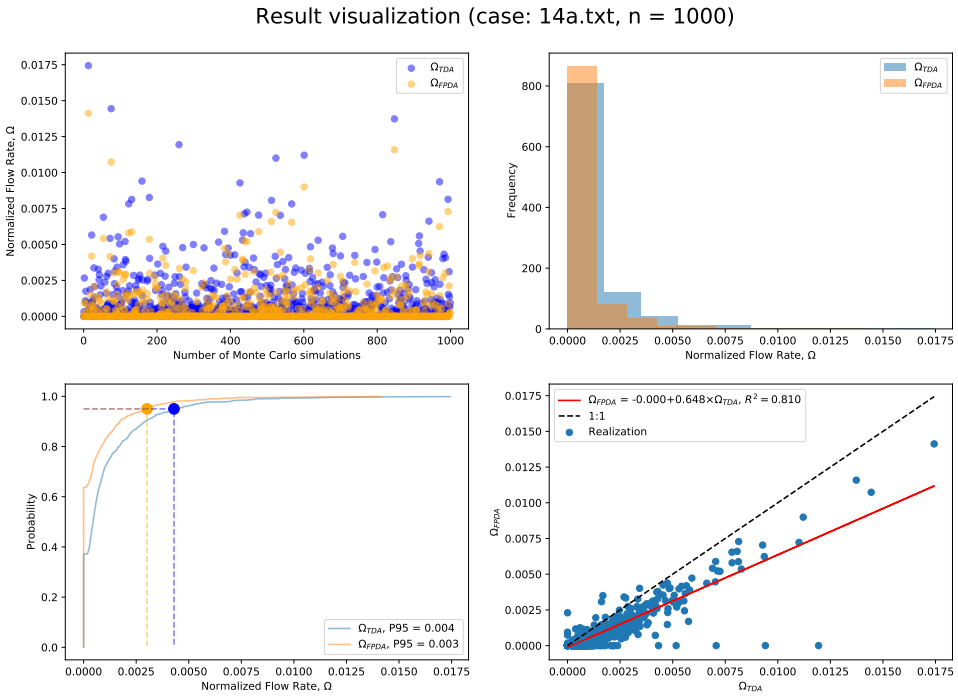

(a) Direct comparison, Ω_{TDA} vs. Ω_{FPDA}

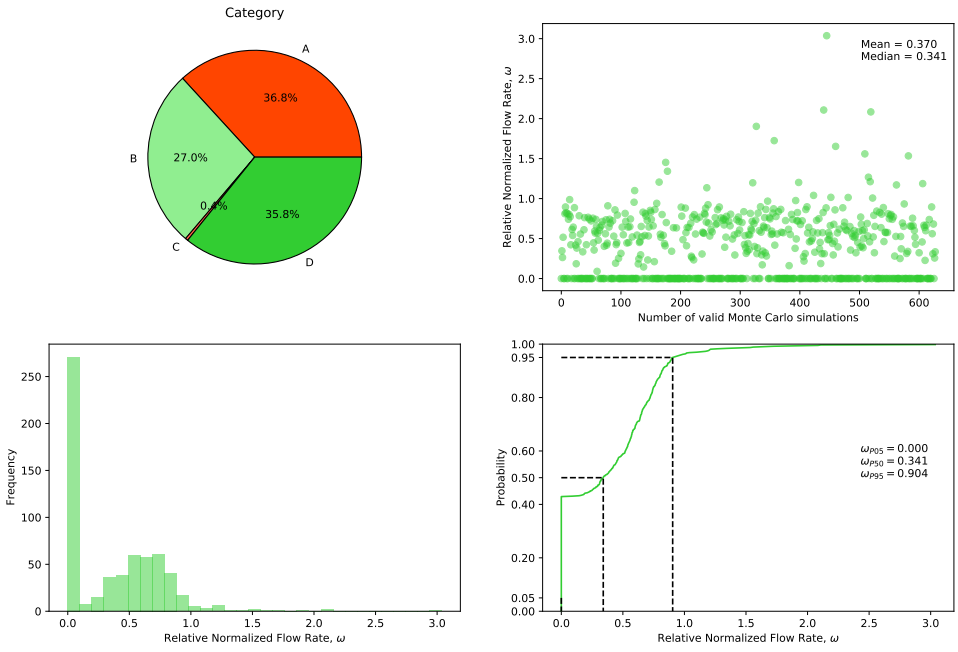

(b) Relative comparison, ω.

Figure E.15: Detailed results for case # 14

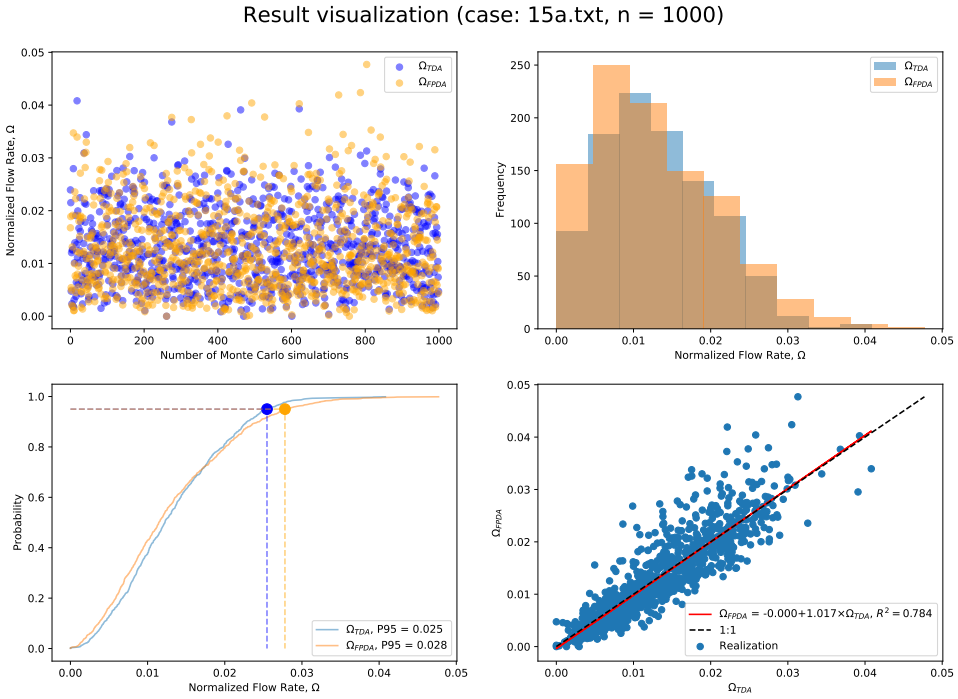

(a) Direct comparison, Ω_{TDA} vs. Ω_{FPDA}

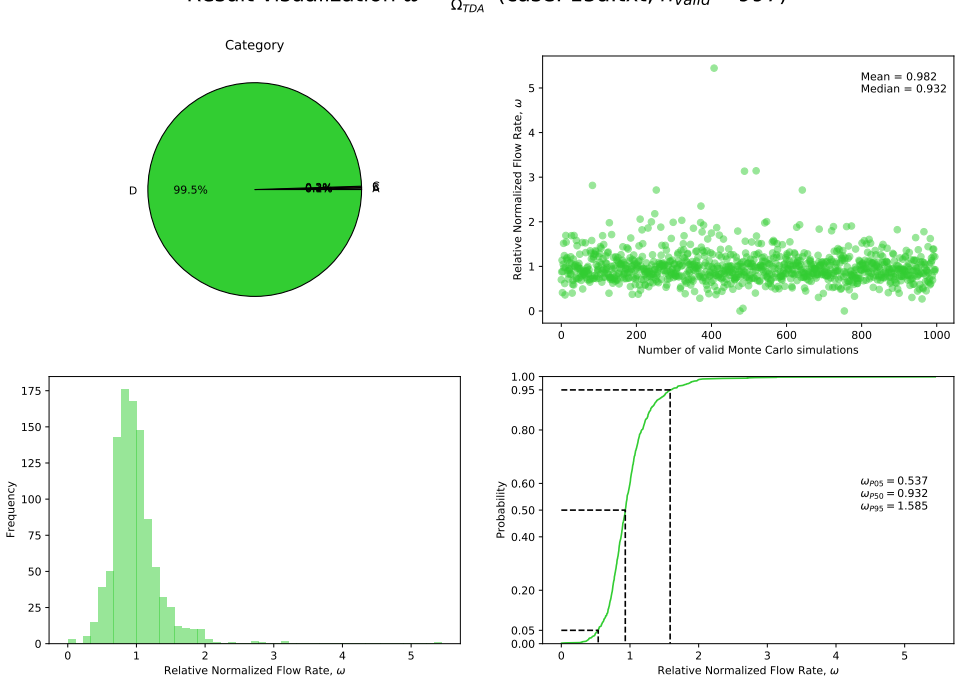

(b) Relative comparison, ω.

Figure E.16: Detailed results for case # 15

Table E.2: Demonstration of convergency. COV_{MC} defined in Appendix C.

Case	Comparison	COV_{MC}
①	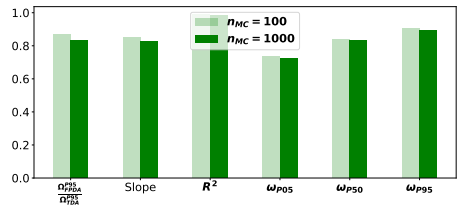	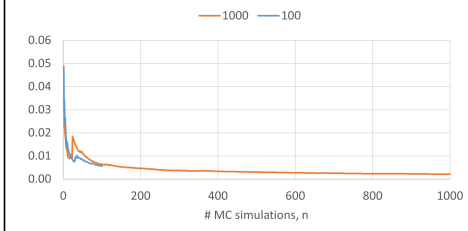
②	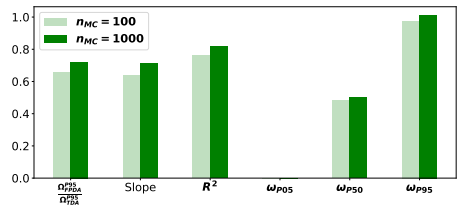	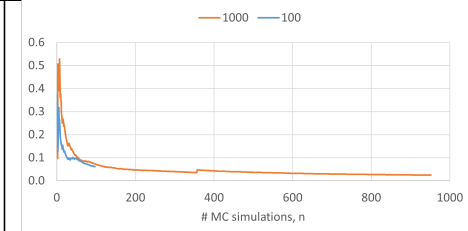
③	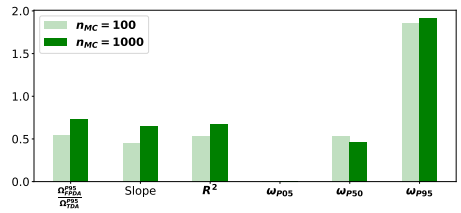	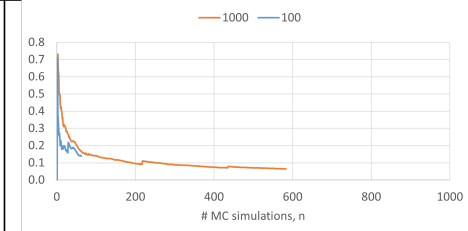
④	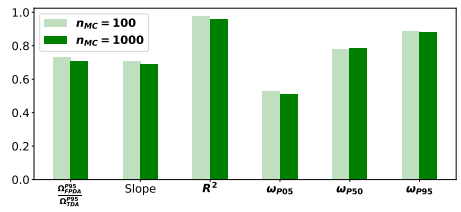	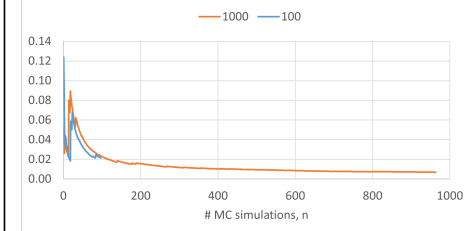
⑤	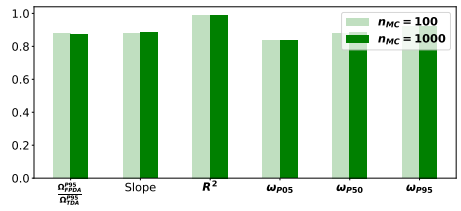	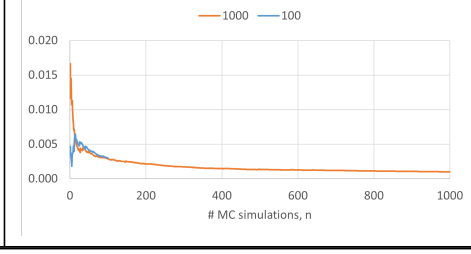

Continued on next page

Table E.2 – continued from previous page

Case	Comparison	COV_{MC}
6	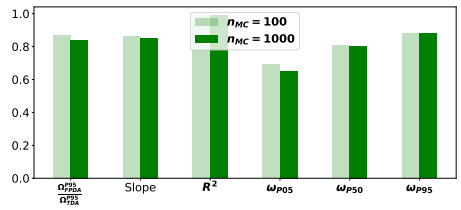	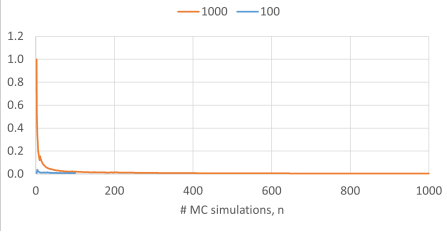
7	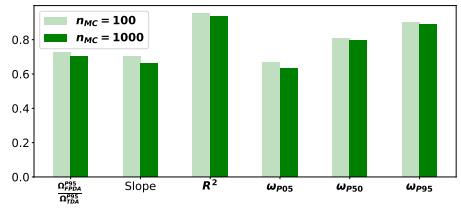	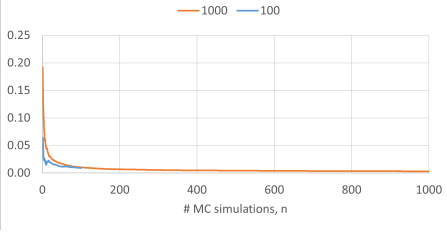
8	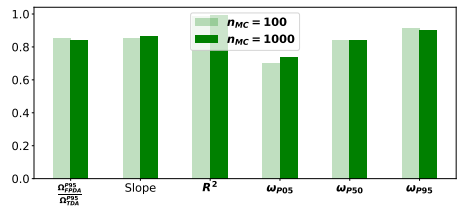	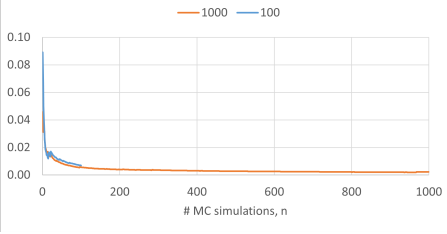
9	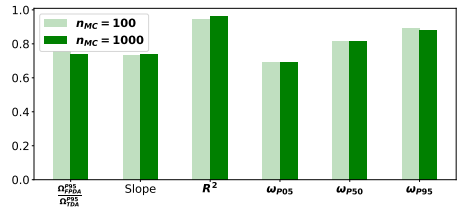	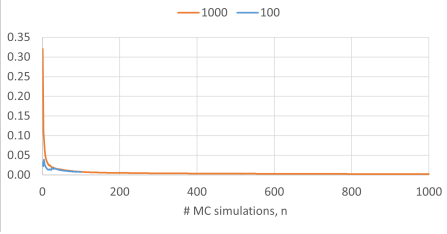
10	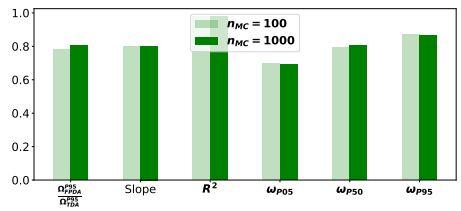	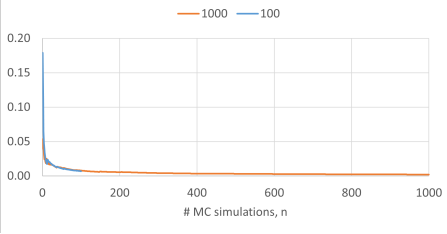

Continued on next page

Table E.2 – continued from previous page

Case	Comparison	COV_{MC}
11	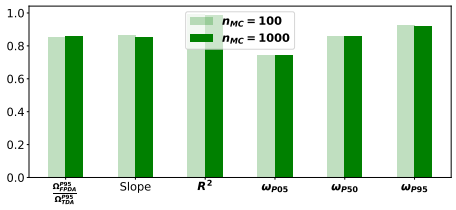	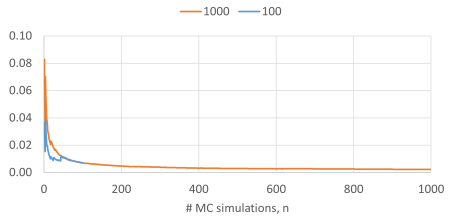
12	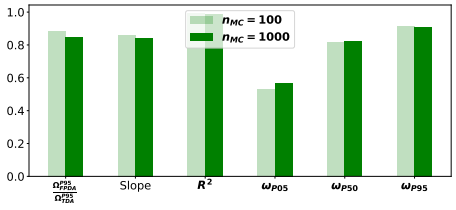	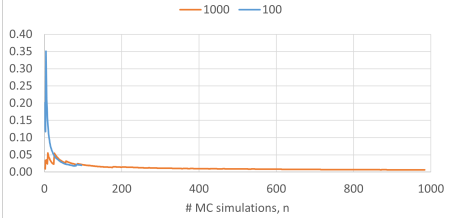
13	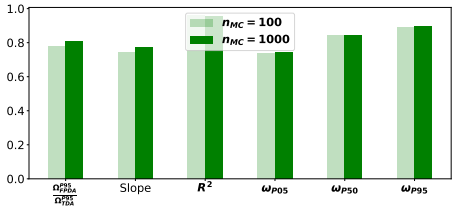	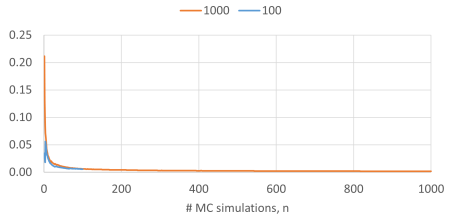
14	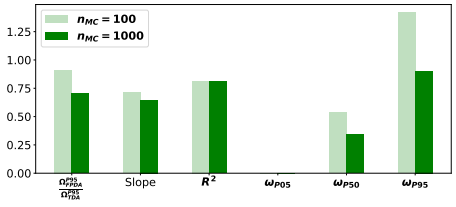	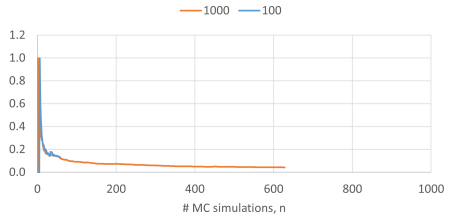
15